University of Texas at El Paso
ScholarWorks@UTEP

Open Access Theses & Dissertations

2022-04-01

Targeting Delivery Of Bcl-2 Family Protein Inhibitor Has The Potential To Treat Cancer And Fibrosis

Mohammad Nurul Huda
University of Texas at El Paso

Follow this and additional works at: https://scholarworks.utep.edu/open_etd

Part of the Oncology Commons, and the Pharmacology Commons

Recommended Citation

Huda, Mohammad Nurul, "Targeting Delivery Of Bcl-2 Family Protein Inhibitor Has The Potential To Treat Cancer And Fibrosis" (2022). *Open Access Theses & Dissertations*. 3879.
https://scholarworks.utep.edu/open_etd/3879

This is brought to you for free and open access by ScholarWorks@UTEP. It has been accepted for inclusion in Open Access Theses & Dissertations by an authorized administrator of ScholarWorks@UTEP. For more information, please contact lweber@utep.edu.

TARGETING DELIVERY OF BCL-2 FAMILY PROTEIN INHIBITOR HAS THE POTENTIAL TO TREAT CANCER AND FIBROSIS

MD NURUL HUDA

Doctoral Program in Environmental Science and Engineering

APPROVED:

Md Nurunnabi, Ph.D., Chair

Marc B. Cox, Ph.D.

Siddhartha Das, Ph.D.

Arshad Khan, Ph.D.

Yong Qin, Ph.D.

Stephen L. Crites, Jr., Ph.D.
Dean of the Graduate School

Copyright ©

by

Md Nurul Huda

2022

DEDICATION

To my parents, better-half, and Zuha

for their love, patience, strength, and support during

the development of this dissertation

TARGETING DELIVERY OF BCL-2 FAMILY PROTEIN INHIBITORS HAS THE POTENTIAL TO TREAT CANCER AND FIBROSIS

by

MD. NURUL HUDA, B.SC.

DISSERTATION

Presented to the Faculty of the Graduate School of

The University of Texas at El Paso

in Partial Fulfillment

of the Requirements

for the Degree of

DOCTOR OF PHILOSOPHY

Environmental Science and Engineering Program

THE UNIVERSITY OF TEXAS AT EL PASO

August 202

ACKNOWLEDGMENTS:

First of all, I would like to thank my doctoral committee – Md Nurunnabi, Ph.D. (chair), Marc B Cox, Ph.D., Siddhartha Das, Ph.D., Arshad M. Khan, Ph.D., and Yong Qin, Ph.D. Collectively they have provided me with tremendous challenge and support, and each has been an outstanding mentor. I am indebted to my Ph.D. mentor, Md Nurunnabi, for his continuous and generous support and mentorship. With his leadership and mentorship, I was able to accomplish this dissertation. Also, his personality and teaching capability inspired me to peruse in an industrial career after my Ph.D. I hope our student-mentor relationship will maintain in the future, and we will collaborate to bring impactful outcomes from our research. I am indebted to Marc B Cox for trusting me with the confidence to take on such an enormous challenge; to Siddhartha Das for sharing his biological insight and helping me to apply theoretical concepts to the translational application; and to Arshad Khan and Yong Qin for their sharp, critical eye, and insightful comments which have dramatically improved the quality of research included in this dissertation. I want to thank Armando Varela Ph.D., Md Nafiujjaman, Ph.D., Isaac G. Deaguero, Ph.D., Vanessa Enriquez, Ph.D., Edgar A Borrego Puerta, Tamanna Islam, and Humayra Afrin for their collaboration and support during the theoretical and experimental period. These people were very open in expressing their opinions and experiences. They showed a lot of excitement for the research topic, which encouraged me to keep going in the direction I wanted. Also, I esteem the research facility UTEP provides to its students. The research facility at Dr. Nurunnabi's lab, school of pharmacy, and BBRC core facility offer me the platform to conduct complex biological assays and increase the standard of this dissertation. Also, I am grateful to UTEP graduate school for giving the Dodson research grant and travel grant during the preparation of this dissertation.

ABSTRACT:

Apoptosis is a naturally occurring cell death mechanism to remove the selective cell population. B-cell leukemia/lymphoma-2 (BCL-2) family protein plays a critical role in activating the upstream apoptosis signaling pathway, primarily the intrinsic apoptosis pathway. The BCL-2 family consists of both pro-and anti-apoptotic proteins, which are structurally and functionally similar, containing up to four BCL-2 homologies (BH) motifs (BH1-4). Defecting apoptosis along this signaling pathway can lead to various events, including malignant cell transformation, tumor metastasis, tissue fibrosis, and drug resistance. In fibrosis, the aberrant apoptosis signaling also activates multiple effector proteins and growth factors, such as TGF-β, CTGF, and IL-6. Activation of TGF-β accumulates higher ECM matrix-like Col1 and α-SMA both on the outside and inside of the cell membrane. Therefore, modalities that can induce apoptosis signaling pathways could target cancer and fibrosis treatment. Navitoclax (NAVI) is a BCL-2 and BCL-xL inhibitor small molecule approved by FDA for cancer treatment. BCL-2 and BCL-xL are anti-apoptotic proteins, and inhibition of these proteins results in the induction of apoptosis. To achieve non-invasive and targeted local delivery, we utilized an ionic liquid composed of Choline bicarbonate and Octanoic Acid (COA) to enhance topical transportation of the small hydrophobic molecules like NAVI. The COA-mediated topical distribution of NAVI improved drug transportation through the skin barrier and retained the drug to stay longer in the deeper skin layers. COA/NAVI had a better cancer-cell killing selectivity than orally administered NAVI, with minor inflammation to healthy human skin cells. In vivo experiments show that it effectively treats melanoma without causing irritation or systemic absorption. The COA/NAVI combination triggered apoptosis in the mouse xenograft model and provided a safe and effective topical administration for the treatment of melanoma. COA-mediated topical delivery of NAVI also heals preexisting fibrosis in a rat model of

scleroderma cutaneous fibrosis by triggering myofibroblast death. Using a BH3 profiling assay, we show that the extent of apoptosis induced by BH3 mimetic drugs correlates with their mitochondrial priming in dermal fibroblasts derived from scleroderma patients, implying that BH3 profiling could predict apoptotic responses of the fibroblasts to BH3 mimetic medicines in scleroderma patients. In scleroderma, topical application of COA/NAVI targeting myofibroblast anti-apoptotic proteins combined with BH3 mimetic medications reduces fibrotic indicators in mouse models. Additionally, topical administration of NAVI combined with COA reduced thrombocytopenia toxicity, which is the biggest challenge for the clinical translation of NAVI. Finally, β-Glucan mediated oral delivery of NAVI induced apoptosis in the paclitaxel resistance tumor model. NAVI can kill paclitaxel-resistant cells by overcoming the barrier associated with the tumor. We demonstrated plausible molecular reasons for the link between paclitaxel medication resistance and how to inhibit MDA MB 231 PTXR tumor growth using a BCL-2 inhibitor in this pilot investigation. In a C57BL/6 mouse model, tumor inhibition and drug resistance reversal were tested using -Glucan mediated Navitoclax oral administration. We have evaluated the hypothesis in both in vitro 2D and in vivo solid tumor models. Both findings confirm that targeting anti-apoptotic proteins, such as BCL-2 and BCL-xL, has the clinical translational capability for skin melanoma and fibrosis treatment.

Keywords: Apoptosis; BCL-2 inhibitor; Ionic liquid; Beta-Glucan; melanoma; fibrosis; drug resistance.

TABLE OF CONTENTS

DEDICATION iii

ACKNOWLEDGMENTS: v

ABSTRACT: vi

LIST OF FIGURES: xii

CHAPTER 1 1

CHAPTER 2: IONIC LIQUID-MEDIATED DELIVERY OF A BCL-2 INHIBITOR FOR TOPICAL TREATMENT OF SKIN MELANOMA 8

ABSTRACT 8

Keywords 8

2.1 INTRODUCTION 9

2.2. RESULTS & DISCUSSION 11

2.2.1. FORMULA PREPARATION AND CHARACTERIZATION 11

2.2.2. COA INCREASES NAVI SOLUBILITY AND TRANSPORTATION OF NAVI THROUGH THE SKIN 13

2.2.3. BCL-2 INHIBITION IN MOUSE CANCER MELANOMA CELLS: 15

2.2.4. COA/NAVI CAN INDUCE APOPTOSIS AND DOWNREGULATE BCL-2 PROTEIN EXPRESSION IN VITRO: 18

2.2.5. *IN VIVO* TREATMENT EFFICACY IN MICE TUMOR MODEL: 20

2.2.6: HISTOLOGY, SERUM BIOCHEMISTRY, AND BLOOD CELL ANALYSES: 21

2.2.6. INHIBITION OF ANTI-APOPTOTIC PROTEIN BCL-2 IN VIVO: 24

2.3. CONCLUSIONS 26

2.4. MATERIALS AND METHODS: 27

2.4.1. MATERIALS: 27

2.4.2. CELL CULTURE 28

2.4.3. SYNTHESIS OF COA 28

2.4.4. PHYSICAL CHARACTERIZATION OF COA 28

2.4.5: SKIN PERMEATION 28

2.4.6. DRUG SOLUBILITY 30

2.4.7. *IN VITRO* CYTOTOXICITY EVALUATION AND CELL IMAGING 30
2.4.8. LACTATE DEHYDROGENASE (LDH) RELEASE ASSAY: 32
2.4.9. *IN VITRO* APOPTOSIS-NECROSIS STUDY: 33
2.4.10. PROTEIN PURIFICATION AND WESTERN BLOT ANALYSIS: 34
2.4.11. MOUSE TUMOR XENOGRAFT AND BODY WEIGHT: 35
2.4.12. HISTOLOGY ANALYSIS: 35
2.4.13. CLINICAL BIOCHEMISTRY PANEL ANALYSIS : 36
2.4.14. PROTEIN EXPRESSION BY IMMUNOHISTOCHEMISTRY 36
2.4.15: TUNEL ASSAY: 37
2.4.16. STATISTICAL ANALYSIS: 38
2.5 ACKNOWLEDGMENTS: 38

CHAPTER 3: TOPICAL BCL-2/BCL-XL INHIBITOR REVERSES BLEOMYCIN-INDUCED SKIN FIBROSIS 39

3.1. ABSTRACT 39

Keywords: 39

GRAPHICAL ABSTRACT: 40

3.2. INTRODUCTION 40

3.3. RESULT & DISCUSSION 43
3.3.1: COA/NAVI FORMULATION INHIBITS FIBROTIC MARKER IN TGF-B INDUCED HS27 FIBROTIC CELL: 43
3.3.2: COA/NAVI-INDUCED APOPTOSIS IN FIBROTIC CELLS VIA MITOCHONDRIAL MEMBRANE DEPOLARIZATION 46
3.3.3 BLEOMYCIN INDUCES FIBROSIS CAN INHIBIT BY COA/NAVI TOPICAL ADMINISTRATION: 49
3.3.4: COA-ASSISTED TOPICAL NAVI DOES NOT SHOW SYSTEMIC TOXICITY 52
3.3.5: COA/NAVI INDUCES APOPTOSIS VIA ANTI-APOPTOTIC BCL-2 PROTEIN INHIBITION 54
3.3.6: TOPICAL DELIVERY OF COA/NAVI IMPROVES SCLERODERMA BY REVERSING FIBROSIS 56

3.4. CONCLUSION 59

3.5. MATERIALS AND METHODS 60

3.5.1. MATERIALS AND CHEMICALS 60

3.5.2. CELL CULTURE 60

3.5.3. SYNTHESIS OF IONIC LIQUID 60

3.5.4. PHYSICAL CHARACTERIZATION OF IONIC LIQUID 61

3.5.5. DRUG SOLUBILITY 61

3.5.6. CELLULAR UPTAKE & IN VITRO FIBROTIC MARKER VISUALIZATION 61

3.5.7 MITOCHONDRIAL MEMBRANE POLARIZATION ASSAY 62

3.5.8. *IN VITRO* PORCINE SKIN DIFFUSION 63

3.5.9. *IN VITRO* APOPTOSIS-NECROSIS STUDY 64

3.5.10. PROTEIN PURIFICATION AND WESTERN BLOT ANALYSIS 65

3.5.11. MOUSE TUMOR XENOGRAFT AND BODY WEIGHT 66

3.5.12. HISTOLOGY ANALYSIS 67

3.5.13. CLINICAL BIOCHEMISTRY PANEL ANALYSIS 67

3.5.14. IMMUNOHISTOCHEMISTRY ANALYSIS OF PROTEIN EXPRESSION 68

3.5.15: TUNEL ASSAY 69

3.5.16. STATISTICAL ANALYSIS 70

3.6. ACKNOWLEDGEMENT 70

CHAPTER 4: ORAL DELIVERY OF BCL-2 INHIBITOR REDUCED PACLITAXEL RESISTANCE MDA MB 231 TUMOR IN A MOUSE MODEL 72

4.1 ABSTRACT 72

Keywords 72

4.2. INTRODUCTION 73

4.4.3. RESULT & DISCUSSION 75

4.3.1 PACLITAXEL RESISTANCE MDA MB 231 CELLS EXPERIENCE APOPTOSIS DUE TO NAVI TREATMENT: 75

4.3.2 IN VITRO SOLUBILITY, STABILITY & IN VIVO BIODISTRIBUTION OF ORAL ADMINISTRATION NAVI AND BG/NAVI IN SD RAT 76

4.3.3 PTXR MDA MB 231 TUMOR XENOGRAFT AND TUMOR VOLUME DURING TREATMENT: 79

4.3.4 SYSTEMIC TOXICITY EVALUATION OF PTXR MDA MB 231 TUMOR MOUSE MODEL 81

4.4. CONCLUSION AND FUTURE DIRECTION 83

4.5. MATERIALS & METHODS: 85

4.5.1 MATERIALS AND CHEMICALS 85

4.5.2 CELL CULTURE AND PACLITAXEL RESISTANCE CELL 85

4.5.3: FORMULATION OF BG/NAVI: 86

4.5.4 CONJUGATION OF NAVI/MTP AND PTX/MTP 86

4.5.5: *IN VITRO* APOPTOSIS-NECROSIS STUDY 86

4.5.6: SOLUBILITY, STABILITY & NAVITOCLAX BIO-DISTRIBUTION STUDY ...87

4.5.7: TUMOR XENOGRAFT MOUSE MODEL AND TUMOR VOLUME MEASUREMENT 88

4.5.8: CLINICAL BIOCHEMISTRY PANEL ANALYSIS AD COMPLETE BLOOD COUNT 88

4.5.9 IMMUNOHISTOCHEMISTRY OF TUMOR SAMPLES 89

4.5.10 STATISTICAL ANALYSIS 90

4.6 ACKNOWLEDGMENT 90

CHAPTER 5: CONCLUSION 92

REFERENCES 96

VITA: 113

LIST OF FIGURES:

Figure 1: Physical and Chemical properties of COA and NAVI……...13

Figure 2: Solubility and ex-vivo skin transportation…….14

Figure 3: In vitro toxicity and internalization……16

Figure 4: In Vitro apoptosis-necrosis & western blotting…….19

Figure 5: (a,b) Tumor volume and body weight were measured during the treatment……22

Figure 6: Hematoxylin and eosin staining, serum biochemistry, and total blood count analysis……...23

Figure 7: Ex-vivo tissue analysis……...25

Figure 8: In vitro fibrotic cell therapy and internalization…….45

Figure 9: In Vitro cell apoptosis and mitochondrial polarization……..47

Figure 10: In Vivo animal study and biochemical analysis……...50

Figure 11: H&E staining, serum, and comprehensive blood analysis of fibrotic mice model……..53

Figure 12: Ex-vivo tissue analysis and apoptosis analysis……55

Figure 13: Biochemical analysis of fibrotic tissue analysis……...57

Figure 14: Tumor gets drug resistance due to consistent chemotherapeutic exposure……..76

Figure 15: Drug solubility and pharmacokinetic study……..78

Figure 16: The treatments were paclitaxel (IV), NAVI (PO), and BG/NAVI (PO)……..80

Figure 17: Serum and complete blood analysis were conducted to evaluate serum toxicity……83

Figure 18: The Col1 and BCL-2 expressions were quantified using immunohistochemistry…..

CHAPTER 1

Finding patient-friendly administration routes and identifying those that can be employed over large dose ranges are two of the most significant disruptions that may be made through the development of small molecule delivery strategies and technology. Drug delivery methods concentrate on changing intravenous administration to more convenient subcutaneous injections or non-invasive transdermal, oral, buccal, nasal, and inhalation routes. The specific barrier challenges that are dependent on the delivery route, the potential advantages of the delivery route, the intended dose and frequency of dosing, and the molecular complexity of the small molecules must all be considered when developing strategies for overcoming delivery barriers to systemic delivery of biologics [1,2]. To date, a variety of non-invasive techniques have effectively negotiated these obstacles and been licensed for biologic delivery in clinics. This dissertation focuses on transdermal and oral delivery of BCL-2 inhibitor Navitoclax to improve local diseases like melanoma and scleroderma. Navitoclax is a protein inhibitor from the B-cell lymphoma 2 (BCL-2) family that was discovered during the clinical development of ABT-737. Navitoclax is a BH3 mimetic medication that binds to the BH3 domain of anti-apoptotic members of the BCL-2 family [3]. After being administered, navitoclax attaches to the BH3 binding groove of BCL-2 proteins in the cytoplasm, causing BIM to be displaced from a pro-apoptotic BH3-only protein BCL-2 [4]. BIM is subsequently left free to induce cell death by triggering the release of tiny heme proteins called cytochrome c from mitochondria [5].

Apoptosis is a pre-programmed cell death [6]. This type of controlled cell death is essential for various physiological processes in adult tissue and fetal development. Many disorders, including cancer, can be exacerbated by a failure to activate apoptosis [7]. The biochemical and

morphological changes during apoptosis are caused by a family of proteases known as caspases. The release of apoptogenic proteins such as Smac/DIABLO, cytochrome c, DDP/TIMM8a, and EndoG is triggered by mitochondrial outer membrane permeabilization (MOMP) during apoptosis [8]. MOMP activation, and hence whether or not a cell initiates apoptosis, is dependent on a dynamic balance between anti-apoptotic and pro-apoptotic proteins like BCL-2 and BAX [9]. Systemic sclerosis is a connective tissue illness characterized by increased extracellular matrix protein production and buildup in the affected skin and other interior organs [10]. The apoptotic process is thought to play a role in developing systemic sclerosis [11]. On the other hand, melanoma cells can self-destruct by apoptosis or programmed cell death. The molecular components of apoptosis in these tumors comprise positive (apoptotic) and negative (anti-apoptotic) regulators. P53, Bid, Noxa, PUMA, Bax, TNF, TRAIL, Fas/FasL, PITSLRE, interferons, and c-KIT/SCF are among the former [12]. Bcl-2, Bcl-XL, Mcl-1, NF-KB, survivin, livin, and ML-IAP are among the latter. Bcl-2 is an anti-apoptotic membrane-associated protein that performs three functions: (1) controlling mitochondrial cytochrome c release and Apaf-1-caspase 9 interaction; (2) binding to Bax; and (3) inhibiting apoptosis triggered by the avian myelocytomatosis viral oncogene homolog (cMyc) [13,14]. When compared to benign naevi, Bcl-2 levels are downregulated in cutaneous malignant melanoma, resulting in higher apoptosis. This downregulation of BCL-2 protein is not enough and further required inhibition of the BCL-2 anti-apoptotic proteins [14]. Therefore, regulating apoptosis in both scleroderma and cutaneous melanoma has the scope of therapeutic benefit and can eliminate current treatment limitations.

<u>Local Diseases and Scope of finding alternative therapeutic approaches</u>: Small molecules' quick approval and clinical use have changed how these medications are administered. As new obstacles and unmet requirements arise, this transition necessitates new delivery options. Accounting for

patient adherence, compliance, and acceptance are among the challenges. Because doses can vary by nearly an order of magnitude, flexible delivery methods that can accommodate a variety of volumes, preparations, and even drug states will be required. A primary focus has been developing and accessing excipients for storage, improving penetration and diffusion, and allowing more time at the injection site to optimize drug absorption at biological barriers.

Skin diseases account for 1.79 percent of the global burden of illness [15]. The American Academy of Dermatology (AAD) stated that one out of four people in the United States has a skin disorder [16]. Multiple local diseases such as seborrheic dermatitis, Rosacea, melanoma, skin lesion/ fibrosis, lupus, psoriasis, eczema, etc., prevail due to genetic, environmental, drug, and radiation exposure [16]. Out of all skin or local diseases, skin melanoma and skin fibrosis are the most neglected treatments and diagnoses. Melanoma originates in the cells (melanocytes) that create melanin, the pigment that gives your skin its color is the most aggressive form of skin cancer. Melanoma may also develop in the eyes and, in rare cases, inside the body, such as the nose or throat [17]. Although the exact cause of all melanomas is unknown, UV radiation from the sun, tanning lights, and beds increase our chances of developing melanoma. By reducing your exposure to UV radiation, you can lower your risk of developing melanoma. Melanoma risk appears to be increasing in people under 40, particularly among women. [17]. This dissertation, chapter 2, is based on alternative topical therapeutic delivery of ionic liquid/navitoclax to skin melanoma tumor mice model. On the other hand, tissue fibrosis is a critical histopathologic hallmark of many clinical diseases, characterized by excessive deposition of ECM and growth factors[18]. For example, excessive collagen deposition can occur in internal organs, such as pulmonary fibrosis or liver cirrhosis [19]. Fibrotic processes frequently damage the skin, and dermal fibrosis is a

pathologic feature of several acquired and heritable cutaneous illnesses [20]. Chapter 3 addresses consistent bleomycin-induced skin lesion and topical fibrosis delivery of ionic liquid/navitoclax.

In chapter 2, the study is based on novel topical delivery of BCL-2 inhibitors for skin melanoma treatment. Melanoma is one of the fastest-growing tumors and one of the most frequent cancers in the United States and worldwide. Although initial melanoma can be surgically removed if identified, advanced metastatic melanoma cannot be treated with surgery alone, necessitating a different and more successful treatment strategy. When surgery is not an option, the direct local application of anti-cancer medications may potentially effectively cure topical malignant skin lesions. Due to the protective structure of the skin and the fact that existing topical treatments can cause skin irritation, burning, scaling, and inflammation, these therapies are severely limited. We develop a topical formulation of Navitoclax (NAVI). This BCL-2 inhibitor upregulates apoptosis with an ionic liquid constituted of Choline bicarbonate Octenoic Acid (COA) and other ingredients to treat early-stage melanoma (1:1). Ionic liquids, for example, have been found to promote cell membrane permeability via improving transit into the stratum corneum and lipid channel navigation [21]. These liquids have also been proven to fluidize cell membranes and remove or displace transport-limiting lipids in the stratum corneum, allowing for better diffusion. Ionic liquids can be specifically tailored to obtain the required solubility, concentration, and viscosity, directly regulating transdermal distribution and delivery, thanks to their tunable physicochemical features [21].

Physical disruption devices, chemical permeation, or penetration enhancers are not required for transdermal biologics using ionic liquids; as a result, combination techniques may be even more effective. Efforts to understand the mechanisms of transdermal transport, evaluate host toxicity, describe interactions with topical microbes, and expand the application to therapeutic usage are

well underway, even though ionic liquids are [22]. When dissolved in 50 percent (DW V/V) COA, NAVI is a small hydrophobic molecule that dissolves at 20% (W/V). NAVI is highly efficient chemotherapy that is poisonous to the blood. As a result, the COA-mediated topical distribution of NAVI improved drug transport through the skin barrier and allowed the drug to stay longer in the deeper skin layers. COA/NAVI had a better cancer-cell killing selectivity than NAVI given orally, with minor damage to healthy human skin cells. Experiments in vivo show that it effectively treats melanoma without causing irritation or systemic absorption. The COA/NAVI combination triggered apoptosis in the mouse xenograft model and provided a safe and effective topical, transdermal administration for the treatment of melanoma.

Chapter 3 focuses on the scleroderma disease mechanism and how to develop a topical ionic liquid-based delivery system. We also utilized a BCL-2 inhibitor and repurposed navitoclax for fibrosis treatment and found it very efficient in inhibiting fibrotic marker development during the disease model. Persistent myofibroblast activation distinguishes pathological fibrosis from physiological wound healing, suggesting that medicines that induce myofibroblast death selectively could limit growth and perhaps repair established fibrosis in disorders such as scleroderma (a heterogeneous autoimmune disease characterized by multi-organ fibrosis). The ionic liquid, comprising octanoic acid and choline bicarbonate (COA), can increase skin pore size and allow its payload to pass through the barrier. Navitoclax (NAVI) is an anti-fibrotic BCl-2 inhibitor that has only been used once in skin fibrosis research. There is also no research on navitoclax as a topical treatment for skin fibrosis. Death signals, such as the pro-apoptotic BH3-only protein BIM, prime mitochondria in activated myofibroblasts but not in quiescent fibroblasts and upregulate the production of the anti-apoptotic protein BCL-xL, which sequesters BIM and ensures myofibroblast survival. Myofibroblasts are more sensitive to apoptosis when treated with ABT-263, a "BH3 mimic" drug

that suppresses BCL-x L. ABT-263 displaces BCL-xL binding to BIM, allowing BIM to induce apoptosis in stiffness-primed myofibroblasts. Therapeutic suppression of BCL-xL with ABT-263 (Navitoclax) heals preexisting fibrosis in a rat model of scleroderma cutaneous fibrosis by triggering myofibroblast death. Using a BH3 profiling assay, we show that the extent of apoptosis induced by BH3 mimetic drugs correlates with their mitochondrial priming in dermal fibroblasts derived from scleroderma patients, implying that BH3 profiling could predict apoptotic responses of the fibroblasts to BH3 mimetic medicines in scleroderma patients. In scleroderma, topical application of COA/NAVI targeting myofibroblast anti-apoptotic proteins combined with BH3 mimetic medications reduces fibrotic indicators in mouse disease models. It improves disease status in the animal model, according to our findings. Additionally, topical administration of NAVI in combination with COA reduced thrombocytopenia toxicity.

Chapter 4 addresses resistance to chemotherapy and molecularly targeted therapies in cancer research. Changes in the drug target, activation of pro-survival pathways, and ineffective induction of cell death are all features of resistance to 'conventional' cytotoxic chemotherapeutics and therapies aimed at specific molecular targets. We wanted to improve anti-cancer pharmaceutical cytotoxicity in cancer cells and animal models by overcoming multi-drug resistance. In this chapter, we identify β-Glucan/NAVI oral delivery compared to only NAVI (PO) and paclitaxel (PTX) (IV), which inhibit tumor volume and show better therapeutic efficiency in the PTX resistance tumor model. Our analysis shows that targeting the mitochondria via inducing apoptosis is another alternative way to treat drug resistance in the breast cancer tumor model. Beta-glucan, a polysaccharide-based of burly origin, showed excellent properties of oral delivery of small molecules. 1,3-glucans, which are glucopyranose polysaccharides with (1,3) glycosidic connections and various degrees of (1,6) branches, are an exciting class of polysaccharides.

Combining heat and humidity, 1,3-glucans can produce single or triple helical structures, exploited to create robust gels [23]. In the PTX resistance tumor model, BG/NAVI oral delivery inhibits tumor volume and shows greater treatment efficacy than simply NAVI (PO) and PTX (IV). According to our findings, targeting the mitochondria by generating apoptosis is another approach for treating medication resistance in the breast cancer tumor model.

Finally, our findings in Chapters 2 and 3 proposed alternate topical delivery of COA/NAVI for skin-related diseases. Skin melanoma topical delivery was successful and therapeutic efficiency was evaluated via molecular biology assays. The data confirmed inhibition of melanoma and showed tumor inhibition due to topical delivery of COA/NAVI. In chapter 3, the bleomycin-induced skin fibrosis pathway was attenuated via topical delivery of COA/NAVI. Bleomycin-induced fibrosis activates TGF-β and eventually upregulates the ECM accumulation such as Col1, CTGF, and α-SMA. Topical delivery of COA/NAVI inhibits ECM accumulation and improves fibrosis conditions after 28 days of treatment. And chapter 3 focuses on oral delivery of BG/NAVI to reverse the drug resistance tumor model. The data from this pilot study conclude that alternative chemotherapeutics target different molecular pathways that can apply to drug-resistant tumors. The drug that can inhibit vasculature and angiogenesis and induce apoptosis in cancer can be a candidate for the drug-resistant tumor model.

CHAPTER 2: IONIC LIQUID-MEDIATED DELIVERY OF A BCL-2 INHIBITOR FOR TOPICAL TREATMENT OF SKIN MELANOMA

ABSTRACT

Skin melanoma is one of the most common types of cancer in both the United States and worldwide, and its incidence continues to grow. Primary skin melanoma can be removed surgically when feasible and if detected at an early stage. Anti-cancer drugs can be applied topically to treat skin cancer lesions and used as an adjunct to surgery to prevent the recurrence of tumor growth. We developed a topical formulation composed of Navitoclax (NAVI), a BCL-2 inhibitor that results in apoptosis, and an ionic liquid of choline octanoate (COA) to treat early-stage melanoma. NAVI is a small hydrophobic molecule that solubilizes at 20% (w/v) when dissolved in 50% COA. Although NAVI is a highly effective chemotherapeutic, it is equally thrombocytopenic. We found that COA-mediated topical delivery of NAVI enhanced its penetration into the skin and held the drug in the deeper skin layers for an extended period. Topical delivery of NAVI produced a higher cancer-cell killing efficacy than orally administrated NAVI. *In vivo* experiments in a mouse model of human melanoma-induced skin cancer confirmed the formulation's effectiveness *via* an apoptotic mechanism without any significant skin irritation or systemic absorption of NAVI. Overall, this topical approach may provide a safe and effective option for better managing skin cancer in the clinic.

Keywords: Topical Delivery; Ionic Liquid; Melanoma; Chemotherapeutic; Apoptosis.

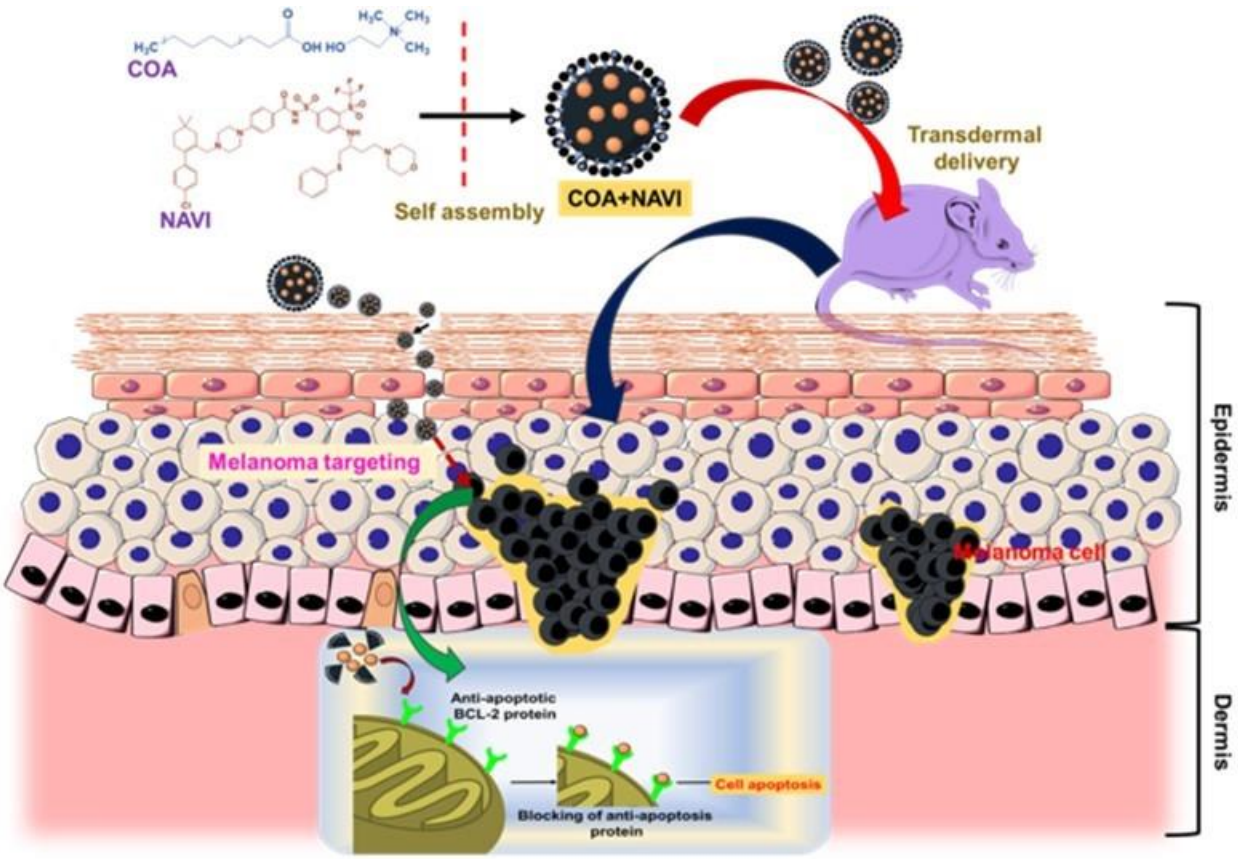

GRAPHICAL ABSTRACT:

Ionic liquid-mediated topical delivery of Navitoclax enhanced transportation through the skin barrier and held the drug in the deeper skin layers for an extended period compared to the control. *In vivo* experiments confirm its efficacy in treating melanoma without irritation or systemic absorption. In a mouse xenograft model, the formulation induced apoptosis and provided a safe and potent topical, transdermal delivery for the treatment of melanoma.

2.1 INTRODUCTION

The American Cancer Society estimates that over 106,000 new skin melanoma cases will be diagnosed in 2021 in the United States [24]. Predicted mortality will exceed 7100 Americans in 2021, and the increased mortality rate is expected to continue over the next few decades [17].

Among Caucasian people, the incidence of melanoma will grow by 3-5%, making it fastest-growing cancer worldwide [12,25]. Many risk factors for melanoma include smoking and excessive exposure to sunlight [26] In addition, alteration of specific oncogenes in skin moles (nevi) or normal skin can lead to melanoma [27,28]. Current treatments for melanoma include surgical excision, chemotherapy, electrodesiccation or Mohs surgery, curettage, immunotherapy, and cryotherapy [29,30] Unfortunately, these treatments are effective only against more localized lesions [30] and can often miss vital points of growth, leading to advanced disease stages.

Currently available topical gels or creams can effectively treat skin cancers when the tumors are located at superficial sites but fail to offer comprehensive treatment within deeper skin layers. Additional limitations of some topical products like hydroquinone, fluorouracil, and Efudex is that the drugs cause inflammation, burning, stinging, and swelling upon skin application [31–34], resulting in reduced patient compliance through physical pain limitation. Immunotherapeutic such as nivolumab, ipilimumab, and pembrolizumab have been approved by the FDA and prescribed to patients with different stages of melanoma; however, all immunotherapy treatments contain the unavoidable caveat of severe side effects, including colitis, renal dysfunction, pneumonitis, and immune-mediated hepatitis [35–37]

Here, we propose a novel topical solution composed of an ionic liquid, choline octanoate (COA), and a BCL-2 inhibitor, navitoclax (NAVI), for the treatment of non-metastatic melanoma. COA ionic liquid was reported to be an effective agent for delivering small hydrophobic molecules, like NAVI, through the skin [38]. COA enhances skin permeation and holds the payload within the dermis and subcutaneous layers [3] NAVI is a safe and effective chemotherapeutic that inhibits the anti-apoptotic proteins BCL-2, BCL-xL, BCL-W, and MCL in tumor cells. The COA/NAVI combination was designed to improve drug penetration into the skin and enhance NAVI retention

in the target area for an extended time. Besides facilitating skin permeation, COA also increases the solubility of NAVI. However, despite the emerging potential of NAVI as a chemotherapeutic agent, its applications are limited due to the risk of severe thrombocytopenia it poses [39]. Therefore, we hypothesized that COA-mediated local delivery of NAVI will prevent systemic absorption and limit toxicity risk.

Here, we show that our COA/NAVI formulation overcomes key limitations of NAVI to facilitate its topical application to accelerate local melanoma treatment. We confirmed that the COA/NAVI formulation delivers and holds the drug at the targeted melanoma site for an extended period. We confirmed this by an *ex-vivo* permeation test (EVPT) using porcine skin. *In vitro* studies conducted using the B16 F10 mouse melanoma cell line demonstrate the potential use of NAVI as a chemotherapeutic for treating melanoma, and COA/NAVI shows significantly higher efficacy than free NAVI (delivered orally; PO) in a xenograft mouse model. The xenograft model was also used to evaluate drug safety and biodistribution. The findings reveal that the COA/NAVI formulation could be an effective and safe therapeutic approach for treating skin melanoma.

2.2. RESULTS & DISCUSSION:

2.2.1. FORMULA PREPARATION AND CHARACTERIZATION:

The COA/NAVI formulation was prepared in the laboratory with regular mixing of both components at equal volumes. The chemical identities of each were studied using ^{1}H-NMR spectroscopy. Figure 1(a,b,c) shows the 1H-NMR results of NAVI (A), COA (B), and COA/NAVI (C). Initially, each sample was dissolved in deuterated chloroform (CDCl3), and the NMR analysis was performed using an Avance III HD NanoBay NMR instrument at an operating frequency of 400 M Hz. The chemical shift δ values of NAVI obtained (in CDCl3) were: δ 0.92 (d, J=6.6, 6H), 1.26 (t, J=7, 4H), 1.6 (Br, s, 1H), 2.06 (s, 2H), 2.14 (Br., s, 2H), 2.31 (d, J=7, 2H), 3.49 (Br., s,

12H), 3.73 (q, J=7.3, 1H) (Fig. S1A). The chemical shift data for COA were: δ 0.87 (t, J=6.8, 3H), 1.27 (Br., s, 8H), 1.55 (p, J=7.4, 2H), 2.21 (t, J=7.8, 2H), 3.23 (s, 9H), 3.55 (m, J=2,5, 2H), 4.02 (m, J=2,2.6, 2H), 6.06 (s, 2H) in CDCl3 (Fig. 1B). Finally, the chemical shift data for NAVI+COA were: δ 0.85 (t, J=7, 3H, 6H), 1.18 (t, J=7, 8H), 1.25 (Br., s, 4H), 1.55 (p, J=7.3, 2H), 1.66 (Br., s, 1H), 2.02 (s, 3H), 2.06 (d, J=7, 2H), 2.11 (s, 2H), 2.19 (t, J=7.8, 2H), 3.21 (s, 9H), 3.4 (s, 12H), 3.53 (m, J=2,5, 2H), 3.65 (q, J=7.3, 1H), 4 (m, J=2,2.6, 2H), 5 (s, 2H) (Fig. 1C). Where J=spin-spin coupling, s= singlet, t= triplet, d= doublet, m= multiplet , q= quartet, p= panlet , and Br.= Broad. These findings demonstrate that COA shows chemical interactions with NAVI, resulting in a stable formulation of the NAVI+COA covalent bond system.

COA/NAVI displayed an average size of 213 nm, placing the formulation well within the size range expected to traverse through the subcutaneous layer to deliver NAVI to the deeper layers of the skin. The standard deviation remained within this range, indicating a consistent formulation that can provide a consistent dosage (Fig. 1D). Like the size evaluation, the measurement of the electrokinetic potential (zeta potential) showed excellent stability. The initial polydispersity index displayed a low amount of dispersion; however, after 10 h, the index rose sharply, as seen in Figure 1E. The varied, time-dependent polydispersity index indicates a requirement to shake well the suspension before use, as is true for most medicinal suspensions. However, mixing COA/NAVI involves sonication using a probe. Therefore, the formulation would have to be prepared or sonicated just before treatment to ensure a consistent and uniform dosage of NAVI at each application. This precipitation seems to be unique to COA compared with H_2O and may result from the electrophoretic relationship between NAVI and COA.

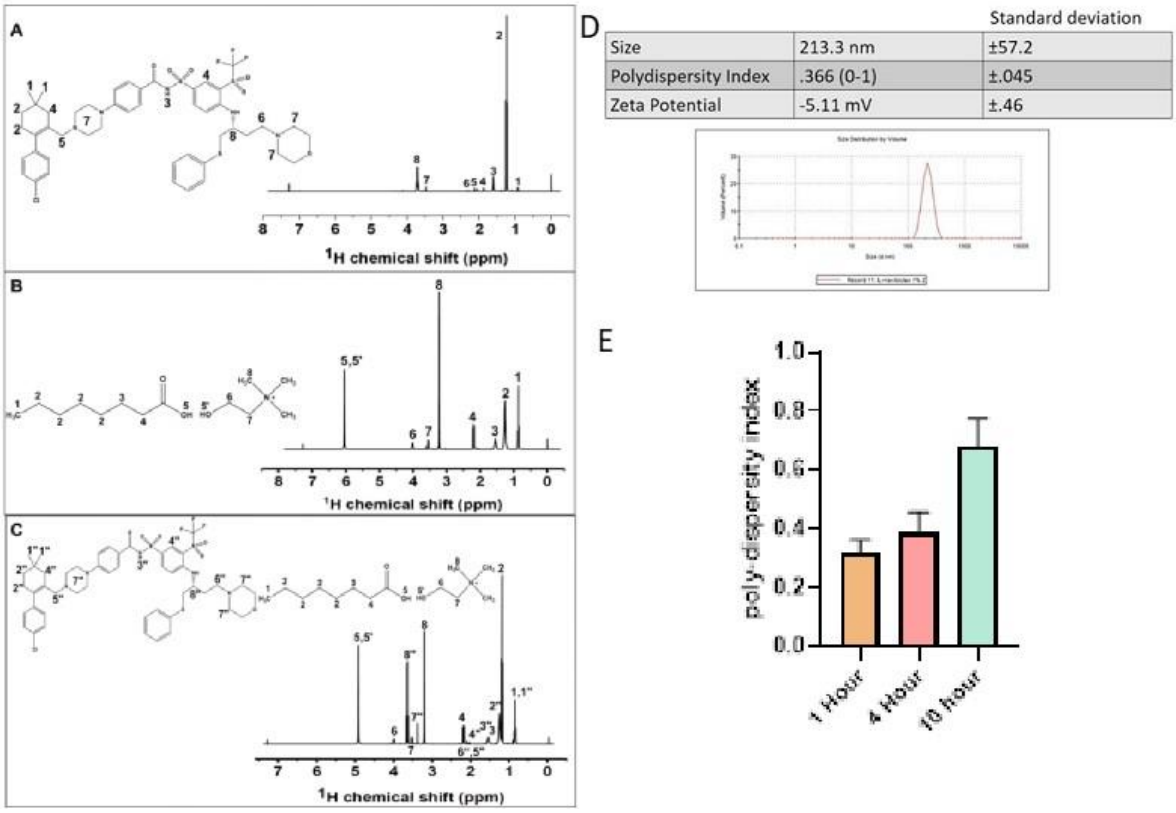

Figure 1: Physical and Chemical properties of COA and NAVI.

(a) Navitoclax 1H-NMR: Chemical shift δ (in CDCl3): δ 0.92 (d, J=6.6, 6H), 1.26 (t, J=7, 4H), 1.6 (Br, s, 1H), 2.06 (s, 2H), 2.14 (Br., s, 2H), 2.31 (d, J=7, 2H), 3.49 (Br., s, 12H), 3.73 (q, J=7.3, 1H). COA 1H-NMR: (b) Chemical shift δ (in CDCl3): δ 0.87 (t, J=6.8, 3H), 1.27 (Br., s, 8H), 1.55 (p, J=7.4, 2H), 2.21 (t, J=7.8, 2H), 3.23 (s, 9H), 3.55 (m, J=2,5, 2H), 4.02 (m, J=2,2.6, 2H), 6.06 (s, 2H). Navitoclax + COA 1H-NMR: (c) Chemical shift δ (in CDCl3): δ 0.85 (t, J=7, 3H, 6H), 1.18 (t, J=7, 8H), 1.25 (Br., s, 4H), 1.55 (p, J=7.3, 2H), 1.66 (Br., s, 1H), 2.02 (s, 3H), 2.06 (d, J=7, 2H), 2.11 (s, 2H), 2.19 (t, J=7.8, 2H), 3.21 (s, 9H), 3.4 (s, 12H), 3.53 (m, J=2,5, 2H), 3.65 (q, J=7.3, 1H), 4 (m, J=2,2.6, 2H), 5 (s, 2H) s= singlet, t= triplet, d= doublet, m= multiplet , q= quartet, p= panlet , Br.= Broad, (d) The COA/NAVI formulation was evaluated to determine size, polydispersity, zeta potential, and maximum load. (e) Polydispersity of NAVI loaded COA varies at different time points within a 10-hr span. Increased time displayed higher diversity as well, displaying instability in the suspension.

2.2.2. COA INCREASES NAVI SOLUBILITY AND TRANSPORTATION OF NAVI THROUGH THE SKIN:

The COA/NAVI formulation was prepared by simple mixing and sonicating. The solubility of NAVI in an aqueous solution is very poor, i.e. < 1 µg/mL in DI water [40–42]. However, COA

can solvate hydrophobic drugs, thus improving their solubility and bioavailability [43–45]. To check the solubility of NAVI in COA, we prepared a stock solution of 5 mg/mL NAVI, serially diluted the stock solution from 5 to 0.002441 mg/mL, and then measured the absorbance of 100 µL of each sample by using a UV plate reader at 345 nm. Transmittance was measured using the formula A =2-log (%T), converted to absorbance, and plotted. As shown in Figure 2A, the highest solubility was observed as 156 µg/ml. Thus, COA increases the solubility of NAVI by ~150 fold compared to DI water or Dulbecco's phosphate-buffered saline.

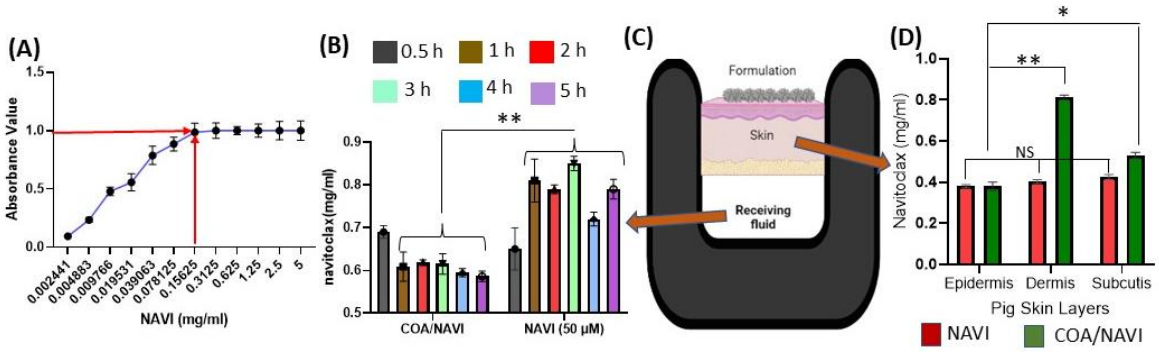

Figure 2: Solubility and ex-vivo skin transportation

(a) COA increases the solubilization of NAVI up to 156 µg in 1 mL, measured as an absorbance value of 0.9987. (b) The in vitro permeation test (IVPT) of NAVI on porcine skin shows that COA (100%)/NAVI (50 µM) provides superior NAVI transportation compared to NAVI treatment alone, at 1 and 3 h. The data validate that COA holds NAVI at the deep layer of porcine skin. (c) The schematic represents how the porcine skin was placed into the cells, and formulations were applied on top to analyze drug transportation via ex-vivo tissue. Figure b represents the navitoclax quantification collected as receiving fluid and represented by the arrow. And figure D represents the amount of navitoclax accumulated into the skin layers due to topical administration of formulations. (D) After applying the COA/NAVI formulation or NAVI, the porcine skin layers were separated to quantify accumulated NAVI in different layers of the skin. Both the dermis and subcutaneous layers of pig skin hold a higher amount of NAVI when delivered with COA than NAVI applied alone. The experiment was performed in triplicate. *Indicates statistical significance, with $p < 0.05$; *** indicates statistical significance, with $p < 0.001$.

The uppermost epidermis and stratum corneum (SC) of the skin constitute an effective barrier that prevents the absorption of a wide range of chemicals, including topical drugs. An ideal topical drug delivery formulation should have high potency to enhance skin permeation while minimizing

skin irritation. Here, we used a porcine skin model to test dermal penetration by two different formulations of COA/NAVI versus NAVI alone: COA (100%)/NAVI (50 µM), COA (50%)/NAVI (50 µM), and NAVI (50 µM). Each treatment was administered topically at 100 µl each. The findings confirm only NAVI topical administration has higher transportation of navitoclax at the percentage of 23.5%, 21%, 27.3%, and 25% at 2, 3, 4, and 5 h respectively through porcine skin compared to COA/NAVI topical administration (Fig. 2B). Due to continuous 1X PBS circulation, this observation enables the NAVI to transport via the skin; on the contrary, COA/NAVI could not penetrate the fat layer of the hypodermal layer. Therefore, we observe a higher accumulation of navitoclax in the deep skin layer in COA/NAVI topical delivery, which is a novel indication of this treatment. This experiment collected the transporting solution in an assigned container at different time points and further quantified navitoclax transportation. The concentration of navitoclax was measured using a standard curve constructed with UV absorbance values recorded at 345 nm. A higher accumulation of navitoclax was found at the dermis and subcutaneous layers at COA (100%)/NAVI (50 µM) topical administration compared to NAVI topical delivery (Fig. 2D). The results show that COA-mediated transportation of NAVI through the skin facilitates the drug's penetration into the dermal and subcutaneous layers. Ionic liquid increases the solubility of NAVI by150-fold due to its chemical properties. This *ex-vivo* analysis also confirmed the tendency of COA to hold the drug deep within the skin layers.

2.2.3. BCL-2 INHIBITION IN MOUSE CANCER MELANOMA CELLS:

To assess the ability of COA to mediate cellular uptake of a hydrophobic "payload", we mixed COA with the hydrophobic fluorescent dye Coumarin 6 (as a substitute for NAVI) and then added the mixture to cultures of B16 F10 mouse melanoma cells. After 6 h, we washed and then visualized the cells using confocal microscopy. Accumulation of Coumarin 6 in B16 F10 cells was

significantly higher when it was mixed with COA, compared to free Coumarin 6 (control), as shown in Figure 3A. Cells treated with standalone Coumarin 6 showed some residual fluorescent flakes post-washing, due to extracellular fluids holding Coumarin 6, or adherence on the plate itself. However, none of these signals overlap the nucleus, labeled with blue dye (Hoechst), indicating they are probably non-specific binding. In contrast, the cells co-incubated with COA/Coumarin 6 display a uniform teal color, a mixture of blue and green, which indicates Coumarin 6 entered almost the entirety of all the cells and reached the nucleus as well. This finding demonstrates that COA acts as a cell membrane penetration enhancer, allowing more potential drug penetration at the cellular and subcellular levels.

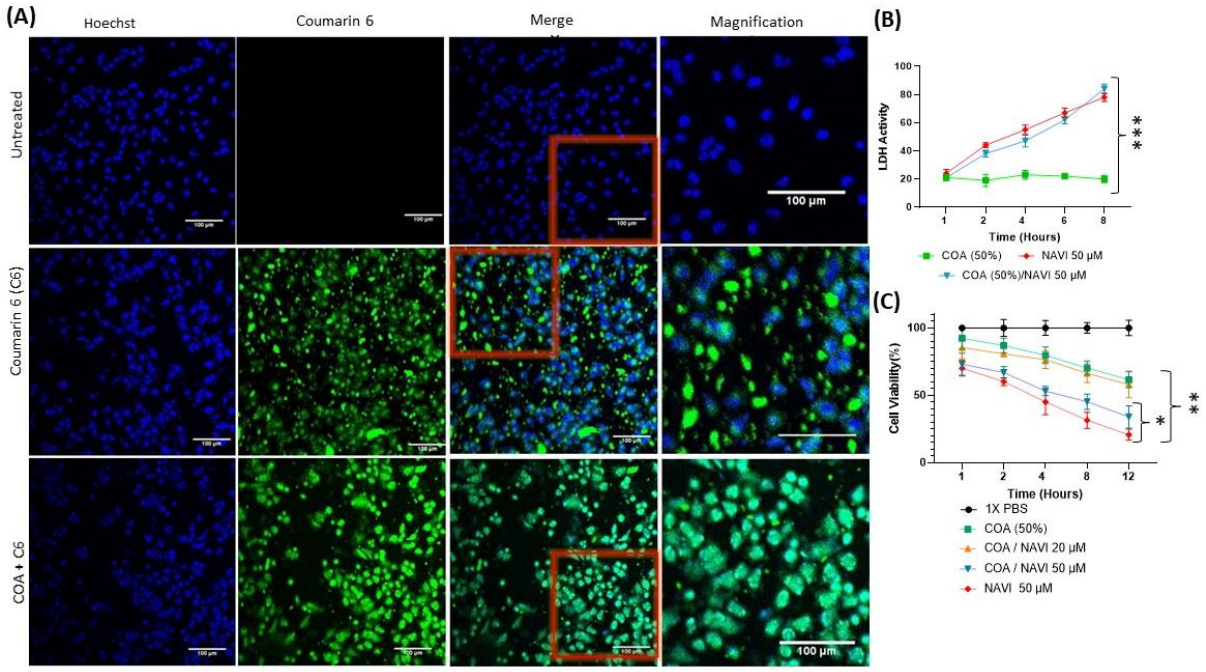

Figure 3: In vitro toxicity and internalization.

(a) Potential of COA to enhance cellular uptake of a payload. The cell internalization study was conducted with Coumarin 6, a small hydrophobic molecule with fluorescence properties. The images show enhanced uptake of Coumarin 6 by B16 F10 mouse melanoma cells when co-incubated with COA compared to free Coumarin 6 after 6 h of incubation. (b) Cytotoxicity of COA, NAVI, and COA/NAVI was investigated by incubating the compounds with B16 F10 cells at various times (1, 2, 4, 6, 8 h). COA alone showed little toxicity, whereas free NAVI and COA/NAVI, NAVI induced 81% LDH activity at 8 h of incubation. (c) The cytotoxicity of COA,

NAVI, and COA/NAVI was investigated by incubating the compounds with B16-F10 cells at various times (1, 2, 4, 8, 12 h) and then measuring cell viability using an MTT assay. Cells treated with COA/NAVI showed 60% and 45% cell viability at 20 µM and 50 µM NAVI, respectively, at 12 h of incubation. Each data point represents the mean ± SD, where n=6. *Indicates statistical significance with $p < 0.05$; *** indicates statistical significance with $p < 0.001$.

The lactate dehydrogenase (LDH) assay detects and quantifies the amount of LDH released from a cell and is a standard indicator of cell death or membrane damage [46]. One concern with enhanced cell penetration is the possibility that apoptosis could also increase due to potential cellular membrane damage involving the utilization of COA. Figure 3B shows the LDH activity released by cells treated with free COA, NAVI, and COA/NAVI. The results indicate that COA is minimally toxic to cells in this assay, as the LDH activity it elicited was constant over 8 h of observation. In contrast, standalone NAVI, and COA/NAVI induced LDH activity directly proportioned to the incubation time, thus demonstrating the cytotoxic effects of NAVI. COA carries cationic and anionic groups that can be toxic to cells at higher concentrations in culture but not in animal studies [21]. This data also confirms that COA does not interfere with the biological activity of navitoclax and acts as a drug carrier to facilitate transportation through the cell membrane. Therefore, we may reduce navitoclax-reported dosing previously and overcome clinically reported thrombocytopenia by the local administration.

To further evaluate the anti-cancer cytotoxicity of COA, COA/NAVI (20 µM and 50 µM), and NAVI (50 µM), we conducted an MTT colorimetric assay, again using the B16 F10 mouse melanoma cell line. Cells treated with saline have been used as a control. We observed that the viability of cells treated with COA/NAVI and NAVI decreased with time. We confirmed that COA (50%) shows some toxicity to cancer cells, as cell viability dropped to around 60% at 12 h of treatment (Fig. 3C). Cells treated with COA/NAVI and NAVI displayed cell viabilities of 40%

and 30%, respectively, at 12 h. Therefore, we can conclude that the COA/NAVI formulation is cytotoxic to B16 F10 melanoma cells *in vitro*. These data reveal that treatment with COA/NAVI has an anti-cancer activity similar to that of NAVI alone.

2.2.4. COA/NAVI CAN INDUCE APOPTOSIS AND DOWNREGULATE BCL-2 PROTEIN EXPRESSION IN VITRO:

Apoptosis is a form of programmed cell death [47]. This programmed cell death plays a critical role in various physiological mechanisms in adult tissue and fetal development. Failure to induce apoptosis can contribute to many diseases, including cancer. A family of proteases known as caspases is responsible for the biochemical and morphological changes during apoptosis [47,48]. In apoptosis, mitochondrial outer membrane permeabilization (MOMP) leads to the release of apoptogenic proteins like cytochrome c, Smac/DIABLO, DDP/TIMM8a, and EndoG. However, MOMP activation, and thus whether a cell initiates apoptosis or not, depends on a dynamic balance between anti-apoptotic and pro-apoptotic proteins such as BCL-2 and BAX, respectively [40,49]. As we noted above, NAVI is a BCL-2 inhibitor, and thus using NAVI to target BCL-2 should induce apoptosis in cancer cells [42]. For instance, genetic knockdown of BCL-2 promoted BIM-dependent apoptosis of melanoma cells (BIM is a pro-apoptotic activator protein). We measured the degree of apoptosis and necrosis introduced by COA/NAVI and compared it with the effects of NAVI alone and controls, as shown in Figure 4A. The following formulations were used as treatments, NAVI (20 μM), NAVI (50 μM), COA/NAVI (20 μM), COA/NAVI (50 μM), COA (50%), and the levels of apoptosis and necrosis were compared to those induced by H_2O_2 (30 μM), DMSO (1%), and saline. annexin V-FITC and PI were used for apoptosis and necrosis detection (Fig. 4A). The samples were processed by using a GALLIOS flow cytometer (Beckman Coulter)

and the data were analyzed with Kaluza analysis software (Beckman Coulter) and graphed (GraphPad Prism). Both doses of COA/NAVI (20 and 50 µM) induced ~70 and 75% apoptosis,

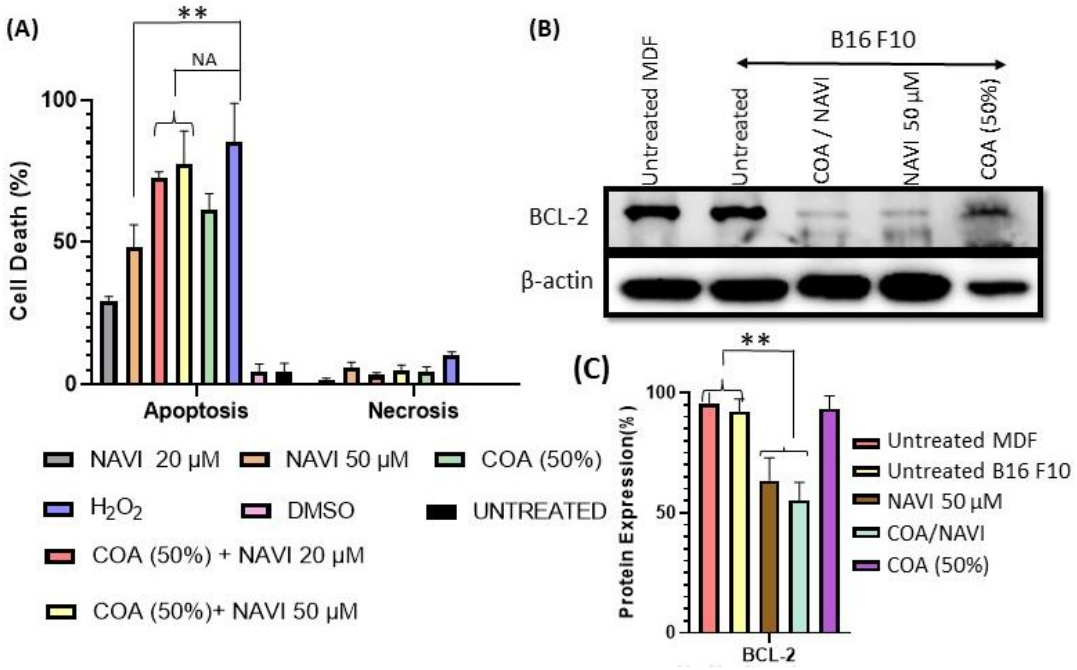

Figure 4: In Vitro apoptosis-necrosis & western blotting.

(a) In the apoptosis-necrosis assay, the formulations COA/NAVI (20 µM) and COA/NAVI (50 µM) showed around 75% and 70% apoptosis, respectively, tested in A375 cells after 24 h of treatment compared to H2O2, as a positive control. However, both treatments showed around 5% necrosis. (b) Western blot analysis was done from Hs27 healthy skin fibroblast and A375 human melanoma cell lysate after treatment with the formulations for 6 h. The experiment shows more inhibition of BCL-2 expression in COA/NAVI and NAVI compared to COA or untreated melanoma and healthy cell. (c) The BCL-2 expression was quantified and represented compared to the housekeeping gene β-actin. Data represent the mean ± SD, where n=6. * Indicates statistical significance with $p < 0.05$; *** indicates statistical significance with $p < 0.001$.

respectively, and COA itself induced 50% apoptosis. Moreover, these treatments induced only 2-10% necrosis (Fig. 4A). These results confirm that the COA/NAVI induces apoptosis of B16 F10 melanoma cells, which validates the NAVI's cytotoxic mechanism hypothesis. Next, we used

western blotting to quantify BCL-2 protein expression in both treated and untreated cells. The housekeeping protein β-Actin was also quantified as a standard. Protein from B16 F10 mouse cells was collected after 6 h of treatment; mouse dermal fibroblast MDF cells were used as healthy control. The experimental groups were untreated MDF cells, untreated B16 F10 cells, and B16 F10 cells treated with COA/NAVI (50 µM), NAVI (50 µM), and COA. We observed significantly reduced expression of BCL-2 in the COA/NAVI and NAVI groups (Fig. 4B). Band quantification confirmed the level of BCL-2 inhibition in the NAVI and COA/NAVI treatment groups to be 52% and 40%, respectively (Fig. 4C). Figures 4B and 4C also support the findings presented in Figure 4A. Taken together, these results (in figure 4) demonstrate the superior ability and potential of COA/NAVI over free NAVI to induce apoptosis in a melanoma cell model and that apoptosis was activated *via* inhibition of anti-apoptotic BCL-2 protein.

2.2.5. *IN VIVO* TREATMENT EFFICACY IN MICE TUMOR MODEL:

The therapeutic efficacy of COA/NAVI was evaluated using the C57BL/6 mouse tumor xenograft model. Twenty tumor-bearing mice were divided into four groups: untreated, COA, NAVI (PO), and COA/NAVI. B16 F10 mouse melanoma cells ($0.1X10^6$ per animal) were injected into the back's subcutaneous layer (SC) to create the melanoma model. Visible tumors were evident in the model by 2 weeks after cell injection. Hair around and on top of the tumor region was trimmed before the treatment to visualize the tumor and better topical administration. COA and COA/NAVI were applied topically, and NAVI alone was administered orally (PO) [50]. We did not administer NAVI (by itself) topically because it is a hydrophobic drug [51]; therefore, orally delivered NAVI is considered a positive control for this study and also prescribed by FDA in the clinical trial. NAVI was dispersed in PBS and administered *via* oral gavage to avoid toxicities associated with organic solvent and thrombocytopenia. The animal's treatment was given thrice a week (T.I.W)

for 3 weeks, and slide calipers were used to measure tumor volume (Fig. 5A) [52]. Mice treated with COA/NAVI showed inhibition of tumor volume by 65% and 55% compared to untreated and NAVI (PO)-treated mice, respectively. Topical application of COA did not produce any sign of tumor volume reduction; however, we observed signs of inflammation, resulting in damage within the superficial cells adjacent to the skin, the inflammation was reversible, and the skin returned to a normal condition once the application of COA was terminated. Oral NAVI showed antitumor effects but was not as effective as the same dose of topically administered NAVI. Body weight was recorded every other day, and the mice in all treatment groups showed continuous increases in body weight, indicating that severe toxicity was not induced by any of the treatments (Fig. 5B). Images of melanoma lesions were recorded in each of the groups and compared to visualize treatment toxicity. Figure 5 confirms that COA induced both skin irritation and lesions, compared to the untreated group. The skin irritation was overcome by diluting COA to 50% of its original concentration, which retained COA's intrinsic topical delivery properties. Surprisingly, we noticed the rapid growth of hair and skin-softening in COA-treated mice. One possible reason could be that COA increases the skin pore diameter and potentially makes the skin structure leaky, resulting in the rapid growth of hair. No deaths occurred during the experiment. The clinical end-point for the animal work was if the tumor volume was> 1000 mm^3 and no animal reached to that point during the experiment.

2.2.6: HISTOLOGY, SERUM BIOCHEMISTRY, AND BLOOD CELL ANALYSES:

Microscopic analysis of hematoxylin and eosin (H&E)-stained sections of xenograft tissue revealed no sign of severe toxicity in any of the treatment groups (Fig. 6A). Compared to healthy mouse skin, we observe higher melanin and iron expression indicated by deformed skin structure and higher purple pigments [53]. Also, we observed nuclear shrinkage and morphological change

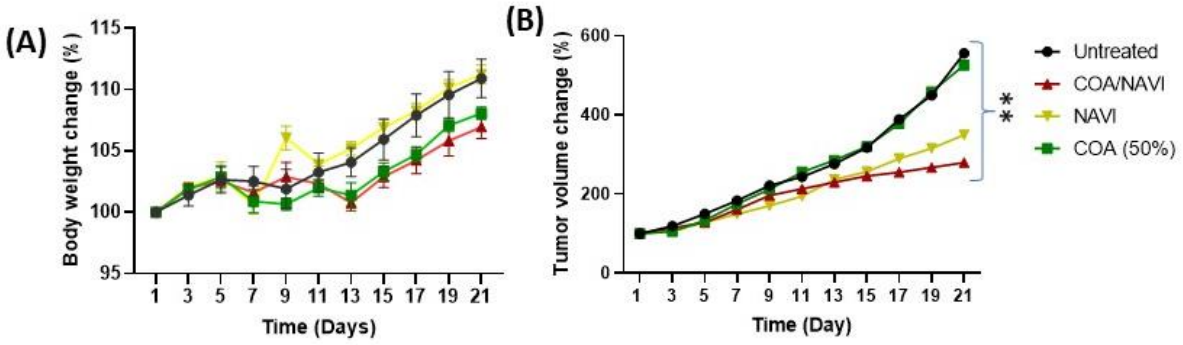

Figure 5: (a,b) Tumor volume and body weight were measured during the treatment.

There was no significant change in body weight among the mouse groups, indicating that COA/NAVI is not systemically toxic to mice. The COA/NAVI formulation could inhibit further tumor growth in the melanoma site. Data represent the mean ± SD, where n=6. *Indicates statistical significance with $p<0.05$.

in melanoma mouse skin. In the COA/NAVI treatment group, we monitor lower melanin and iron levels similar to healthy control compared to the NAVI treatment group. Therefore, we observed higher tumor reduction in the COA/NAVI treatment group than in the NAVI (PO) administration. Serum biochemistry studies were conducted using blood serum collected at the end of the study. Both liver and kidney metabolic markers were analyzed to test for COA/NAVI and NAVI toxicity in mice after 21 days of treatment (figure 6B). In untreated xenografted mice, creatinine, blood urea nitrogen, alanine aminotransferase (ALT), and alkaline phosphatase were much higher than in the control and treatment groups, which indicates that unconstrained tumor development was associated with the upregulation of these biomarkers. Notably, treatment with NAVI or COA/NAVI reduced the biomarker levels to the normal range. Elevated ALT levels in COA-treated mice indicate liver toxicity, resulting from systemic absorption of free COA. In contrast, no liver toxicity was observed in the COA/NAVI-treated group. Moreover, liver and kidney function markers were within the normal range in COA/NAVI-treated mice. The serum biochemistry analysis indicates that COA/NAVI formulations are potentially safer to use and

therefore promising for clinical translation upon further evaluation. In the total blood count analysis, we observed that the platelet (PLT), red blood cell (RBC), white blood cell (WBC), and hemoglobin (Hb) counts were all within the normal ranges across all treatment groups (Fig. 6C).

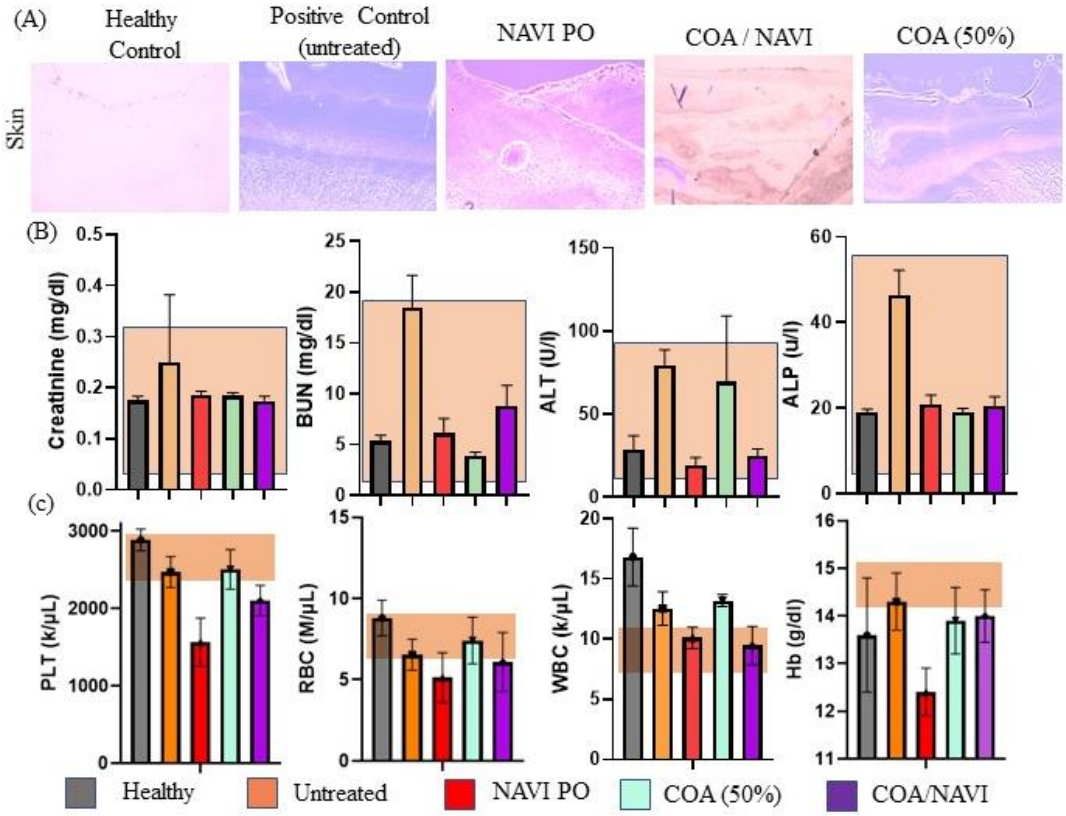

Figure 6: Hematoxylin and eosin staining, serum biochemistry, and total blood count analysis.

(a) The safety of treatments was evaluated by hematoxylin and eosin (H&E) staining and serum analysis. Skin tissue was embedded in OCT and sectioned using a cryotome at 15 µm thickness. The tissue was then stained with H&E and imaged with a microscope. The images were taken at 10× magnification with similar gain and exposure settings. (b) We observed no liver or kidney toxicity based on serum analysis across all treatment groups. The alanine aminotransferase (ALT) value was elevated in the COA treatment group, unlike in the untreated group. Nonetheless, all serum biochemistry values are within the normal range, represented by the light brown rectangle in each graph. Serum analysis and H&E staining data also validate that NAVI PO administration reduces the cytotoxicity caused by IV administration of navitoclax reported in multiple studies [53,54]. (c) A Hemavet 1700 (Drew Scientific) was used to determine blood cell count. The data also confirm the reduction of thrombocytopenia by PO administration compared to intravenous injection of NAVI in other studies [55,56]. Both platelet (PLT) and hemoglobin (Hb) levels were within normal ranges for healthy mice. Data represent the mean ± SD, where n=6.

However, PLT, Hb, and RBC were reduced for the oral NAVI group. Previously, in multiple studies, NAVI was shown to induce platelet apoptosis, resulting in severe thrombocytopenia [56–58]. Platelet production and survival depend on Bcl-xL protein, a BCL-2 family member [59]. Notably, our data in Figure 6C do not show any sign of COA/NAVI-mediated thrombocytopenia. One possible explanation for this apparent protective effect is that COA may hold the drug in the dermis layer for longer, and only smaller amounts reach the circulation. If so, then COA provides a better vehicle for NAVI to reach the melanoma site. Thus, COA/NAVI is a safer platform for skin melanoma treatment.

2.2.6. INHIBITION OF ANTI-APOPTOTIC PROTEIN BCL-2 IN VIVO:

NAVI inhibits BCL-2, leading to depolarization of the mitochondrial membrane and mitochondrial outer membrane permeabilization (MOMP), which results in the release of apoptogenic proteins like cytochrome c, Smac/DIABLO, DDP/TIMM8a, and EndoG [42]. As a result of this inhibition, we showed that NAVI induces apoptosis in the melanoma disease model. Here, we examined the molecular mechanism of the anti-cancer efficacy of COA/NAVI by western blotting, immunohistochemistry, and TUNEL apoptosis analysis. Figure 6A shows a western blot of BCL-2 protein in the different treatment groups compared with untreated healthy skin and untreated melanoma. Compared to the untreated and healthy skin groups, we observed reduced BCL-2 expression in the COA/NAVI and NAVI (PO) treatment groups. These data support our hypothesis that BCL-2 inhibition by NAVI results in increased apoptosis in melanoma tissue and aligns with our *in vitro* findings. We observed 52% and 44% Bcl-2 protein expression inhibition compared to the untreated mouse group for NAVI and COA/NAVI respectively. This finding confirms that NAVI can inhibit anti-apoptotic BCL-2 protein and activate intrinsic apoptotic pathways in

melanoma tissue. In Figure 7B, we quantified the protein bands using ImageJ software. We observed more significant inhibition of BCL-2 protein expression by COA/NAVI or topical NAVI when compared to the untreated and healthy groups. Figure 7C shows the immunostaining of

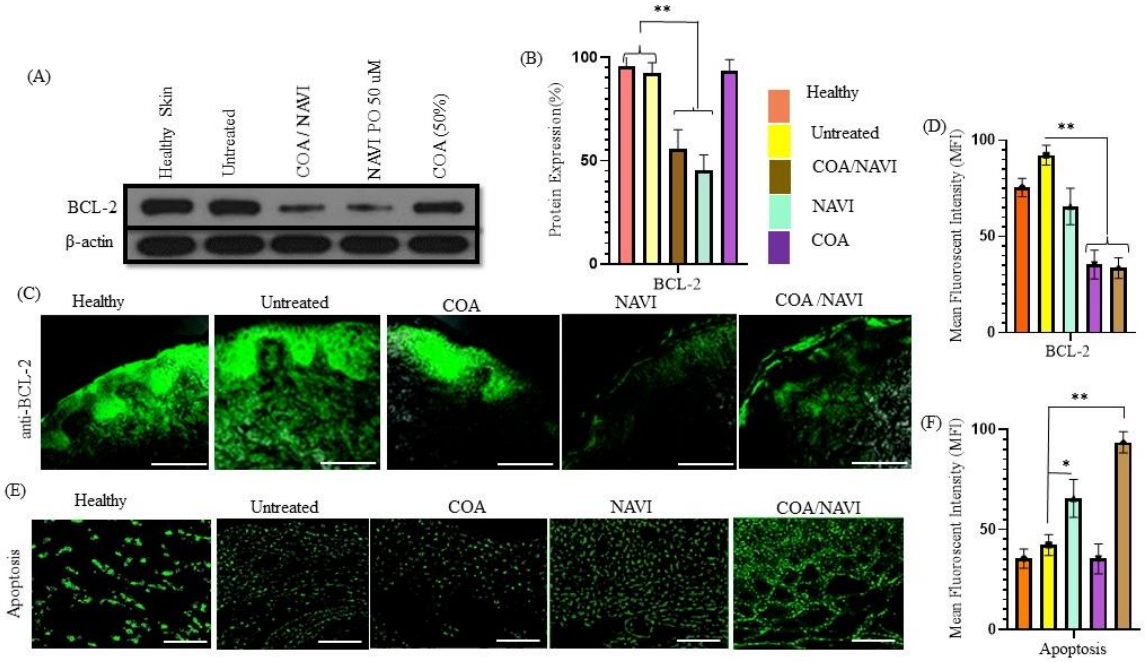

Figure 7: Ex-vivo tissue analysis.

Western blot of skin melanoma tissue shows that BCL-2 expression was inhibited significantly in COA/NAVI- and NAVI (PO)-treated animals compared to healthy skin and untreated melanoma. (b) BCL-2 protein levels on the western blot were quantified using ImageJ software and compared to the control protein β-actin. (c) Immunostaining melanoma and healthy skin with anti-BCL-2 primary antibody (1:100) and Alexa 488 goat anti-rabbit secondary antibody (1:200) was used to visualize BCL-2 expression. The images were recorded using an LSM700 confocal microscope and 20× magnification. COA/NAVI and NAVI treatment inhibited the expression of BCL-2 in tissue. (d) BCL-2 expression in panel C was qualified using ImageJ software. We observed significantly lower expression (mean fluorescence intensity, MFI) in the NAVI and COA/NAVI groups compared to the untreated and healthy control groups. (e) *In situ* TUNEL assay was used to quantify apoptosis in melanoma in mouse skin. The images were captured with an LSM 700 confocal microscope. (f) The fluorescence in panel E was quantified by using ImageJ software. The TUNEL assay findings correlate with our previous *in vitro* finding of increased apoptosis due to COA/NAVI treatment. Data represent the mean±SD, where n=6. *Indicates statistical significance with $p<0.05$; ***indicates statistical significance with $p< 0.001$. Scale bar = 200 µm

BCL-2 in sectioned skin tissue and confirms the treatment efficacy. We observed lower expression in the NAVI and COA/NAVI treatment groups compared with the other groups, COA only,

untreated, and healthy skin. The fluorescent expression of Figure 7C was quantified using ImageJ software measuring mean fluorescent intensity and graphed as figure 7D. We observed lower BCL-2 protein signal in CAO/NAVI and NAVI treatment groups, which correlate with our western blot and *in vitro* assays. Finally, we conducted an *in situ* apoptosis assay using TUNEL to quantify the apoptosis activity in those tissues. In figure 7E, the apoptosis signal indicates DNA breakdown in the nucleus of that tissue, and the higher the fluorescent signal (green), the higher the apoptotic activity. We also measured the MFI of TUNEL assays (Figure 7F). Figure 6F indicates 45% and 20% higher apoptosis in COA/NAVI and NAVI treatment represented by MFI of green fluorescent signal, respectively, compared to the untreated melanoma group. This confirms our previous finding that NAVI inhibits BCL-2, leading to activating an intrinsic apoptosis pathway and inducing apoptosis in melanoma tissue. Analysis by two-way ANOVA confirms statistically significant differences in BCL-2 expression between COA/NAVI and NAVI PO treatment. These findings demonstrate the anti-cancer activity of topical COA/NAVI to melanoma, thus opening a new avenue to investigate topical delivery of NAVI and other chemotherapeutics using COA.

2.3. CONCLUSIONS

Our findings from this study support using an ionic liquid, choline octanoate 1:2, as a platform for topical delivery of a BCL-2 inhibitor for treating early-stage skin melanoma. COA is an excellent vehicle for topical delivery of small hydrophobic molecules because it enhances drug solubility and permeability through the skin non-invasively. NAVI seems to be a very potent anti-cancer drug, but it is highly hydrophobic and has severe adverse effects related to thrombocytopenia. Our *in vitro* experiments confirm that the COA/NAVI formulation is biologically active and possesses anti-cancer activity. Both *in vitro* and *in vivo* studies demonstrate that NAVI induces apoptosis in B16 F10 mouse melanoma cells and tumors and activates the intrinsic apoptosis pathway by

inhibiting BCL-2 anti-apoptotic protein. The feasibility study in the *in vivo* mouse xenograft model evaluated both the safety and efficacy profiles of topically administered COA/NAVI compared with orally administered NAVI. Molecular biology and immunohistochemistry studies prove that COA-assisted topical NAVI kills melanoma cells without killing platelets effectively. The western blotting and immunostaining of tissue collected from treatment and non-treatment groups identified underlying molecules responsible for apoptosis in melanoma tissue. We observed by western blot analysis that BCL-2 expression was lower or inhibited in the NAVI and COA/NAVI treatment groups compared to untreated and healthy skin tissue. The immunostaining findings also support the inhibition of BCL-2 expression in the NAVI and COA/NAVI treatment groups. This discovery may improve skin melanoma treatment with advanced topically administrable formulations such as COA. We aim to continue this work to investigate other BCL-2 inhibitors by utilizing the BCL-2 knock-in animal model. This topical formulation has promising potential in developing more effective therapeutic modalities for the noninvasive treatment of skin diseases such as nonmetastatic melanoma.

2.4. MATERIALS AND METHODS:

2.4.1. MATERIALS:

Pigskin was purchased from a local butcher store in El Paso, TX, USA. Deionized water (resistivity of 18.2 MΩ) used for all experiments was obtained from an in-lab Milli-Q® IQ 7000 Ultrapure Water System (EMD Millipore, Bedford, MA, USA). Phosphate-buffered saline (PBS) (pH 7.4) was procured from Fisher Chemicals (Fair Lawn, NJ, USA). COA was synthesized according to the method reported earlier [45] and described briefly in the synthesis methodology below. Cell culture reagents, including Dulbecco's Modified Eagle Medium (DMEM), fetal bovine serum (FBS), Dulbecco's PBS, penicillin/streptomycin, and trypsin/ EDTA, were purchased from Gibco

BRL (Carlsbad, CA, USA) CyQUANT MTT Cell Proliferation Assay Kit (V13154), CyQUANT™ LDH Cytotoxicity Assay Kit (C20301), Invitrogen™ eBioscience™ Annexin V-FITC Apoptosis Detection Kit (15581947) and Click-iT™ TUNEL Alexa Fluor™ 488 Imaging Assay, for microscopy & HCS (C10245) were from Thermo Fisher. Anti-BCL-2 and anti-β-actin antibodies were purchased from Abclonal.

2.4.2. CELL CULTURE:

The B16-F10 mouse melanoma and Hs27 cell lines were purchased from ATCC and were cultured according to the supplier's instructions. Both cell lines were cultured in DMEM with 10% FBS and 1% penicillin-streptomycin (PS). We used passage numbers 6-8 of Hs27 cells.

2.4.3. SYNTHESIS OF COA:

The ionic liquid is based on octanoic acid and choline bicarbonate. Octanoic acid and choline bicarbonate were combined slowly in a 1:2 molar ratio, stirring at 37°C overnight. CO_2 and water byproducts were removed by rotary evaporation at 30 mbar, 60 ^{o} C for 2 h. The ionic liquid was then dried in a vacuum over (-100 kPa) for 48 h. The final product is a clear, viscous fluid. Successful synthesis is confirmed with proton NMR spectroscopy.

2.4.4. PHYSICAL CHARACTERIZATION OF COA:

Dynamic light scattering (DLS) was used to determine the size and poly-disparity index, and zeta potential. 100 µL of COA/NAVI were diluted in 10 mL of deionized water. This formulation was sonicated for 5 min to ensure consistent dispersion, and measurements were taken using a Malvern Zetasizer (Nano series ZS90, Malvern, Worcestershire, UK) at 25°C.

2.4.5: SKIN PERMEATION:

Skin penetration studies were performed using skin from locally harvested porcine sources originating on the animal's belly. Skin samples were stored at -20°C until needed. For the

experiment, the samples were thawed for 24 h at 4°C and then left to equilibrate at 24 °C for 20 min, and then lightly shaved to remove any hair. Several layers of muscle and fat tissues were attached to the skin. These were carefully removed using a scalpel, not disturbing or piercing the skin. Special consideration was given to ensure that a minimum amount of scar tissue was present on these samples to ensure a consistent flow among the various samples and improve the permeation results. The skin was then soaked in 150 mL of PBS (pH 7.4) for 20 min for rehydration. The skin was then cut into squares of approximately 1.8 cm × 1.8 cm to fit into the ILC07 automated flow-through system (Permegear Inc. Hellertown, PA, USA). The skin was then placed individually in one of the seven donor/receptor compartments. These receptor compartments were locked in place, with a small lower chamber that pumped PBS (pH 7.4) directly underneath the skin at a flow rate of 4 mL/h at 37 °C to simulate typical flow conditions of the human body. The pump used was a multi-channel peristaltic pump IPC (Ismatec, Zurich, Switzerland), and the heating source was a Julabo BC4 circulating water bath (Julabo Pumps, Seelbach, Germany). The liquid that flowed through the chambers was collected in 20-mL scintillation vials and changed at various time points (0.5, 1, 2, 3, 4, 5, 6, 7, and 8 h) to determine how much drug had penetrated the final skin layer and could potentially enter the bloodstream. The stratum corneum (SC) epidermis, dermis, and hypodermis layers were removed using a tape strip and scrape method to quantify the amount of drug left in the skin. The skin was carefully detached from the holding frame and placed on a flat metal surface. The skin was gently dabbed to remove excess formulation, and a piece of Scotch tape was pressed on the skin to ensure maximum adherence. This strip was removed with a light pulling force and discarded. An additional tape was placed on the skin, and the SC was then forcefully ripped from the other layers quickly in a single pull. This process was repeated ten times.

Additionally, a surgical scalpel was used to carefully scrape away and collect any SC left after the tape stripping. The tape strips and the SC were collected in conical tubes and dissolved in 10 mL of ethanol. The remaining dermal layers were cut with surgical scissors into the smallest pieces mechanically possible and placed into their respective conical tubes. Each tube was then filled with 10 mL of ethanol and sonicated for 30 min. The tubes were left overnight to soak at 4 °C. Finally, the solution was centrifuged at 15,000 rpm for 30 min at 4 °C, and the supernatant was collected for drug quantification by a UV spectrophotometer.

2.4.6. DRUG SOLUBILITY*:*

NAVI was dissolved in COA at a concentration of 5 mg/mL and this stock solution was serially diluted to 2.5 mg/mL, 1.25 mg/mL, 0.625 mg/mL, 0.3125 mg/mL, 0.15625 mg/mL, 0.078125 mg/mL, 0.0390625 mg/mL, 0.019531 mg/mL, 0.009765 mg/mL, 0.004882 mg/ml, and 0.002441 mg/mL in DI water. Absorbance was read at 345 nm using a SYNERGY H1 96 plate reader. The amount of drug accumulated in each layer of porcine skin was then quantified using the same method. Briefly, the epidermis, dermis, and subcutaneous layers of porcine skin were separated and ground into a liquid homogenate in 2 mL of 1X PBS. After centrifugation of the homogenized tissue, the supernatant was collected and measured by UV spectroscopy to determine the concentration of NAVI. Absorbance vs. concentration was plotted with GraphPad Prism software.

2.4.7. *IN VITRO* CYTOTOXICITY EVALUATION AND CELL IMAGING:

In vitro cytotoxicity studies of the COA/ NAVI were carried out using B16-F10 mouse melanoma cells (ATCC catalog CRL-6475). Cells were grown in DMEM supplemented with 10% fetal bovine serum and 0.5% Penicillin-Streptomycin (PS) at 37°C and 5% CO_2 in a humidified atmosphere. The cells (5×10^4 cells/mL) were grown in a cell culture flask and harvested with 0.25% trypsin-0.03% EDTA solution. A sample of 200 μL of cells was plated in 96-well plates

and incubated for 24-36 h. The complete medium was then suctioned. COA, COA/NAVI (20 µM and 50 µM), NAVI, and 1X PBS in a complete medium were added to the wells, and the plates were incubated for a time duration (1, 2, 4, and 8 h). For this experiment, 1X PBS was used as a positive control, and blank wells were used as a negative control. According to the manufacturer's instructions, a Cyquant MTT cell proliferation assay kit was used to measure cell viability [60]. In brief, a 12 mM MTT stock solution was prepared by adding 1 mL of sterile PBS to one 5-mg vial of MTT (Component A). The solution was vortexed or sonicated to mix the solution until the MTT was dissolved. During the experiment, 10 µL of the 12 mM MTT stock solution was added to each well containing 100 µL of the medium. Next, the cells were incubated for 2 h, as the cell density per well was > 100,000 cells. After incubation, all but 25 µL of the medium was removed from the wells, and 50 µL of DMSO was added to each well, then pipetted up and down thoroughly to mix. The plate was then incubated at 37˚C for 10 min. The absorbance of MTT was measured by using a SYNERGY H1 microplate reader (BioTek) at a wavelength of 540 nm after the solution was pipetted up and down to remix each sample. The cell viability was calculated using the following equation:

$$Cell\ Viability\ (\%) = \frac{Absorbance\ of\ sample\ cells - Absorbance\ of\ th\ blank\ well}{\text{Absorbance of control cells} - \text{Absorbance of blank well}}$$

To observe the cellular uptake of COA, B16-F10 mouse melanoma cells were cultured in DMEM with 10% FBS and 0.5% PS. When the cells reached 70-80% confluence, they were split and seeded in 96-well plates with approximately 1000 cells per well. Fifteen wells were prepared for the three treatment groups (5 wells each). After 48 h of seeding, the treatment was added to the corresponding well. Coumarin 6, a fluorescent agent, was used to substitute for the drug to offer a visual representation for imaging purposes. The bright glow provides insight into COA's behavior

and penetrative capabilities and clearly shows if COA acts as a penetration enhancer at the cellular level. Three different treatment groups were utilized: a control group with medium only, Coumarin 6 treatment group, and COA with Coumarin 6 treatment group. Coumarin 6 was diluted to 1 mg/mL in DI H_2O. COA and Coumarin 6 treatments were prepared at a 1:1 ratio. After 6 h of treatment, the cells were washed three times with 1X PBS and replaced with 190 mL of fresh media in each well. Then, 10 µL of Hoechst 33342 dye was added to stain the live-cell nucleus. After 20 min of incubation, the cells were washed three times with 1X PBS and replaced with 200 µL of fresh medium in each well. An LSM 300 confocal microscope was used to capture fluorescent images. The images were taken at 20× magnification at both green (488 nm for Coumarin) and violet (410 nm for Hoechst) wavelengths.

2.4.8. LACTATE DEHYDROGENASE (LDH) RELEASE ASSAY:

B16-F10 mouse melanoma cells were cultured in DMEM, 10% FBS, and 0.5% PS. When the cells reached 70-80% confluence, they were split and seeded in 96-well plates at around 3000 cells per well. After 48 h of seeding, the cell treatment was initiated. Four different treatments were used: a control group with medium only, NAVI, COA, and COA + NAVI. A Cyquant LDH cytotoxicity assay kit was used per the manufacturer's instructions [61]. 3000 cells per well were plated in 100 µL of the medium in triplicate wells in a 96-well tissue culture plate. The LDH activity of B16 F10 mouse melanoma cells was measured in all four different treatments at 1, 2, 4, and 6 h time points. The set of triplicate wells served to quantify the maximum, spontaneous, and chemical-associated LDH activity for all treatments. For the maximum, we added 10 µL of 10X lysis buffer; for spontaneous we added 10 µL of sterile ultrapure water; and chemical-associated, 10 µL of the vehicle containing the chemical compound. The samples were mixed by gently tapping the plate. 50 µL of each sample medium were transferred to a 96-well flat-bottom plate in triplicate wells.

50 µL of Reaction Mixture was added to each sample well, then mixed thoroughly. The plate was then incubated at room temperature for 30 min while protected from light, after which 50 µL of stop solution was added to each well. Finally, absorbance was measured at both 490 and 680 nm. To determine LDH activity, the 680 nm absorbance value (background) was subtracted from the 490 nm absorbance before calculating the percent cytotoxicity, as follows:

$$\text{LDH Cytotoxicity (\%)} = \frac{\text{[LDH] compound activity} - \text{[LDH] spontaneous activity}}{\text{[LDH] maximum} - \text{[LDH] spontaneous activity}}$$

2.4.9. *IN VITRO* APOPTOSIS-NECROSIS STUDY:

Apoptosis was measured using the Annexin V-FITC kit (Beckman Coulter, Miami, FL, USA), which measures the externalization of phosphatidylserine [62]. B16F10 cells were seeded at a density of 1×10^5 cells per 1 mL of medium in a 24-well plate and were left overnight under cell culture conditions. The next day, cells were treated with NAVI dissolved in DMSO, COA/NAVI, and COA (50%); as vehicle control, cells were treated with 1% DMSO; as a positive control, cells were treated with 1.6 mM H_2O_2; and as a negative control, cells were left untreated. Cells were plated as 100,000 cells/well in 24-well plates. After 24 h of cell seeding, formulations or individual entities were added depending on the optimal dose of 50 µM (see Fig. 4A). After 24 h of co-incubation, the cell medium from each well was collected into an individual tube. Trypsin was then added to separate the layer and promptly centrifuged at 1200 rpm to spin the cells into a pellet. Afterward, the supernatant was discarded, and a master mix of 2.5 µL propidium iodide (PI) + 100 µL of 1X binding buffer + 1 µL of Annexin-V was added to the cell pellet. After 15 min of incubation on ice in a dark room, 300 µL of 1X binding buffer was added. Cells were collected in pre-cooled flow cytometry tubes (5-mL tubes) and centrifuged at 1200 rpm for 5 min at 4°C, the supernatant was discarded. Then, cells were gently resuspended in 400 µL of binding buffer and

immediately examined by flow cytometry (Gallios, Beckman Coulter). Fluorescence signals emitted by FITC and PI were captured with FL1 and FL2 detectors, respectively [63] Cells positive for just FITC were considered early apoptotic cells, whereas cells stained by PI alone indicate necrotic cells. Cells that are FITC and PI-positive represent cells in late apoptosis [64].

2.4.10. PROTEIN PURIFICATION AND WESTERN BLOT ANALYSIS:

B16 F10 and MDF cells were seeded at a density of 1×10^6/well in a 6-well plate and allowed to grow for 48 h. Then, the old medium was changed, and the treatments were applied for a total of 6 h. Five different groups were used, including healthy (non-melanoma) cells (MDF) and four groups for mouse melanoma cells, as follows: untreated, COA (50%), NAVI (50 µM), and COA/NAVI (50 µM). After treatment, the cell lysate was collected in a cocktail buffer containing RIPA and a freshly prepared protease inhibitor. Then, the solution was sonicated and vortexed for 5 min, and this process was repeated 5-6 times followed by incubation on ice. The samples were then centrifuged at 3000 rpm for 15 min, the pellet was discarded, and the supernatant was collected. Protein concentration was quantified using a BSA standard curve at 280 nm. 100 µg/30 µL protein was loaded in each well, and proteins were separated using 12% SDS-PAGE under reducing conditions [65,66]. The separated proteins were electrophoretically transferred onto a PVDF membrane. After transfer, the membranes were blocked overnight at 4°C with 5% BSA in TBS-Tween solution. The next day, the membranes were washed twice for 5 min with TBS-Tween 20, and incubated with diluted primary antibody for 1 h at room temperature. Antibodies against β-actin and BCL-2 were obtained from Invitrogen and Abclonal, respectively. The blot was washed with TBS-Tween 5 times for 5 min with constant agitation. The blot was incubated with a secondary antibody for 1 h at room temperature. The chemiluminescence signal was developed using ECL western blotting substrate (Thermo Scientific Super Signal ECL substrates). Protein

bands were developed using a Bio-Rad ChemiDoc MP Imaging System. Quantification of the digitized images of the Western blot bands was performed using ImageJ software (National Institutes of Health, Bethesda, MD).

2.4.11. MOUSE TUMOR XENOGRAFT AND BODY WEIGHT:

All experiments pertaining to animal use were performed according to protocols approved by the Institutional Animal Care and Use Committee of the University of Texas at El Paso. Six- to seven-week-old C57BL/6 mice (21-30 g) were purchased from Charles River Laboratories International, Inc. and maintained under specific pathogen-free conditions. Cultured B16-F10 cells (mouse melanoma) were trypsinized, washed twice with serum-free DMEM, and suspended at 0.1×10^6 cells/mL PBS. 100 µL of the suspended cells were subcutaneously (SC) injected into the back of the mice, on Day 14 of post-injection, the tumors were visible, and twelve mice were randomly divided into four treatment groups: untreated, NAVI (50 µM) (PO), COA (50%), COA/NAVI (50 µM). All treatments were given thrice a week (T.I.W) for 3 weeks either *via* cotton swab for topical delivery or orally the navitoclax (which was standard of care). Treatment was terminated on day 35 of tumor cell inoculation. Mouse weight and tumor volume were measured during the treatment period and plotted against time (Day). Tumor growth was determined by measuring three orthogonal tumor dimensions. Tumor volume was calculated by utilizing the following formula:

$$\text{Volume} = \left(\text{Length (mm)} * \text{Width (mm)} * \text{ Width (mm)}\right) * 0.5$$

2.4.12. HISTOLOGY ANALYSIS:

The harvested tumor was fixed in 4% PFA for 4 h, then washed with saline and dehydrated. Afterward, the tumor was embedded in the optimal cutting temperature compound (OCT compound), sectioned (10-15 µm), and stained with hematoxylin and eosin (H&E), according to

the method published earlier [67] The stained slides were examined by light microscopy through a 160× objective lens.

2.4.13. CLINICAL BIOCHEMISTRY PANEL ANALYSIS :

Complete blood count (CBC) and serum biochemistry were determined for the xenografted mice described in section 2.12. On day 35, after tumor cell injection, the mice were euthanized, and 1-1.5 mL of blood was collected from heart puncture; 0.5 mL of blood was collected in heparin-coated tubes for CBC analysis, and the remaining 1 mL of blood was used for a biochemistry panel assay [68] Each blood sample (0.5 mL) was put in an anticoagulant (EDTA) coated bottle (K3EDTA bottle, ACUETTER, Greiner, Austria) to prevent coagulation and was centrifuged at 3000 rpm for 7 min. Serum biochemistry analysis included parameters related to liver and kidney function, e.g., aspartate aminotransferase (AST), alanine aminotransferase (ALT/GPT), alkaline phosphatase (ALP), total protein (TP), blood urea nitrogen (BUN), and creatinine (Cr). Biochemical analyses were quantified using a chemical analyzer (Element-DC by HESKA), and the results were presented using GraphPad prism software. Total blood count analysis was conducted using 20-µL blood samples from each treatment group and a Hemavet 950 (Drew Scientific). We measured red blood cell (RBC), white blood cell (WBC), platelet (PLT), and hemoglobin (Hb) values. The data were tabulated *via* GraphPad Prism software.

2.4.14. PROTEIN EXPRESSION BY IMMUNOHISTOCHEMISTRY:

Fixed tissues were cut using a cryotome (20 µm thickness), and tissues were kept in an anti-freeze medium at 4°C until the immunohistochemistry experiment was completed. Anti-freeze medium is composed of sodium phosphate monobasic (0.5 mm, 0.79 g) and dibasic (2.73 g), ethylene glycol (300mL), and glycerol (200mL) in DI water q.s. to 1 liter, which prevents any fixed tissue from

drying. Immunohistochemistry was performed using a protocol obtained from Thermo Fisher and Abcam, and modified in our laboratory with troubleshooting [69,70]. In brief, tissue samples were washed with PBS and once with 400 µL of wash buffer (0.1% BSA in 1X PBS). Then, non-specific staining was blocked by adding 400 µL of blocking buffer (10% normal donkey/goat serum, 0.3% Triton® X-100 in 1X PBS) and incubated for 45 min at room temperature. This buffer also acted as a permeabilization buffer. Diluted unconjugated primary antibody in dilution buffer was added according to the manufacturer's instructions and incubated overnight at 4 °C. The tissue was washed four times for 5 min the next day using 400 µL of wash buffer. The tissue was incubated with diluted secondary antibody in PBS for 1 h, protected from light. The tissue was washed two times for 5 min using wash buffer. Next, the wash buffer was removed, and the tissue was air-dried before adding a mounting medium and a coverslip. Confocal images were captured by using an LSM 700 microscope and analyzed in ImageJ software [71].

2.4.15: TUNEL ASSAY:

We utilized the Click-iT™ Plus TUNEL Assay (Thermo Fisher) and an Alexa Fluor™ 488 dye assay kit for *in situ* detection of apoptosis according to the manufacturer's instructions, as follows. Depilated skin samples were fixed in 4% paraformaldehyde (PFA) for 2 h at 37˚C. The samples were washed twice in PBS for 5 min and then incubated for 15 min with 1X Proteinase K solution (Component H in the assay kit was diluted 1:25 in PBS). The samples were again fixed in 4% PFA for 20 min and washed with PBS for 5 min. To induce DNA-stand breakdown in the skin,, skin samples were incubated with 1 unit of DNase I (diluted in 1X DNase I Reaction Buffer (20 mM Tris-HCl, pH 8.4, 2 mM $MgCl_2$, 50 mM KCl)) for 30 min at room temperature. After incubation, the samples were washed with DI water. 100 µL of TDT Reaction Buffer (Component A in the kit) were added to each well and incubated for 10 min. The TDT reaction buffer was removed and

replaced with 50 µL of the prepared TDT reaction mixture in each well for 1 h. Next, the reaction mixture was removed, and each well was rinsed with DI water. After rinsing, the samples were incubated in 3% BSA and 0.1% Triton™ X-100 in PBS for 5 min with gentle shaking. The samples were rinsed with 1X PBS, and then 50 µL of freshly prepared Click-iT™ Plus TUNEL Reaction cocktail was immediately added to each well for 30 min in the dark. The reaction cocktail was removed and replaced with 3% BSA in PBS for 5 min. The samples were rinsed with 1X PBS and prepared for imaging by placing the tissue on a glass slide and adding a mounting medium and a coverslip. The slides were incubated for 1 h at 4˚c and then imaged using an LSM700 confocal microscope at 20× magnification and the same image settings for all groups.

2.4.16. STATISTICAL ANALYSIS:

All experiments were carried out in triplicates, and the results are indicated as mean ± SD unless stated otherwise. Student T-test, one-way analysis of variance (ANOVA), and two-way ANOVA were performed using GraphPad Prism nonlinear regression software (GraphPad Software Inc.) [72]. A P value of <0.05 was considered significant. * Indicates statistical significance with $p < 0.05$; *** indicates statistical significance with $p < 0.001$.

2.5 ACKNOWLEDGMENTS:

The research reported in this publication was supported by a Research Centers at Minority Institutions grant funded by the National Institute on Minority Health and Health Disparities (NIMHD) of the National Institutes of Health (NIH) under Award No. U54MD007592. We also acknowledge Cancer Prevention Research Institute of Texas (CPRIT) funding through a Texas Regional Excellence in Cancer Award (TREC) under Award No. PR210153. The contents of this paper are solely the authors' responsibility and do not necessarily represent the official views of NCRR or NIH.

CHAPTER 3: TOPICAL BCL-2/BCL-XL INHIBITOR REVERSES BLEOMYCIN-INDUCED SKIN FIBROSIS

3.1. ABSTRACT:

Pathological fibrosis is distinguished from physiological wound healing by persistent myofibroblast activation, suggesting that therapies that induce myofibroblast apoptosis selectively could prevent progression and potentially reverse the established fibrosis, for instance, scleroderma (a heterogeneous autoimmune disease characterized by multi-organ fibrosis). Navitoclax (NAVI) is a BCl-2/ BCL-xL inhibitor with anti-fibrotic properties and has been investigated for skin fibrosis study. NAVI, a "BH3 mimic" medication that inhibits BCL-xL, makes myofibroblast particularly vulnerable to apoptosis. Despite significant potency, NAVI's potential application has been controlled and limited due to its risk of tremendous thrombocytopenia. Therefore, in this project, we have utilized a newly developed ionic liquid topical to deliver the NAVI directly to the fibroblast by avoiding systemic circulation. The ionic liquid composed of octanoic acid and choline bicarbonate (COA) has intrinsic properties of increasing skin pore size and allowing its payload to cross the skin barriers. By causing myofibroblast death, therapeutic Inhibition of BCL-xL with NAVI efficiently cures preexisting fibrosis tested in a scleroderma mouse model. Together, our findings elucidate that topical delivery of NAVI inhibits anti-apoptotic proteins BCL-2/BCL-xL in myofibroblast with minimal presence of the drug in the systemic circulation, resulting in accelerating therapeutic effect with no mentionable drug-associated toxicity.

Keywords: Ionic Liquid; Navitoclax; Apoptosis; Scleroderma;

GRAPHICAL ABSTRACT:

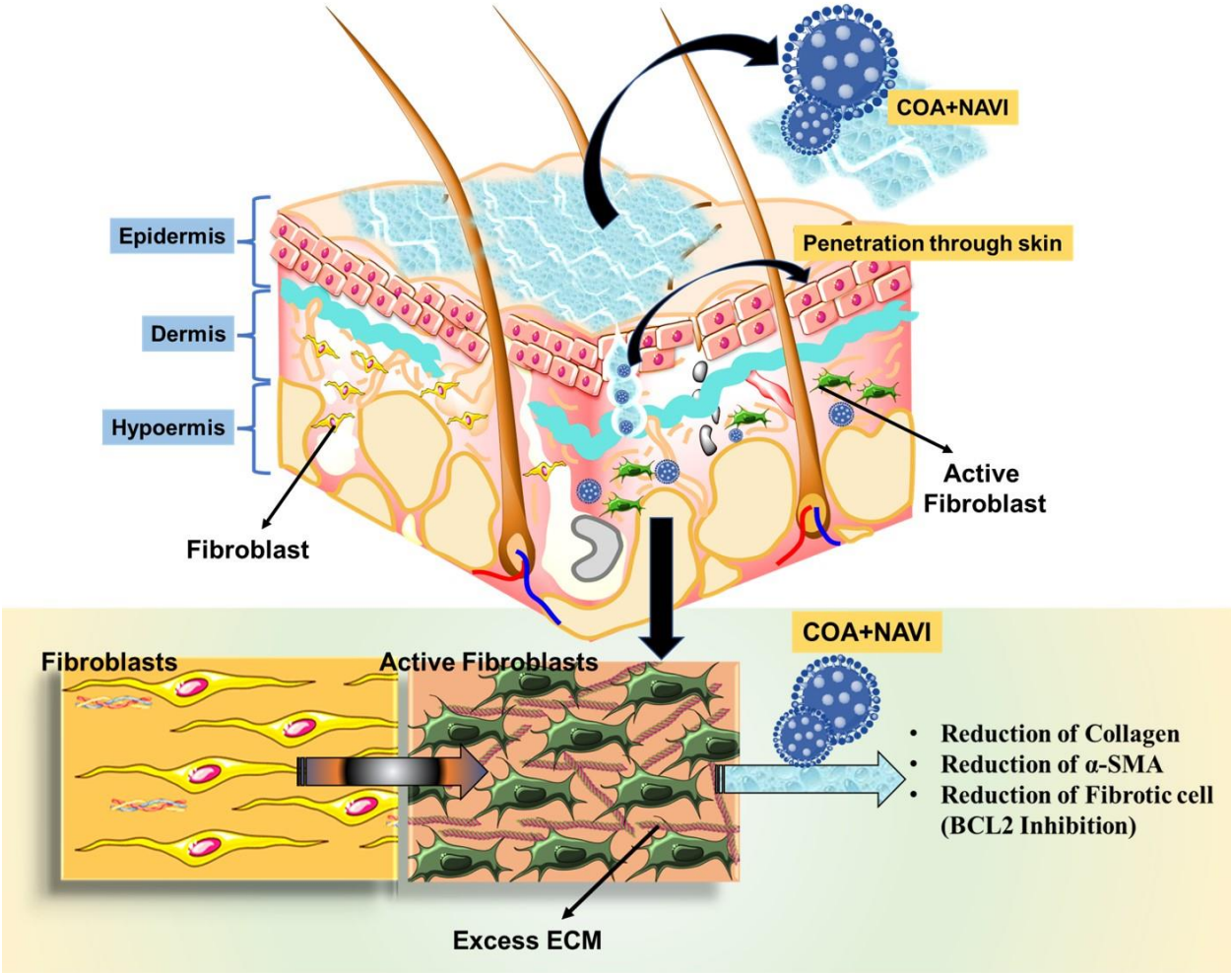

3.2. INTRODUCTION:

Annually, 75,000 to 100,000 cases of scleroderma are diagnosed in the U.S and more often affect women [73]. The initiation of scleroderma can result from aberrant wound-healing responses to autoimmune tissue injury, leading to activation of the myofibroblasts, the effector scar-forming cells in fibrosis. Failure of myofibroblasts to undergo apoptosis distinguishes non-resolving pathological fibrosis from self-limited physiological wound healing [74,75]. However, current treatments for skin fibrosis consist of immune-suppressant medications and surgery [76]. But the available treatments can only improve the fibrotic condition by slowing down the progress of the fibrosis [77]. Lagares et al. first reported

that inhibition of anti-apoptotic protein could reverse the fibrosis, tested in a skin fibrosis mice model. They have investigated the therapeutic potential of navitoclax (NAVI), a clinical trial BCL-2/BCL-xL inhibitor small molecule, and found the potential to treat skin fibrosis by inducing apoptosis [78]. However, the concerns related to the risk of thrombocytopenia and extreme hydrophobic properties of NAVI resulted in limitations for their potential for applications and clinical translations.

Fibrosis usually accompanies chronic inflammation and an increase of fibrous connective tissues in the dermis or subcutis [79]. This condition characterizes the proliferation of fibroblasts and collagen fibers in the dermis or surrounding hair follicles, usually parallel to the epidermis. Fibrosis can develop further into the dermis and subcutis in more severe cases [79]. Typically, skin fibroblasts synthesize little extracellular matrix (ECM) due to negative signaling and inhibitory influence of the non-cellular matrix. But due to the over-activation of fibroblast, different growth factors like IL-1, prostaglandin E, PDGF, connective tissue growth factor (CTGF), IL-6, and TGF-β [75]. This upstream activation triggers the release of extracellular matrix and accumulates in fibroblast cells' outer or cytoplasmic regions. In fibrosis, the cells become more rigid, lose functionality, and stop apoptosis. And eventually, all these tissue abnormality leads to organ failure [80].

The programmed cell death is critical in adult tissue and fetal development [81]. Failure to induce apoptosis can contribute to many diseases such as cancer, fibrosis, stroke, heart failure, and neurodegeneration. The molecular mechanism of apoptosis has been elucidated [82]. A family of proteases known as caspases has been identified; these are responsible for the biochemical and morphological changes during apoptosis. In apoptosis, mitochondrial outer membrane (MOMP) permeabilization leads to the release of apoptogenic proteins like cytochrome c, Smac/DIABLO,

DDP/TIMM8a, and EndoG [83]. MOMP permeabilization depends on anti-apoptotic BCL-2 family protein activation, translocation, and multidomain oligomerization. BCL-2 family protein acts as a gatekeeper to the apoptotic response [84]. The short sequence of amino acids related to the BCL-2 family is known as BCL-2 homolog (BM) motifs [8]. BCL-2 family members are classified into 3 functional groups: pro-apoptotic effector (BAX, BAK, BOK), pro-apoptotic activators (BID, BIM, BAD, NOXA, PUMA) and anti-apoptotic proteins (BCL-2, BCL-xL, Bcl-W, MCL and Bcl-B) [85]. Apoptosis promoting the effect of both activator and effector inhibits the anti-apoptotic BCL-2 family by direct interaction. BCL-2 inhibitors are designed to bind and sequester BH-3-only activators and prevent them from interacting with the pore-forming effector [9]. When the pore-forming process is blocked, pro-apoptotic protein cannot penetrate the mitochondrial membrane and induce apoptosis. The dynamic balance between anti-apoptotic members like BCL-2 and pro-apoptotic members helps determine whether the cell initiates apoptosis.

This project hypothesizes that a topical formulation that can solubilize the therapeutic molecule and enhance permeation to the skin but prevent their absorption into the systemic circulation can overcome the existing limitations. Thereby, NAVI could be used for treating skin fibrosis without exerting any toxicity related to thrombocytopenia. In this project, we have considered utilizing an ionic liquid based on choline bicarbonate, and octanoic acid (COA) has shown the capability of solubilizing the hydrophobic NAVI without adding any solubilizing agent. More importantly, COA-mediated topical delivery is a highly effective method of transporting NAVI to the epidermis layer of the skin. The main challenges in treating fibrosis with chemotherapeutics are epidermal layer penetration, appropriate drug concentration, and drug retention within the epidermis/dermis layer for an extended period. The COA-mediated topical delivery strategy likely can overcome all

the odds. The COA-mediated topical delivery strategy likely can overcome all these hurdles. COA can enhance the solubility of NAVI up to 150 µg/mL and allow 72.23% less NAVI transportation compared to NAVI itself (figure 2(a) of chapter 2 and figure 10(a) of chapter 3) [86]. The in vitro studies demonstrate that the transported NAVI was on hold within the epidermis/dermis/subcutis layer for more than 12 h, an experiment conducted on pigskin in vitro permeation test (IVPT) (chapter 2). In vitro studies performed on the human skin, fibrotic skin fibroblast cell line Hs27 show its potential use as a chemotherapeutic agent for fibrosis treatment, and COA/NAVI shows significantly greater efficacy than free NAVI. NAVI is a BH3 mimetic drug molecule with a high potency of anti-apoptotic protein B cell lymphoma/leukemia (BCL-2/BCL-xL) inhibition.

Here, we performed *in vivo* studies in a bleomycin-induced mouse model to evaluate the drugs' effectiveness, safety, and biodistribution. COA/NAVI was found to be very effective in inducing apoptosis by inhabiting BCL-2 and BCL-xL proteins. We have also observed a reduction in extracellular metrics (collagen and (-SMA) within the fibrosis skin as a therapeutic readout. With the development of COA/NAVI formulations, we have overcome the limitations of NAVI and facilitated its topical application to accelerate the treatment of local fibrosis. The findings indicate that the COA/NAVI formulation can be considered an effective and safe treatment approach for treating cutaneous fibrosis. Therefore, we aim to investigate the potential of a COA/NAVI formulation as a topical delivery platform and investigate their therapeutic feasibility and biocompatibility in a chemically induced skin fibrosis mice model.

3.3. RESULT & DISCUSSION:

3.3.1: COA/NAVI FORMULATION INHIBITS FIBROTIC MARKER IN TGF-B INDUCED HS27 FIBROTIC CELL:

COA, an ionic liquid composed of **C**holine bicarbonate and **O**ctanoic **A**cid was synthesized by our collaborator Eden Tunner's previously reported method [87]. COA is an organic salt and maintains its liquid property at room temperature, but more importantly, facilitates solubilizing of hydrophobic molecules, for instance, NAVI at a concentration of 156 µg/mL, without adding any organic solubilizer. In a recent *ex-vivo* skin penetration study, we observed slower skin penetration by COA/NAVI, signifying that COA holds the payload (NAVI) longer in the skin layer (figure 3(a) [88,89]. These studies allow us to explore the COA/NAVI therapeutic avenue in fibrosis treatment. Skin fibrosis is defined as extracellular matrix accumulation and increased fibroblast proliferation [90]. This phenomenon has clinical ramifications, including organ dysfunction and failure. We utilize COA intrinsic properties and NAVI anti-fibrotic effect to dual effect against fibrosis signaling. There are multiple signaling cascades in fibrosis pathogenesis. TGF-β is overexpressed in fibrotic diseases and displays a pro-fibrotic effect in fibroblasts [91]. TGF-β is one of the primary mediators in the fibrotic process, associated with a long list of pathologies related to chronic inflammation and scarring, and affects all types of organs and tissues. The Hs27 cells were treated with recombinant TGF-β (10 ng/mL) for 24 hours [91].

After 24 h, we washed the cells and plate cells to evaluate different fibrotic markers and COA/NAVI therapeutic efficiency in vitro studies. 1000 cells/well were plated in 12 wells in 96 flat bottom well-plate. After making the cells fibrosis (mentioned above) in 6 wells, treatment was added to 4 wells and incubated for 6 h [92]. After antibody incubation, we stained each well with Hoechst (1:500) for 30 minutes at 37 ˚C. In this in vitro assay, we have confirmed that cells with TGF-β-induced fibrotic cells' coincubation express higher fibrotic markers like Col1 and α-SMA compared to healthy Hs27 cells [93]. Figure 8(c) showed the anti-fibrotic activity of COA/NAVI treatment as indicated by the reduction of the Col1 and α-SMA protein expression. With only 6 h

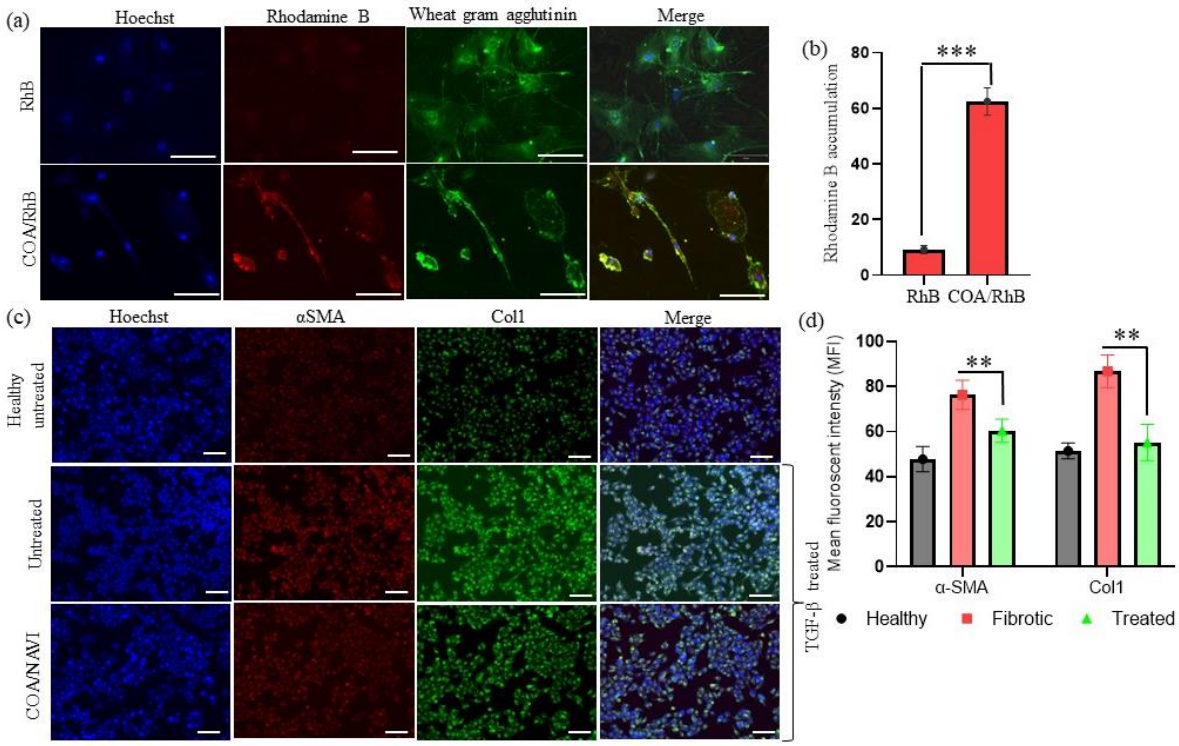

Figure 8: In vitro fibrotic cell therapy and internalization.

(c) Hs27 cells were cultured in 12 well plates 1000/well the cells were incubated with Col1 (1:500) anti-goat and α-SMA (1:1000) anti-rabbit in the same well for 2 h at RT. Then incubate with F(ab')2-goat anti-mouse and rabbit anti-mouse IgG (H+L) cross-adsorbed secondary antibody, Alexa fluor plus 488 (1:500) and Alexa fluor plus 546 for 1 h at RT, respectively. The image was taken using LSM700 at 20 X magnification. The scale bar represents here is 100 µm. Higher expression of Col1 and α-SMA in untreated TGF-β panels validate our approach to making the healthy Hs27 cell fibrotic. (a) Hs27 cells were treated with TGF-β, and we evaluated the cell internalization properties of COA. Fibrotic cells were treated with free Rhodamine B (RhB) and COA/RhB for 6 hr. Then cells were washed and stained with Hoechst (live nucleus) and wheat gram agglutinin (plasma membrane staining) [94]. Higher accumulation of RhB in COA/RhB treatment was observed in the fibrotic cell compared to free RhB treatment. Images acquired by epi-fluorescent microscope confirm COA's intrinsic properties of carrying a payload to penetrate the cell membrane and delivery it to the cell cytoplasm. The image was taken using Leica DMi8 epi-fluorescent microscope at 40X magnification. The scale bar represents in the image is 200 µm. (b) The RhB accumulation was quantified. The RhB MFI value of COA/RhB is statistically higher than the RhB treatments. Data represent mean ± SD, where n=6. * Indicates statistical significance with $p < 0.05$; *** indicates statistical significance with $p < 0.001$.

of treatment with COA/NAVI, the amount of both Col1 and α-SMA was reduced dramatically.

This in vitro experiment validates the initial claim of COA/NAVI anti-fibrotic therapeutic

efficiency *in vitro* assay. We also quantify the mean fluorescent intensity of Col1 and α-SMA and graphed in figure 8 (d). The treatment inhibits both fibrotic markers and the data is statistically significant.

Further concern was if COA could facilitate the internalization of the drug molecule into the activated fibroblast cells. To prove the hypothesis, the drug molecule was replaced with fluorescent dye rhodamine B (RhB) to visualize the cellular internalization of hydrophobic molecules assisted by COA. The COA/RhB formulation was prepared following the same method as for COA/NAVI. In figure 8 (a), a higher accumulation of RhB was observed within the cells treated with COA/RhB compared to the cells treated with only RhB. This data demonstrates COA's intrinsic properties of carrying a hydrophobic payload to fibrotic cells. Figure 8(b) shows that COA-associated RhB internalization was recorded as much as seven-fold higher. The findings indicate that NAVI can be considered a potential therapeutic against fibrosis pathogenesis that can reverse the fibrotic cells in a healthy phenotype. And COA facilitates the NAVI to penetrate the skin layer and allows the drug to initiate apoptosis in the site of action.

3.3.2: COA/NAVI-INDUCED APOPTOSIS IN FIBROTIC CELLS VIA MITOCHONDRIAL MEMBRANE DEPOLARIZATION:

NAVI is an inhibitor of the anti-apoptotic protein BCL-2, and genetic knockdown of BCL-2 promotes BIM-dependent apoptosis of fibrotic tissue [3], so we expected to see an increased level of apoptosis caused by NAVI in the skin fibrosis model. After 24 h of treatment with COA/NAVI or NAVI alone, cells were washed with 3 X PBS and incubated with Annexin-V and propidium iodide (PI) to quantify the levels of apoptosis and necrosis. We tested the following formulations and controls: NAVI (20 µM), NAVI (50 µM), COA/NAVI (20 µM), COA/NAVI (50 µM), COA, H_2O_2, DMSO, and saline. Figure 2(a) reveals that apoptosis is heavily induced by both COA/NAVI

and free NAVI. However, COA/NAVI induced 20-30% more apoptosis than free NAVI at an equivalent concentration. We observed 70% and 75% apoptosis induced by 20 μM and 50 μM COA/NAVI, respectively. Figure 9(a) shows that COA induces 50% apoptotic cell death [95]. As NAVI is not soluble in water, a solvent of 0.1% (v/v) DMSO was added to prepare NAVI for these *in vitro* experiments. Low apoptosis (<5%) with DMSO treatment was observed. Finally, in contrast to the high levels of apoptotic cell death, we observed a low percentage of necrosis induction by the formulations, including COA/NAVI. COA/NAVI induces higher apoptosis likely because of the ability of COA to enhance the cellular internalization of NAVI.

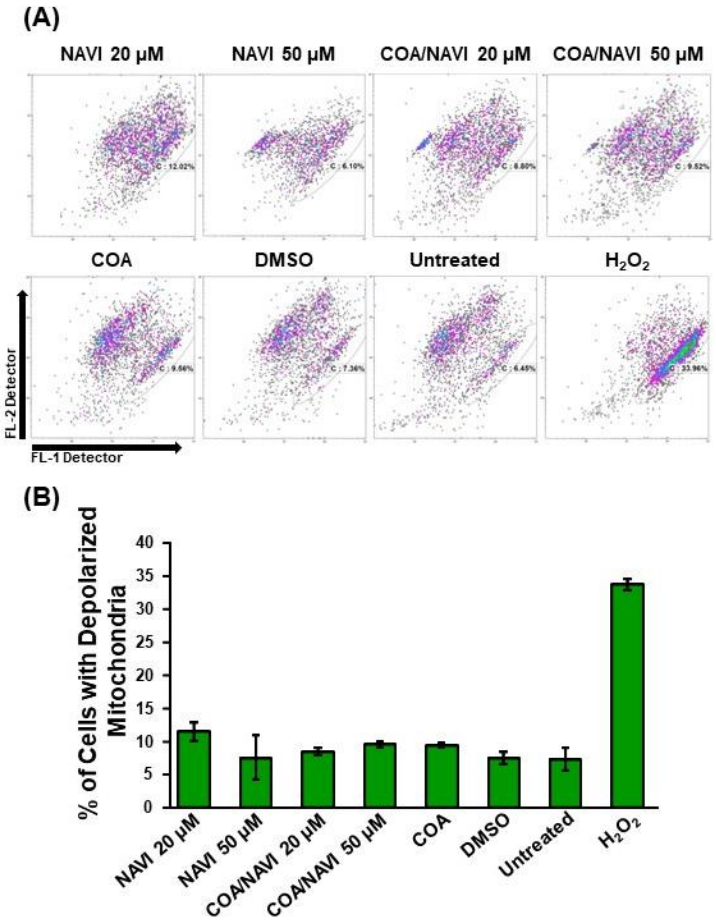

Figure 9: In Vitro cell apoptosis and mitochondrial polarization.

(a) Mitochondrial membrane potential study. (A) Representative flow cytometric dot plots showing cells with aggregates or monomers (oval gate) of JC1 dye; the FL-2 detector was positioned on the y-axis, whereas the FL-1 detector was set on the x-axis. (B) The bar graph does not indicate any significant depolarization changes in mitochondrial membrane potential between the experimental treated cells with NAVI, COA, or COA/NAVI, compared to the DMSO (solvent control) and untreated (negative control) cells. Also, H2O2 was included as the positive control of mitochondrial depolarization. *Indicates statistical significance with $p < 0.05$; *** indicates statistical significance with $p < 0.001$.

Following by apoptosis and necrosis study, we aim to evaluate the mechanism of how NAVI induces apoptosis in fibrotic cells. From the literature review, it has been understood that NAVI inhibits anti-apoptotic proteins BCL-2 and BCL-xL and concurrently changes the mitochondrial polarization to block the transportation of anti-apoptotic proteins [96]. Thus, we further evaluated how NAVI converts the mitochondrial membrane potential of fibrotic cell and block the transport of BCL-2 and BCL-xL.

We used a mitochondrial JC-1 Dye (Mitochondrial Membrane Potential Probe) assay kit to evaluate the polarization change. JC-1 is a novel cationic carbocyanine dye that forms J-aggregates at higher concentrations. These aggregation characteristics make JC-1 a sensitive marker for mitochondrial membrane potential [97]. Typically, under homeostatic conditions, cells display polarized mitochondria. The depolarization of mitochondrial membrane potential ($\Delta\Psi m$) is considered evidence of activation of the intrinsic apoptosis pathway [64]. The JC-1 reagent can form aggregates or monomers emitting red or green signals, respectively. A red fluorescent signal indicates the polarized and healthy condition of mitochondria. In contrast, a green fluorescence signal indicates depolarized and unhealthy conditions. The red and green fluorescence signals were monitored by flow cytometry using FL2 and FL1 detectors [98]. In Figures 9(b), the JC-1 expression is plotted using the green signal numerical values from the Gallios flow cytometry analysis. The JC-1 membrane potential value was measured using Kaluza data analysis software

and represented as the percentage of depolarized positive cells compared to the overall population [99]. COA/NAVI treatments caused an increase in the membrane potential compared to the untreated group. And both NAVI and COA/NAVI treatment induced similar JC-1 monomer expression. COA/NAVI treatment induced significant depolarization in the fibrotic cells compared to untreated cells. Also, both COA/NAVI and NAVI alone produced similar membrane potential values. These results confirm that COA by itself is not effective in changing cell polarization, and NAVI is biologically active in the COA/NAVI formulations. Therefore, COA/NAVI induced apoptosis in fibrotic Hs27 skin fibroblast cells and changed the membrane potential during apoptosis.

3.3.3 BLEOMYCIN INDUCES FIBROSIS CAN INHIBIT BY COA/NAVI TOPICAL ADMINISTRATION:

Bleomycin-induced skin fibrosis is a mouse model used to study disease pathology and therapeutic efficacy. The animal experiments were designed according to IACUC's approval of the University of Texas at El Paso. Bleomycin-induced skin fibrosis should be performed using > 5-week-old C57BL/6 male mice. We recommend using healthy, inbred, young (5 to 6 weeks old) mice of the gender kept under proper housing conditions to reduce variations of obtained data. To minimize stress: (1) avoid combining adult (>5 weeks) males with unfamiliar males due to increased aggression, (2) place mice into an experimental cage or room at least one week before the experiment, and (3) remove additional or socially incompatible mice from experimental cages. We injected 200 µg/mL (100 µL per dose) of bleomycin per animal three times five days apart.

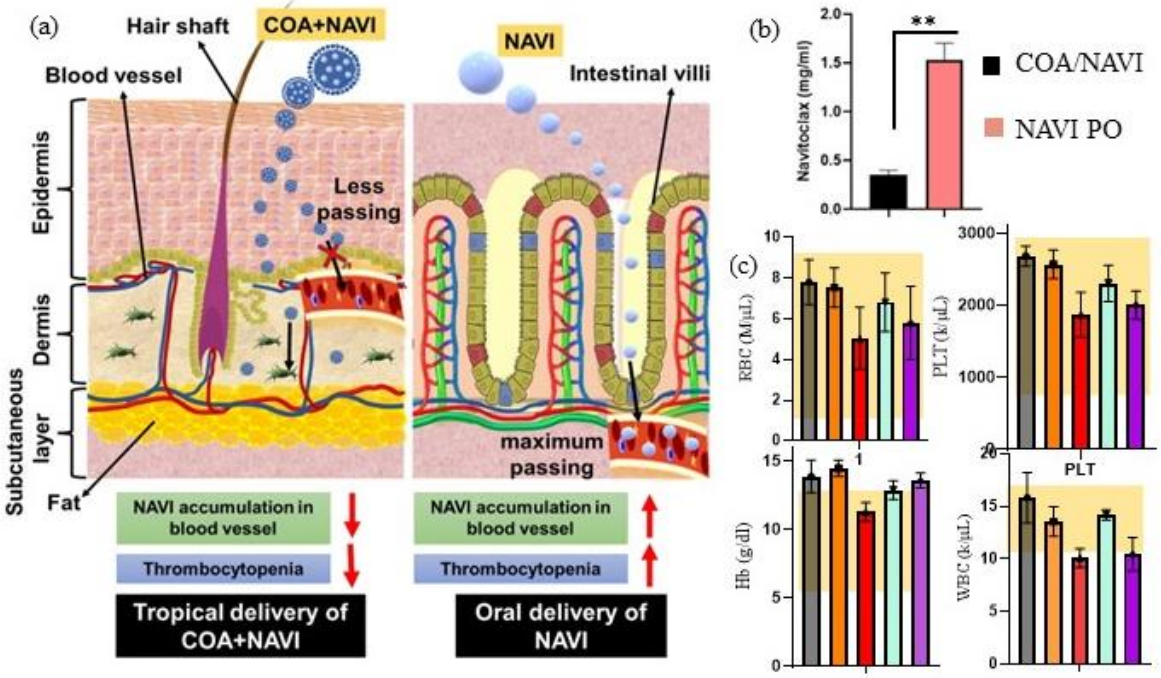

Figure 10: In Vivo animal study and biochemical analysis.

C57BL/6 animals have injected bleomycin at a 200 µg/mL dose per animal for three doses five days apart. After three doses, we waited for another two weeks to make the scleroderma model. After mice were randomly distributed into four groups, treatments were given for four weeks. The treatment groups were untreated, NAVI (50 µM) (PO), topical administration of COA (50%), and COA/NAVI (50 µM). (a) The schematic representation of how NAVI is transported via the topical and oral route of administration. Topical COA/NAVI delivery ensures a higher percentage of NAVI in the fibrotic area than NAVI PO administration. Also, topical COA/NAVI holds the drug longer in the fibrotic region and allows less NAVI transportation in the systemic circulation. Thus, we observe lower thrombocytopenia in COA/NAVI topical administration than in NAVI PO. (b) The blood samples were quantified using a UV absorbance at 345 nm to quantify the concentration of NAVI 6 h of post-administration. The graph showed higher transport of NAVI (1.61 mg/mL) via GI track than COA/NAVI (0.38 mg/mL) via skin fat layers. (c) One of the concerns of using NAVI is the thrombocytopenia side-effect. In total blood cell analysis was done by hemavet. The platelet number is lower in both NAVI treatment groups. But COA/NAVI topical delivery has a higher platelet number (~ 2400 k/µL) compared to NAVI (PO) (~ 1900 k/µL); both are in the normal range. These platelet numbers correlate with the amount of NAVI being transported via skin or GI tract. (d) We measure the body weight during the treatments. We observe no sudden bodyweight reduction, indicating our treatments were safe to administer to mice. (e) We also measure the fibrotic area from the beginning of treatment. We observed the fibrotic area was inhibited by 120% compared to the untreated group after four weeks of treatment. This data validates the initial claim of COA/NAVI anti-fibrotic therapeutic efficiency. Data also according to the platelet number we observe in the total blood count. The data shown here is mean ± SD; the experiment was performed in N = 3.

The rationale was rather than giving a lower dose of bleomycin every other day, administering three moderate doses five days apart with a higher dose (200 µg/dose/animal). Other research articles confirmed that the dose is not lethal and observed no mortality during dosing and treatment [100],[101]. Then we waited another two weeks to start the treatments. Treatment groups were untreated, COA (50%), NAVI (50 µM), and COA (50%)/NAVI (50 µM). We administer COA and CAO/NAVI topically and NAVI (50 µM) per oral for four weeks using a cotton swab and oral gavage. The rationale for oral administration of NAVI was to follow FDA-prescribed guidelines to avoid the risk of thrombocytopenia caused by IV injection NAVI. Treatments were given every other day 14 times in 4 weeks.

Figure 10(a) shows how NAVI is transported via topical and oral administration. COA-assisted topical delivery held the drug longer and allowed the very minimal drug to be absorbed into the systemic circulation. On the other hand, orally administered NAVI initially reaches the systemic circulation via intestinal absorption, and a fraction of the NAVI diffuses to the skin, in other words, to the site of disease. Further, we have measured how much NAVI is being transported and absorbed into the systemic circulation for topical and oral administration. Figure 10(b) shows that the concentration of NAVI in blood was 0.62 and 1.335 mg/mL for topical and oral administration, respectively. One of the limitations of clinical translation of NAVI is thrombocytopenia. The severity of NAVI-associated thrombocytopenia is published in phase I clinical study on multiple disease model diffuse large B-cell lymphoma (DLBCL), chronic lymphoid leukemia (CLL), small lymphocytic lymphoma (SLL), mantle-cell lymphoma (MCL), follicular lymphoma (FL), and classic Hodgkin's lymphoma, NK/T-cell lymphoma, and marginal zone lymphoma [102–105].

The mice were grouped and treated as NAVI (PO; oral), COA, and COA/NAVI topical and compared with the untreated disease model to distinguish the route of administration-dependent

thrombocytopenia. In Figure 10(c), the blood toxicity analysis confirms that oral NAVI provoked comparatively higher thrombocytopenia than COA-assisted topical NAVI. However, the platelet count was within the normal range for oral NAVI and comparable to the value of the healthy control group. These data also confirm that topical delivery of COA/NAVI can improve the thrombocytopenia side-effect in the mouse model.

Based on visual observation, the fibrotic area improved (softened) after treatment with COA/NAVI, becoming more like healthy skin tissue. We also observed some skin lesions due to COA-only administration after one week of treatment. Therefore, we skipped three consecutive treatments, then lowered the COA dose to 50% of its original concentration, and thereafter observed no skin irritation during the remainder of the COA treatments. The experimental results confirm that topical COA/NAVI is an efficacious treatment for skin fibrosis. We further evaluated this efficacy result by using histology and biological analysis of fibrotic markers. All animals were euthanized at the end of the treatment, and blood, skin tissue, and organs were collected for further analysis. Blood serum analysis, skin tissue histology, skin immunohistochemistry, and western blotting were conducted to identify biological and molecular correlates to the therapeutic efficacy, as described in the following two sections.

3.3.4: COA-ASSISTED TOPICAL NAVI DOES NOT SHOW SYSTEMIC TOXICITY:

The animal experiments evaluated dose-response, toxicity, prophylactic, and therapeutic responses to topical COA/NAVI, and NAVI PO administration. The treatment groups were COA/NAVI (50 μM) as the developed delivery therapy, NAVI (50 μM) as the standard of care, and COA as a control. After the animal studies, all animals were euthanized, and all significant organs and blood were collected for biochemical analysis to check for any cytotoxicity and organ toxicity. Figure 11(a) shows hematoxylin and eosin (H&E)-stained skin tissue sections, in which areas of fibrosis

(white regions) are prominent in both the untreated and COA treatment groups. Such fibrotic areas are not apparent in the COA/NAVI group; in fact, the latter's skin is comparable to that of healthy tissue. Other than skin, no sign of toxicity was observed in any organ, based on histological analysis.

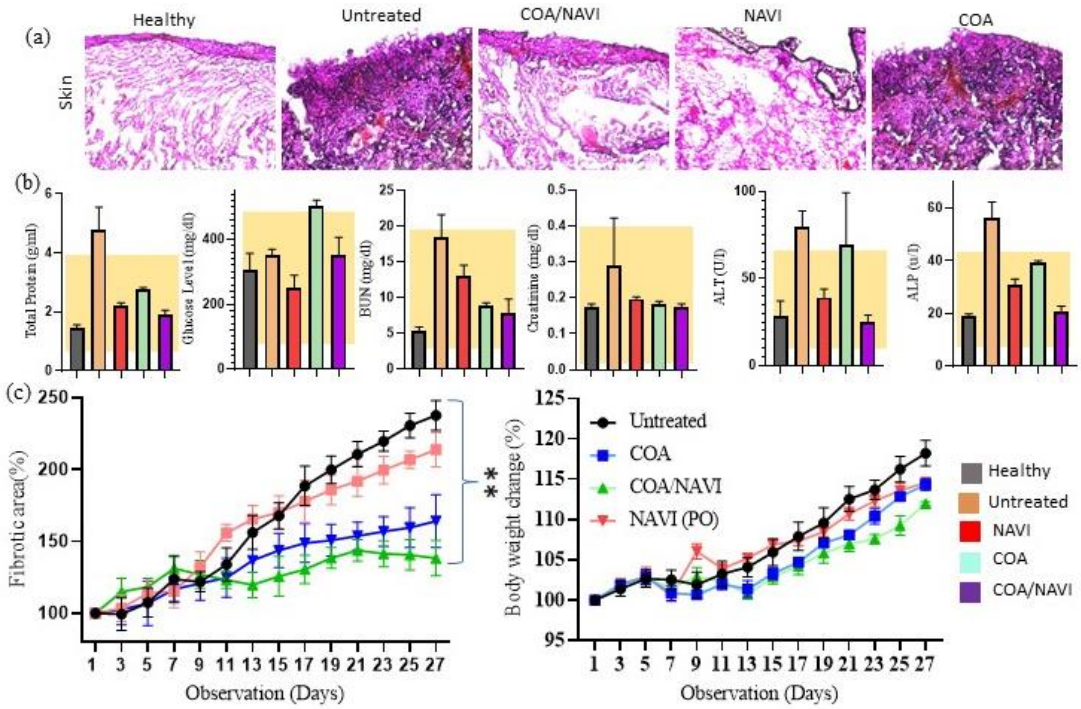

Figure 11: H&E staining, serum, and comprehensive blood analysis of fibrotic mice model.

(a) Hematoxylin and eosin (H&E) staining was conducted according to the protocol described in the method section. The samples were prepared for the H&E staining panel of skin and observed no toxicity markers or indications in the panels. The H&E staining indicated fibrotic regions in the diseased untreated groups. Also found downregulation fibrotic marker with topical administration of COA/NAVI groups. There was similar physiological morphology, structural resemblance, and no abnormal cell & tissue component across different treatment groups in the significant organ panels. Therefore, topical, and oral treatments of NAVI didn't have any toxicity in major organs and their function. (b) In serum biochemistry analysis, liver and kidney function values were regular arbitrary ranges indicated by the yellow rectangle in figure 4(b). A higher total protein value was observed in the diseased untreated group representing the body's immune system fighting against fibrosis pathogenesis. And a lower protein level after four weeks of COA/NAVI treatment indicates the body fighting against the fibrotic signaling pathway. (c) We measure the body weight during the treatments. We observe no sudden bodyweight reduction, indicating our treatments were safe to administer to mice. (c) We also measure the fibrotic area from the

beginning of treatment. We observed the fibrotic area was inhibited by 120% compared to the untreated group after four weeks of treatment. This data validates the initial claim of COA/NAVI anti-fibrotic therapeutic efficiency. Data also according to the platelet number we observe in the total blood count. The data shown here is mean ± SD; the experiment was performed in N = 3.

Serum was separated via centrifugation at 3000 rpm for 15 min. Using a biochemical analyzer, we measured different serum parameters: aspartate aminotransferase (AST), blood urea nitrogen (BUN), alkaline phosphatase (ALP), and alanine aminotransferase (ALT/GPT), creatinine (Cr), and total protein (TP) [68]. Figure 11(b) shows that the liver and kidney biomarker profiles of all treatment groups were similar to those of the control group and within the normal range across all treatment groups. In Figure 11(d), the fibrotic area was measured in all treatment groups and graphed from day 1 to day 27 of treatment. Interestingly, we identified levels of inhibition of the fibrotic area of 120% and 40% in the COA/NAVI group compared to the untreated and NAVI (PO) groups, respectively, on day 27 of treatment. We did not observe any drastic reduction in body weight during the treatments, indicating the safety of the topical therapies in this animal model (Figure 11(e)). The animal body weight, H&E imaging, and fibrotic area inhibition showed that the treatments had therapeutic efficacy against skin fibrosis. Furthermore, COA-assisted NAVI did not generate any significant toxicity, as suggested by the biochemistry and histology data. Therefore, the treatments were safe, as they caused no notable toxicity in blood and major organs.

3.3.5: COA/NAVI INDUCES APOPTOSIS VIA ANTI-APOPTOTIC BCL-2 PROTEIN INHIBITION:

Apoptosis has been identified as a potential initiator that assists in disease progression [47]. Increased apoptosis of fibrotic cells is a pathological characteristic of damaged skin during fibrosis [106]. BCL-2 family proteins act as the apoptotic response gatekeeper [107].

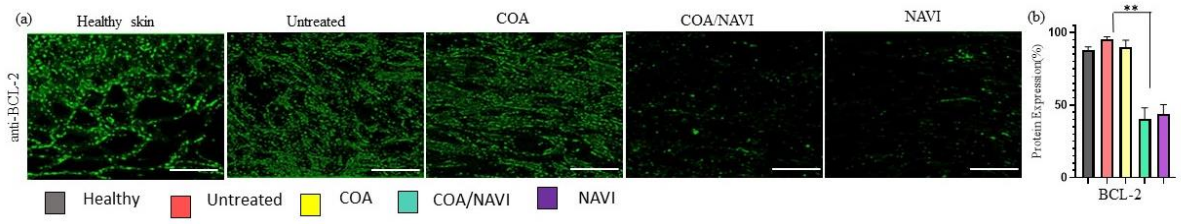

Figure 12: Ex-vivo tissue analysis and apoptosis analysis.

(a) Immunohistochemistry of skin fibrosis to visualize BCL-2 anti-apoptotic protein inhibition during navitoclax administration either PO or topical delivery via ionic liquid. The treatment groups were healthy skin tissue, untreated fibrosis tissue, and treatment with COA (50%), NAVI (50 µM), COA/NAVI, and the untreated group. The BCL-2 antibody concentration was 1:200 and secondary anti-rabbit Alexa 488 (1:250). The image was acquired using LSM 700 confocal imaging microscope, 20X magnification, and a scale bar representing 200 µm. (b) The anti-BCL-2 antibody signal was quantified *via* ImageJ. Signals were dimmed in COA/NAVI treatment group. The data confirm that topical delivery holds biological properties of navitoclax.The experiment was performed in N = 3. *** Indicates statistical significance with $p < 0.001$; ** indicates statistical significance with $p < 0.01$ and * indicates statistical significance with $p < 0.05$.

NAVI is a small molecule inhibitor of BCL-2 family proteins and has a higher affinity toward BCL-2, BCL-xL, and Bcl-w [108]. NAVI binds to the BH3 binding groove of BCL-2 proteins in the cytoplasmic region of the polypeptide, causing the displacement of the pro-apoptotic BH3-only protein (BIM) from the BCL-2 family protein [4]. Thus, free BIM triggers cell apoptosis by releasing cytochrome c from mitochondria [4]. Figure 12(a) shows the expression level of the BCL-2 protein in immuno-stained skin tissue. Tissue from the COA/NAVI-treated group had the lowest expression of BCL-2, followed by the oral NAVI group, compared to untreated and healthy skin tissue. The quantitative expression of BCL-2 measured by ImageJ is shown in Figure 12(b). Expression of BCL-2 protein was observed to be 60-70% and 50-60% lower in the NAVI/COA- and NAVI (PO)- treated groups, respectively. The inhibition of BCL-2 due to treatment with COA/NAVI is statistically significant ($P < 0.001$) when compared to the untreated group.

We next isolated proteins from skin tissue to quantify BCL-2 and BCL-xL expression via western blotting (WB). Protein was loaded at 100 µg/30 µL in each well, and proteins were separated using

12% SDS-PAGE under reducing conditions. The WB data are give a similar profile to the immunohistochemistry data. For WB analysis, β-actin was used as the housekeeping (reference) protein. In addition to BCL-2, we also observed inhibition of BCL-xL for both COA/NAVI and NAVI (PO). These data align with previous findings of NAVI's inhibitory activity against BCL-2 family proteins [3]. The data also validate that COA/NAVI is biologically active and its topical administration can inhibit the anti-apoptotic proteins BCL-2 and BCL-xL. The quantified BCL-2 and BCL-xL expression observed by WB is 60-70% lower in the COA/NAVI and NAVI (PO) groups compared to the untreated and healthy groups. The immunohistochemical and WB data validate the therapeutic efficacy of the COA/NAVI formulation in skin fibrosis. As we discussed earlier, inhibition of the anti-apoptotic proteins BCL-2 and BCL-xL results in activation of the intrinsic apoptosis pathway.

3.3.6: TOPICAL DELIVERY OF COA/NAVI IMPROVES SCLERODERMA BY REVERSING FIBROSIS:

Skin fibrosis is defined as the accumulation of excessive ECM in the dermis layer [109]. Systemic sclerosis (SSc) or scleroderma is an autoimmune disorder that typically results in fibrosis of the dermis layer of the skin and internal organs. Although the pathogenesis of scleroderma is still unclear, thickened dermis due to uncontrolled deposition of ECM is the primary hallmark of this disease [110]. The expression levels of various ECM components, mainly type I collagen (Col 1 α1) and α-SMA, are upregulated at the transcriptional level in fibroblasts isolated from sclerotic lesions of SSc patients, evaluated by *in vitro* assay [111,112].

Figure 13(a) shows immuno-stained specimens to visualize the presence of the fibrotic markers Col1 and α-SMA in mouse skin from the following groups: healthy, untreated, NAVI, COA/NAVI, and COA. As seen in the first row of panel (a), Col 1 α1 expression was low in

healthy tissue and downregulated in both the NAVI (PO; 50 µM, equivalent mouse dose of 150 mg/kg) and COA/NAVI (50 µM) treatment groups compared to the untreated fibrosis group.

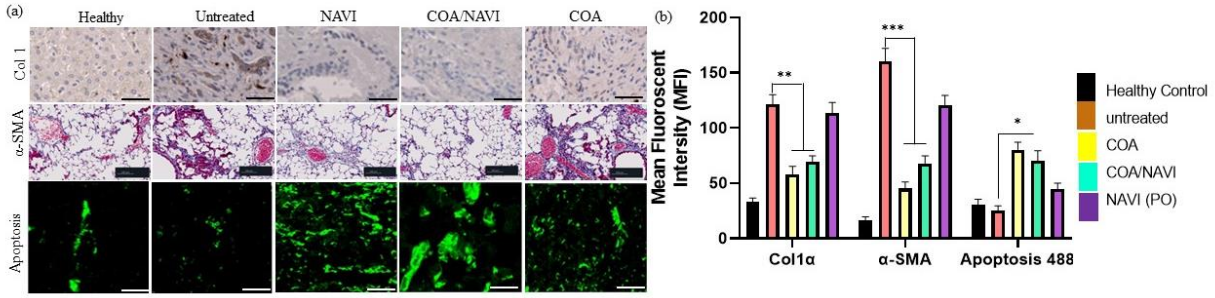

Figure 13: Biochemical analysis of fibrotic tissue analysis.

(a) We ran immunohistochemistry of our skin tissue samples to quantify the Col1 α1 and α-SMA fibrotic marker. Compared to the untreated group, we observe higher inhibition of fibrotic markers in COA/NAVI treatment groups. We had another control group, only NAVI, and COA. The findings consolidate western blot data. In the 3rd row, we represent the apoptosis in fibrotic skin tissue due to the treatments. This data matches the finding's in vitro apoptosis-necrosis assay. We observe a higher apoptosis rate in the COA/NAVI treatment area than in other treatment groups. (b) We also quantified both the immunohistochemistry marker and the TUNEL assay signal. The experiment was performed in triplicate.* indicates statistical significance with $p < 0.05$; *** indicates statistical significance with $p < 0.001$.

We observed greater downregulation of Col1-α1 in the COA/NAVI-treated group than in the NAVI (PO)-treated group at an equivalent dose. The amount of Col1 α1 in COA/NAVI-treated skin was quantified as less than 50% compared to the untreated skin. NAVI (PO) was also found to be effective in reducing Col1 α1 but was not as effective as COA/NAVI (Figure 13b). Immunostaining of α-SMA is shown in Figure 13(a). We observed a similar trend of downregulation of α-SMA expression in both the NAVI and COA/NAVI treatment groups and the findings were significant compared to untreated skin. Qualitative and quantitative analysis of both fibrotic markers confirms that COA/NAVI is efficacious in reducing the expression of fibrotic markers, presumably by inhibiting the downstream fibrotic signaling pathway.

The topical formulation was also investigated for apoptosis activity by using an *in-situ* TUNEL assay. The bottom panel of Figure 13(a) shows higher induction of apoptosis in the skin of mice treated with NAVI and COA/NAVI compared to the untreated healthy and untreated skin samples. However, as expected, the apoptosis rate was higher in mice treated with COA/NAVI than in NAVI. The ability of COA to enhance permeation of NAVI into the skin and hold the drug within the epidermis/dermis layer for a longer duration resulted in higher apoptosis, lower α-SMA, and lower Col1. This promising topical delivery system has two major advantages: 1) it reverses the fibrotic condition by inhibiting fibrotic markers like Col1 and α-SMA, and 2) it significantly reduces transportation of NAVI to the systemic circulation, lowering the risk of thrombocytopenia [113]. The protein and apoptosis signals were quantified by using ImageJ, and the expression levels were compared among the treatment groups. Figure 13(b) gives the quantitative values of Col1 and α-SMA expression, revealing significant reductions — by 45% and 69%, respectively, following COA/NAVI treatment as compared to the untreated diseased group. This inhibition by COA/NAVI is clinically relevant and correlates with the results of preclinical skin fibrosis studies. Topically administered NAVI shows competitive outcomes against an equivalent dose of orally administered NAVI.

In addition to immunohistochemistry, western blotting (WB) of the tissue samples shows excessive deposition of CTGF and α-SMA within the ECM of untreated diseased animals versus that of healthy controls. Thereby, the WB analysis confirms the development of the skin fibrosis animal model. The WB data also reveal that both oral and topical administration of NAVI resulted in the downregulation of the fibrotic markers Col1, CTGF, and α-SMA. This observation agrees with the immunohistochemistry experiment and confirms the efficacy of COA/NAVI as an anti-fibrotic therapeutic modality. The WB bands were quantified using ImageJ software and graphed using

GraphPad Prism software. The quantified data show downregulation of both α-SMA and CTGF protein expression by 50% and 20%, respectively, compared to untreated fibrotic tissue. Thus, COA/NAVI topical administration greatly improves the fibrotic condition in an animal model. This novel topical approach is non-invasive and repurposes NAVI in fibrosis therapy. Finally, we proved that COA/NAVI-induced apoptosis was at least part of the therapeutic mechanism operating to reverse the fibrotic condition in the rodent fibrotic model.

3.4. CONCLUSION:

Currently available therapeutic approaches such as laser surgery, topical cream administration, and drugs or therapy such as D-penicillamine, bovine collagen, methotrexate, mycophenolate mofetil, and allogeneic bone marrow transplantation are only capable of improving the fibrosis condition rather treating the disease by blocking the pathologic mechanism. Therefore, in this study, we have investigated repositioning the anti-apoptotic drug NAVI for the effective and efficient treatment of fibrosis. Furthermore, we have also investigated the feasibility of topical delivery of NAVI to avoid any excessive systemic toxicity. By limiting extreme systemic concentrations of NAVI, an adequate amount of the drug could be retained within the skin layers for an extended period, thus improving therapeutic outcomes. This novel topical delivery system can be developed as a skin gel or patch for patient convenience. NAVI can induce apoptosis of fibrotic cells, and surprisingly it inhibits the fibrotic markers Col1 α1, CTGF, and α-SMA. By limiting the systemic absorption of NAVI, this topical delivery system could significantly reduce the risk of thrombocytopenia. However, as fibrosis results from a complex cascade of events that involves inflammatory effector cells and dysregulation in multiple pathways, we further aim to investigate combination therapy to target multiple signaling pathways. To solidify our hypothesis, we also aim to investigate the COA/NAVI formulation in a BCL-2 knock-out and humanized mouse model.

3.5. MATERIALS AND METHODS

3.5.1. MATERIALS AND CHEMICALS:

Octanoic acid (OA) and choline bicarbonate (CB) were purchased from Merck, Germany. Dulbecco's Modified Eagle Medium (DMEM), Dulbecco's phosphate buffer saline (DPBS), fetal bovine serum (FBS), trypsin/ EDTA, and penicillin/streptomycin were obtained from Gibco BRL (Carlsbad, CA, USA). CyQUANT MTT Cell Proliferation Assay Kit (V13154), CyQUANT™ LDH Cytotoxicity Assay kit, Invitrogen™ eBioscience™ Annexin V-FITC Apoptosis Detection Kit (15581947), and Click-iT™ TUNEL Alexa Fluor™ 488 Imaging Assay for microscopy and HCS (C10245) were purchased from Thermo Fisher. Anti-BcL2, anti-αSMA, anti-β-actin, goat anti-rabbit Alexa 488 secondary, and goat anti-rabbit IgG H&L (HRP) were purchased from ABclonal. Mili-Q water was obtained using in-lab Milli-Q® IQ 7000 Ultrapure Water System (EMD Millipore, Bedford, MA, USA) and used for all experiments.

3.5.2. CELL CULTURE:

HS27 was used for in vitro assays purchased from ATCC. The cells are separately cultured in the DMEM medium, having 10% of FBS and 1% ABT following the manufacturer guidelines. Hs27 cells were used in the experiment and have passage numbers between 4-9.

3.5.3. SYNTHESIS OF IONIC LIQUID:

OA and CB-based ionic liquid has been synthesized using the methods published elsewhere [114]. In brief, the 1:2 molar ratio of OA and CB were taken separately. Then OA was slowly added to CB (1 mL/min) to avoid liquid dropping off the flask caused by the high pressure of CO_2 during escaping. The reaction was led to continue overnight at a temperature of 37 ºC. After the reaction, the solution turned cloudy and still had some foam on the surface. To remove the water and

remaining CO_2, the solution was put in a rotavapor at a 30 mbar with a temperature of 60 ºC for 2 hr and slowly decreased the pressure to avoid CO_2 moving back to the liquid. The final solution was obtained as clear. Later the solution was dried in a vacuum oven for 48 h. The final product was obtained as a highly viscous white solution.

3.5.4. PHYSICAL CHARACTERIZATION OF IONIC LIQUID:

The synthesized formulation's size and zeta potential were measured utilizing the principle of dynamic light scattering (DLS) using Malvern Instruments Ltd, Zetasizer-Nano ZS series [115]. To do the measurement, 100 µL of COA was dispersed in 10 mL of deionized water by sonicating in an ultrasonic bath for 5 minutes.

3.5.5. DRUG SOLUBILITY:

NAVI was dissolved in COA at a 5 mg/mL concentration. A series of dilutions were carried out with a concentration of 2.5, 1.25, 0.625, 0.3125, 0.15625, 0.078125, 0.0390625, 0.019531, 0.009765, 0.004882, and 0.002441 mg/mL respectively from the previously prepared NAVI/COA stock solution. The freshly prepared NAVI/COA absorbance was determined at 345 nm using a SYNERGY H1 96 plate reader. The plot of absorbance vs. the concentration of NAVI/COA was obtained using GraphPad Prism software.

3.5.6. CELLULAR UPTAKE & IN VITRO FIBROTIC MARKER VISUALIZATION:

Hs27 cell lines were used to study the cellular uptake of the COA and NAVI/COA [116]. 1000 cells were seeded in 96 well plates, among which 15 wells were prepared for three different treatment groups, including COA, Rhodamine B/COA, and control with medium only. Rhodamine B was used as the substitute for NAVI to visualize the cellular uptake and penetration capacity of the ionic liquid into the cell. The treatment was initiated after 48 h of incubation of the cells. Firstly,

Rhodamine B was dissolved in DI water at a 1 mg/mL concentration. Then 1:1 ratio of dissolved Rhodamine B and COA was mixed to prepare the treatment. After 6 h of incubation with different treatments, the medium from the well plates was aspirated out, and the cells were washed three times with 1×PBS followed by adding fresh 190 mL medium to each well plate. After the treatment, the live cells were stained by adding 10 µL of the Hoechst. After 20 min of incubation with Hoechst, the cells were washed with 1×PBS three times, and a fresh 200 µL medium was added after removing the old medium. The fluorescence images were collected at 546 nm for Rhodamine B and 410 nm for Hoechst.

We seeded 1 X 10^3 cells per well (used 12 wells) in 96 well plates [117]. After 24 h of seeding, we added TGF-β (10 ng/ml) for 24 h to 8 of the wells. After 24 hours of incubation, we washed with 3 X PBS each well and added COA/NAVI for 6 hours to 4 wells previously treated with TGF-β. After 6 h of treatments, all wells were washed with 3X PBS. Then we fixed all cells 10% normal donkey/goat serum, 0.3% Triton® X-100 for 20 min and permeabilized with 1X PBS, 1% BSA, 1% normal donkey/goat serum, 0.3% Triton X-100, and 0.01% sodium azide. After permeabilization, wells were washed with 3 X PBS, added anti-Col one and anti-α-SMA 1˚antibody (Ab), and incubated for 1 h at RT. After 1 h, we washed 5 X PBS and added goat anti-rabbit Alexa 488 2˚ Ab to each well for 45 min at RT. After a 2˚Ab incubation period, we washed 3 X PBS again, and images were taken using LSM 700. All images were taken at 20 X image magnification and a similar setting.

3.5.7 MITOCHONDRIAL MEMBRANE POLARIZATION ASSAY:

The Hs27 cells were seeded at 50000/wells density in 24 well-plate to evaluate the mitochondrial membrane potentials. After 24 h of incubation, cells were treated with 10 mg/mL TGF-β to make them fibrosis. Then, treatments to each well were applied and incubated for 6 hr. After the

treatment incubation, cells were collected in flow cytometry tubes and stained with two µM JC-1 (5,5',6,6'-tetrachloro-1,1',3,3'- tetraethylbenzimidazolylcarbocyanine iodide) dye according to the manufacturer's instructions (Mito Probe; Life Technologies, Grand Island, NY). Concomitantly, untreated cells treated with just the solvent were used as controls. Approximately 10,000 events (cells) were collected per sample using the Gallios flow cytometer (Beckman Coulter). The data acquisition and analysis were performed using Kaluza software [118].

3.5.8. *IN VITRO* PORCINE SKIN DIFFUSION:

The skin penetration studies were carried out using the skin sample from local porcine [119]. This is because they have almost similar properties compared to human skin. The samples were preserved at -20 ºC till use. When used for the experiment, the skin samples were thawed at 4 ºC overnight and then allowed to equilibrate at room temperature for 20 min. Once they were equilibrated, the skin samples were shaved carefully to remove any hair. The muscle and fat tissues were removed from the skin using a scalpel. The process was done very carefully, ensuring that the scalpel would not disturb the skin in any way. Care was taken to ensure that all the tissue samples had similar characteristics to maintain a consistent flow. For rehydration, the skin samples were submerged in 150 mL of PBS (pH 7.4) for rehydration (20 min). After rehydration, the skin was cut into 0.7x0.7 inches to fit into the ILC07 automated flow-through system (Permegear Inc. Hellertown, PA, USA). Skin samples were placed in each of the seven donor/receptor compartments. These skin samples were locked in place and pumped PBS directly over the skin at physiological temperature (37 ºC) with a 4 mL/h flow rate. This was done to mimic the typical flow condition of the body. A peristaltic multi-channel IPC pump was used from Ismatec, Zurich, Switzerland. The heating source used was Julabo BC4 from Julabo Pumps, Seelbach, Germany. The experiment was run for 8 h to study how much COA penetrated the skin. The residues were

collected in 20 mL scintillation vials after 0.5, 1, 2, 3, 4, 5, 6, 7, and 8 h. Adhesion Tapes were used for removing the Stratum Corneum (SC) layer of the skin using the strip and scrape method for finding out the drug left in the skin. After the diffusion process, the skin was carefully removed from the cells and placed on a flat metal surface. The skin was then cleaned to remove all excess formulation. After that, SC forcefully ripped off using tape ten times. The tape strips of SC were collected in conical tubes and dissolved in 10 mL of ethanol. Dermal layers were cut using surgical scissors for placing them in small pieces. Each tube was sonicated for 30 min. After that, the tubes were left at 4ºC overnight. The solution was centrifuged at 4ºC at 15000 rpm for 30 min. The supernatant was collected to measure drug absorbance using a UV spectrophotometer at 354 nm. Finally, the drug concentration was qualified using NAVI standard curve.

3.5.9. *IN VITRO* APOPTOSIS-NECROSIS STUDY:

The measurement of phosphatidylserine externalization could be used as an indicator for apoptosis [120]. The Annexin V-FITC kit (Beckman Coulter, Miami, FL, USA) was used. For this study, Hs27 cells were used. The cells were grown on 24-well plate dishes at a density of 1x105 cells using 1 mL media per well overnight in an incubator. After 24 h of seeding, we add TGF-β at a dose of 10 ng/mL. The next day we washed each well with 3 X PBS and treated with treatments, saline, DMSO, H_2O_2, NAVI (20 µM, and 50m µM), COA/NAVI (20 µM, and 50 µM), and COA (50%). Cells were treated with 0.1% DMSO (v/v) for the vehicle control study. For positive control, cells were treated with H_2O_2 (1.6 mM), and for negative control, cells were left untreated. After treating the cells, they were kept in the incubator for 24 hr. The cells were collected in pre-cooled 5 mL tubes for centrifugation after the incubation time. After centrifugation, the cells were resuspended in a 100 µL solution (1x binding buffer containing 1 µL of Annexin V-FITC reagent and 2.5 µL of Propodeum Iodide) prepared based on previous reports [121]. The cells were then

kept in the dark and incubated in 300 µL of 1x binding buffer. After incubation, each tube was examined through flow cytometry (Gallios, Beckman Coulter). FL1 and FL2 detectors captured fluorescence signals emitted by FITC and PI, respectively. Cells that showed PI positivity were identified as necrotic cells, and those that were FITC positive were identified as early apoptotic cells. Cells emitting FITC and PI signals were defined as the late apoptosis subpopulation [122]. The total percentage of apoptotic cells subpopulation was defined as the sum of both early and late phases of apoptosis (Annexin V-FITC positive), top and bottom right quadrants in the flow cytometric dot plots, respectively [64].

3.5.10. PROTEIN PURIFICATION AND WESTERN BLOT ANALYSIS:

For western blot (WB) analysis, both HS27 and fibrotic Hs27 cells were used. 1 million cells per well were placed in a 6-well plate dish. These cells were grown for 48 h in incubators. The media was changed once after 24 hours, and the treatments were added for 6 hours. The study included five different groups. The healthy Hs27 cells and one skin fibrosis cell were used as control. The skin fibrosis cells were treated with COA (50%), NAVI (50 µM), and COA/NAVI (50 µM). The homogenizer used homogenizer to ground the tissue into fine particles in animal tissue protein samples. Then we centrifuge at 3000 rpm for 20 min. After centrifugation, we discard the supernatant and add the cocktail buffer (RIPA+ protease inhibitor) to collect protein. The five groups collected the protein samples using a cocktail buffer (RIPA+ protease inhibitor). The solution was sonicated and vortexed at five-minute intervals 5-6 times. The solutions were kept on ice during intermediate times. The final system was then centrifuged at 4 ºC for 15 min at 3000 RPM. The supernatant was carefully collected, and the pellet was discarded. BSA standard curve was used for protein quantification from the collected samples using 280 nm wavelength light. The protein concentration was taken from the quantified samples as 100 µg/30 µL for loading in 12%

SDS-PAGE gel. Protein separation was done using the electrophoresis technique, and the proteins were transferred onto a PVDF membrane [123]. The PVDF membrane was blocked by incubating overnight in 5% BSA solution (in 1xTBST) at 4ºC for minimizing non-specific adsorption. After that, the membrane was washed two times with 1xTBST. The washed membranes were incubated for one hour at room temperature with diluted primary antibodies. β-actin was purchased from Invitrogen and BCL-2 from Abclonal. After incubation, the membrane was washed with TBST 5 times for removing all the unconjugated primary antibodies. The primary antibody conjugated membrane was placed in the secondary antibody-containing solution and incubated for an hour. The PVDF films were incubated in ECL (Thermo Scientific Super Signal ECL substrates) for development using BioRad ChemiDoc MP Imaging System. Protein quantification from the bands was performed using ImageJ software (National Institutes of Health, Bethesda, MD).

3.5.11. MOUSE TUMOR XENOGRAFT AND BODY WEIGHT:

The animal experiments were conducted following the protocols approved by the Institutional Animal Care and Use Committee of the University of Texas at El Paso (protocol no A-201910-1). The mice were bought from Charles River Laboratories International, Inc. All the purchased C57BL/6 (21-30 g) mice were six to seven weeks old. These mice were kept in pathogen-free conditions. The mice were injected with 3 doses of bleomycin (200 µg/dose) five days apart to create the fibrotic model. We waited two weeks to let the mice become fibrotic. The mice were divided into the following groups: untreated, NAVI (PO, 50 µM), COA (50%), and COA/NAVI (50 µM). Each mouse group was given its respective treatment every other day for 21 days after bleomycin-induced fibrosis. The treatments were carried out for three weeks. Mouse weight was measured daily during the treatment period and plotted as fibrotic area vs. body weight change in days. The fibrotic area was measured based on the following formula:

Fibrotic area (mm^2) = Length (mm)*Width (mm)

3.5.12. HISTOLOGY ANALYSIS:

For the histology analysis, all the necessary organs (spleen, heart, lung, kidney, liver, and tumors) were initially washed with saline and, after dehydration, fixed using 4% paraformaldehyde. These organ samples were sectioned into 10-15 µm pieces after embedding in optimal cutting temperature compound (OCT compound) [124]. Then these were stained with hematoxylin and eosin (H&E). For H&E, the protocol was developed from previously described papers [125]. Initially, the slides were rinsed three times (three minutes each time) using xylene and blotted. These slides were then dipped in 100% ethanol for three minutes three times and then in 90% and 85% ethanol for three minutes one time. The washing was carried out with DI water for five minutes. These were then dipped in hematoxylin one more time for 3 min. After that, all the excess hematoxylin was wiped away using Kim Wipes along with all the oxidized particles. The slides were then rinsed with DI and placed in tap water for 5 min to allow the stains to develop. The slides were then dipped 8-10 times in acidic ethanol solution for distaining. The slides were rinsed with DI two times. The slides were entirely dried before starting eosin staining. The slides were initially dipped in eosin solution for 30 seconds for staining. This was followed by dipping in 95% and 100% ethanol solutions three times for three minutes. These slides were then placed in xylene solution for 15 min. Coverslips were placed on these using paramount and allowed to dry overnight. The stained slides were examined using light microscopy using an objective lens (160x). Histological analysis was carried out for determining toxicity and efficacy of COA in skin fibrosis treatment. The analysis was carried out to see if the COA had caused any tissue damage or some other pathological effect.

3.5.13. CLINICAL BIOCHEMISTRY PANEL ANALYSIS:

In the case of animal studies, animals were randomly divided into four different groups. Each group contained three mice. To study the skin fibrosis, COA (50%), NAVI (50 µM, PO), or COA/NABI (50 µM) of 30 µL were administered to each of the mice. The study was continued for 14 dosages and was administered during these 28 days at one-day intervals. For the study, C57BL/6 (21-30 g) of six- to seven-week-old were purchased from Charles River Laboratories International, Inc. These animals were kept under pathogen-free conditions till bleomycin (20 µg/dose) was injected into each mouse three times with five days apart. These mice were sacrificed on day 29 of treatment, and 0.5-0.6 mL of whole blood was collected from the heart of each specimen. During the blood collection process, 0.3 mL was collected in a low molecular weight heparin-containing tube for counting skin fibrosis cells in the blood. The biochemistry panel analysis used the remaining 0.2-0.3 mL of blood serum. To prevent the blood from coagulating EDTA containing K3EDTA bottles, ACUETTER, Greiner, Austria bottles. 0.5 ml of the whole blood sample was taken in a Serum Sep Clot Activator bottle (VACUETTER, Greiner, Austria) and centrifuged at 3000 rpm for 15 min. The serum (supernatant) was collected for the biochemistry analysis. Serological parameters of the kidney and liver were determined. Furthermore, we analyzed various enzymes like aspartate aminotransferase (AST), blood urea nitrogen (BUN), alkaline phosphatase (ALP), alanine aminotransferase (ALT/GPT), creatinine (Cr), and total protein (TP). We also ran a total blood count to analyze blood functions like red blood cells (RBC), white blood cells (WBC), platelet (PLT), and hemoglobin (Hb). GraphPad Prism was used to analyze results from the biochemical assay. The total blood count was done using an Element-DC by HESKA chemical analyzer and Hemavet from Drew scientific. (Drew Scientific, Miami Lakes, FL).

3.5.14. IMMUNOHISTOCHEMISTRY ANALYSIS OF PROTEIN EXPRESSION:

After freezing, the fixed tissues were cut into 20 µm size pieces using cryo-tome. The cut tissues were kept in antifreeze solution till immunohistochemistry experiments. Immunohistochemistry was performed based on a protocol modified from fisher scientific and Abcam. The modified protocol was optimized based on our laboratory's specifications. Initially, the tissues were washed with PBS and washing buffer (400 µL). After that, the tissues were incubated in a 400 µL blocking buffer for 45 min to minimize non-specific blocking. The composition of the washing buffer was 0.1% BSA in 1-X PBS. At the same time, the blocking buffer was prepared by taking 10% donkey/goat serum and 0.3% Triton® X-100 in 1X PBS. According to the manufacturer's specification, the unconjugated primary antibodies were initially mixed with dilution buffer to perform the immunostaining. The tissues were incubated overnight at 4 ºC with the diluted primary antibodies. The next day excess primary antibodies were washed away using washing buffer. Each tissue was washed four times for five minutes. Then the tissues were incubated for 1 h at room temperature in a light protected environment with secondary antibodies. The unbonded secondary antibodies were removed using the washing buffer two times for 5 min. After that, the tissues were dried in air and mounted using the mounting media. The mounting was done on a transparent coverslip, and confocal images at 20x magnification were taken using LSM 700 instrument. Finally, all the images were analyzed using ImageJ software.

3.5.15: TUNEL ASSAY:

The *in-situ* apoptosis process was analyzed using Alexa Fluor™ 488 dyes with the Click-iT™ Plus TUNEL Assay. For the TUNEL assay, the protocol from the vendor was used. Initially, all the skin tissues were washed to remove hairs. These cleaned tissues were then fixed using 4% paraformaldehyde (PFA) at 37ºC for 2 h. The fixed tissues were then washed for five minutes with PBS. After washing, the fixed tissues were incubated in PBS with 1X Proteinase K solution

(Component H in the assay kit diluted in a 1:25 ratio) for 15 min. The fixing and washing steps were repeated. This time the 4% PFA fixing was done for 20 min. The DNA strands were broken using DNase I diluted in 1X DNase reaction buffer for 30 min at room temperature. The reaction buffer was prepared by mixing 20 mM Tris-HCl of pH 8.4 with two mM $MgCl_2$ and 50 mM KCl. Each of the tissue samples was then washed with DI. Then 100 µL of TDT reaction buffer (Component A in the kit) was added to each well containing the washed tissue sample. After incubation for 10 min, the TDT reaction buffer was removed, and 50 µL of the TDT reaction mixture was added to each well and left for 1 hr. The tissue wells were rinsed with DI after the incubation process. with mild shaking; Permeabilization was carried out with PBS solution containing 3% BSA and 0.1% Triton™ X-100 for 5 min. The wells were rinsed with DI again. Then 50 uL of freshly prepared Click-iT™ Plus TUNEL reaction mixture was added to each well and kept in the dark for 30 min. Then the mixture was removed, and PBS with 3% BSA was added to each well. After 5 min, the wells were washed with PBS. The tissues were placed on a slide and covered with mounting media. Then a coverslip was placed on top to prevent air contact, and the system was incubated for an hour at 4 ºC. Finally, the images were obtained using LSM700 confocal microscope with 20x magnification while keeping all settings fixed.

3.5.16. STATISTICAL ANALYSIS:

To ensure reproducibility, all experiments were repeated three times. The results were reported for the mean ± SD of these three experiments. GraphPad Prism (GraphPad Software Inc.) was utilized for performing the Student T-test, one-way analysis of variance (ANOVA), and two-way ANOVA. For all statistical analyses, when the P-value was < 0.05, it was considered significant.

3.6. ACKNOWLEDGEMENT:

Research reported in this publication was supported by the Research Centers at Minority Institutions grant funded by the National Institute on Minority Health and Health Disparities of the National Institutes of Health under Award No. U54MD007592. We also acknowledge Cancer Prevention Research Institute of Texas (CPRIT) funding through Texas Regional Excellence in Cancer Award (TREC) under Award No. PR210153. We want to thank the Staff of the Cytometry, Screening, and Imaging (CSI) Core Facility for the services and facilities provided. This Core Facility is supported by grant 8G12MD007592 to the Border Biomedical Research Center (BBRC) from the National Institutes on Minority Health and Health Disparities (NIMHD), a component of the National Institutes of Health (NIH). Its contents are solely the authors' responsibility and do not necessarily represent the official views of NCRR or NIH.

CHAPTER 4: ORAL DELIVERY OF BCL-2 INHIBITOR REDUCED PACLITAXEL RESISTANCE MDA MB 231 TUMOR IN A MOUSE MODEL

4.1 ABSTRACT:

Cancer cell resistance to anti-cancer drugs can be caused by various causes, including individual genetic variations, particularly in tumoral somatic cells. Drug resistance can also be acquired, and it can be caused by various processes, such as multi-drug resistance, cell death inhibition (apoptosis suppression), changes in drug metabolism, epigenetic and drug targets, improved DNA repair, and gene amplification. However, there are now unparallel opportunities to understand and overcome chemotherapeutic resistance using predictive biomarkers to enable patient stratification and the clinical assessment of rational therapeutic drug combinations. Apoptosis plays a crucial role in the tumor microenvironment and is an escape mechanism of tumor cells from therapy and immune surveillance cells. Our research aimed to overcome the drug resistance mechanism by targeting the intrinsic apoptosis pathway by inhibiting BCL-2 anti-apoptotic protein in cancer cells and animal models. In this pilot study, we showed potential mechanistic explanations for the association between the Paclitaxel drug resistance mechanism and how to inhibit the MDA MB 231 PTXR tumor growth via BCL-2 inhibitor. The tumor inhibition and reversal of drug resistance mechanism were evaluated in the C57BL/6 mouse model dosing with β-Glucan mediated Navitoclax oral delivery.

Keywords: Drug resistance; Cancer therapy; Oral delivery; BCL-2 inhibitor.

4.2. INTRODUCTION:

Drug resistance is common when cancer cells grow resistant to medicinal therapies. This theory was first proposed when bacteria developed resistance to specific antibiotics, but similar mechanisms have been discovered in other diseases, including cancer [126]. Some drug resistance mechanisms are disease-specific, but others, such as drug efflux, which is found in microorganisms and human drug-resistant tumors, have evolved to be disease-specific. Many tumors are initially responsive to drugs, but they can develop resistance over time due to mechanisms such as DNA mutations and metabolic changes that enhance medication inhibition and degradation. Due to current treatments, drug resistance produces in cancer, including drug inactivation, drug target alteration, drug efflux, DNA damage repair, cell death inhibition, and the epithelial-mesenchymal transition (EMT) [127,128]. As a result, novel therapeutic techniques aimed at addressing the essential enabling traits and acquired capacities that turn normal cells and tissues into cancers began to emerge [129,130]. Recent investigations have established a foundation for future research into the complex link between cancer resistance and TME in pathological settings. In cancer treatment, drug resistance is still a significant clinical concern [131]. One way tumor cells develop resistance to cytotoxic medicines and radiation is through apoptosis resistance. Apoptosis is a well-ordered and pre-programmed cell death mechanism. Death receptor activation on cell surface membranes (extrinsic pathway) or a set of biological events mainly processed at mitochondria (intrinsic pathway) can both initiate apoptosis (intrinsic pathway) [132]. Apoptosis' relevance in carcinogenesis and cancer treatment has been shown. Defects in apoptosis can increase the number of malignant cells in a tumor population [133].

Therefore, there needs to be an alternative approach of different therapeutic activating apoptosis in the drug-resistant tumor. This pilot study utilizes consistent Paclitaxel (PTX) dosing to develop

the drug-resistant cell line. After four months of consistent dosing, the MDA MB 231 PTXR cells were created for drug resistance mechanism and therapeutic efficiency Navitoclax (NAVI). Breast cancer, ovarian cancer, and lung cancer are treated with paclitaxel [134]. It's also used to treat Kaposi's sarcoma, linked to AIDS. The injection of paclitaxel (with polyoxyethylated castor oil) may significantly reduce the number of white blood cells (WBC) in our blood [135]. This increases our chances of contracting a severe infection. Navitoclax is a small synthetic molecule with the orally active antagonist of a subset of B-cell leukemia 2 (BcL-2) family of proteins with potential anti-cancer efficacy [56]. Navitoclax binds to the apoptotic suppressor proteins BcL-2, BcL-xL, and Bcl-w, which are overexpressed in several malignancies, including lymphoma, breast cancer, lung cancer, prostate cancer, and colon cancer, and have been been been associated with tumor drug resistance [58]. These apoptosis suppressors are inhibited, which prevents them from interacting with the apoptotic effectors Bax and Bak proteins, inducing apoptosis in cells overexpressing BcL-2, BcL-xL, and Bcl-w.

Beta-Glucans (BG) are a group of β-D-glucose polysaccharides found naturally in the cell walls of cereals, bacteria, and fungus, with physicochemical properties that vary greatly depending on the source [136,137]. BG in this study is used with low molecular weight (179 K Da) origin from burley. The project's novelty is considering BG as a better vehicle for oral drug delivery of chemotherapeutic proteins and antibodies. The treatments were PTX (IV), NAVI (PO), and BG/NAVI (PO). Here, we identify BG/NAVI oral delivery compared to only NAVI (PO) and PTX (IV), which inhibit tumor volume and show better therapeutic efficiency in the PTX resistance tumor model. Our analysis shows that targeting the mitochondria by inducing apoptosis is another alternative way to treat drug resistance in the breast cancer tumor model.

4.4.3. RESULT & DISCUSSION:

4.3.1 PACLITAXEL RESISTANCE MDA MB 231 CELLS EXPERIENCE APOPTOSIS DUE TO NAVI TREATMENT:

Tumors are composed of heterogeneous cell populations, including the subset of undifferentiated cancer cells with stem cell-like features [138,139]. Also, different cytokines and growth factors active during malignant tumor progression become dysfunctional. Epithelial to mesenchymal transitions (EMT) are trans-differentiation programs that trigger the dysregulation of these signaling cytokines and growth factors [139]. Also, cancer cells develop drug resistance to chemotherapeutics via several cell transmembrane proteins. Most of the proteins belong to the ATP-binding cassette (ABC) transporter family. Therefore, drug resistance development is a common mechanism for cancer cells during development and metastasis. Treating the drug resistance cells with different chemotherapeutics or inhibiting the tumor progression is an alternate way to overcome the drug resistance process. This study used NAVI to evaluate how it tackles the paclitaxel drug resistance mechanism. The MDA MB 231 and MDA MB 231 PTXR cells were cultured and seeded at 10000/wells of a 24-well plate. Treatments were NAVI, NAVI/MtP, PTX, and PTX/MtP. Cells were treated for 24 h and washed with 3 X PBS the next day.

Then the cells were separated and prepared according to the method described in vitro apoptosis-necrosis study section. Cell samples were run through a Gallios cell sorter, and 10000 events were measured for each sample. The MDA MB 231 cells showed 55% apoptosis than H_2O_2 positive control (figure 14(a)). But NAVI/MtP and NAVI showed similar cell apoptosis activity in either MDA MB 231 or PTXR cells (both figures a & b). Both PTX & PTX/MtP only induced around 15% apoptosis in MDB MB 231 cells (figure 14(b)). Lower apoptosis by paclitaxel is because, until recently, it’s not clear what will the clinically relevant dose for cell culture studies. Doses are

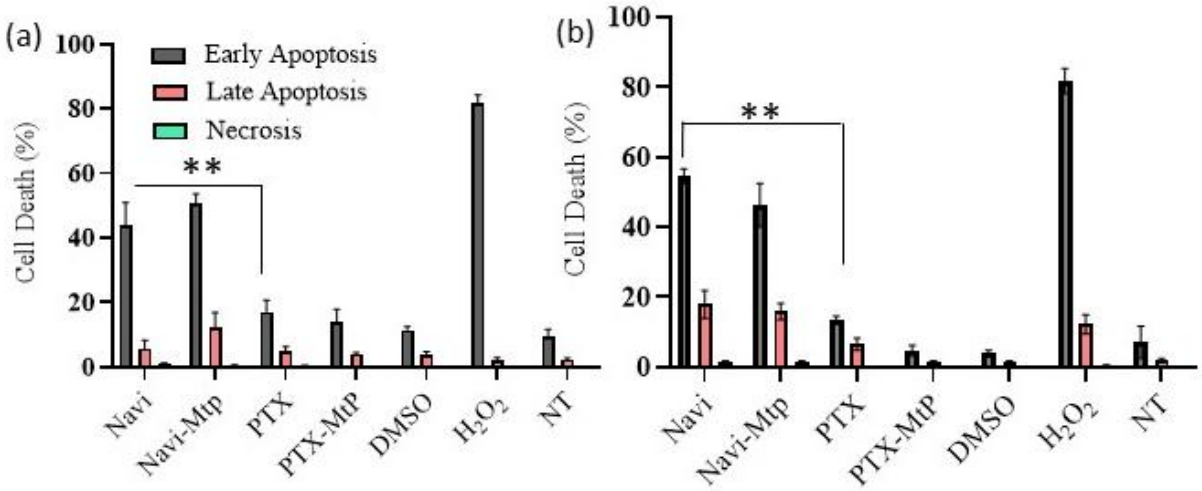

Figure 14: Tumor gets drug resistance due to consistent chemotherapeutic exposure.

To evaluate how Navitoclax reverses the paclitaxel resistance of MDA MB 231 cells. To compare the drug resistance reversal process, both MDA MB 231 and MDA MB 231 PTXR cells were cultured and evaluated for apoptosis. To evaluate the drug mechanism, NAVI and PTX were conjugated with mitochondrial targeting peptide (MtP) to induce apoptosis via the intrinsic apoptotic pathway. Therefore, treatments were NAVI, NAVI/MtP, PTX, PTX/MtP, DMSO, H_2O_2, and untreated (UT). (a) MDA MB 231 cells were plated 10000/well in a 24-well plate and allowed 24 h post-seeding. After 24 h, the treatments were added for another 24 h. After the treatment incubation, cells were trypsinized and stained with Annexin-V and PI in iced cold conditions. Compared to H2O2, NAVI and NAVI/MtP showed 55% apoptosis. But PTX and PTX/MtP showed lower apoptosis percentages and less anti-cancer activity than NAVI. (b) In PTXR cells, NAVI and NAVI/MtP showed similar apoptosis events of 50-55 % compared to MDA MB 231 cells. Data represent mean ± SD, where n=3. * Indicates statistical significance with $p < 0.05$; *** indicates statistical significance with $p < 0.001$.

different depending on disease condition and chemotherapeutic regimen. Also, the concentration of PTX goes down due to rapid clearance by the cell plasma membrane. Interestingly, NAVI accumulates via mitochondria and triggers the intrinsic apoptosis pathway. Therefore, the role of NAVI in tumor volume inhibition will be further evaluated in MDA MB 231 and MDA MB 231 PTXR tumor models.

4.3.2 IN VITRO SOLUBILITY, STABILITY & IN VIVO BIODISTRIBUTION OF ORAL ADMINISTRATION NAVI AND BG/NAVI IN SD RAT:

Beta-glucan (β-glucan, BG) is a soluble fiber readily available from barley oat grains that have been gaining interest due to its bioactive and multiple functional beneficiaries. Its beneficial role in dyslipidemia, hypertension, insulin resistance, and obesity is continuously documented [136]. BG/NAVI solubility and room temperature stability were measured by measuring absorbance at 345 nm. NAVI was dissolved in BG solution at 1 mg/ml and serially diluted using DI water at 0.5, 0.25, 0.125, 0.06250, 0.03125, and 0.015625 mg/ml. Figure 15 (a) represents absorbance taken of all serially diluted samples along with blank. Data plot here (absorbance – blank) vs concentration. We know absorbance is inversely proportional to transmittance. Therefore any absorbance value below 1 represents NAVI solubility in BG. From figure 15(a), we observe that NAVI is soluble in BG at a concentration of around 575 μg/ml. Then, we further ran a stability test of BG/NAVI at room temperature for 6 h. This time we only consider 500 μg/ml BG/NAVI dosing. We again measure the absorbance of BG/NAVI and only BG as blank at 0, 0.5, 1, 2, 3, 4, 5, and 6 h time-point. Figure 15(b) represents absorbance recorded at 345 nm. The absorbance is stable for 6 h and indicates BG/NAVI is stable and no precipitation observes during the experiment.

Next, the bio-distribution of NAVI and BG/NAVI was evaluated. NAVI has thrombocytopenia, a condition in which patients have a low blood platelet count [140]. And this severe toxicity has been reported in multiple studies, and clinical trials in phases [58,103,141]. Therefore, an alternate approach will be the oral administration of NAVI. NAVI is an orally bioavailable drug. In this study, β-glucan was used as a carrier for NAVI transportation.

Low molecular weight BG (179 KDa) was used, and the hydrogel was prepared at a 2 mg/ml concentration. Then the single NAVI dose was measured (500 mg/kg), and the rest of the BG hydrogel was added to the dose to make it 100 μl. And for NAVI only, NAVI stock was diluted into DI water to make a dose of 100 μl containing 500 mg/kg of NAVI. During experiment day,

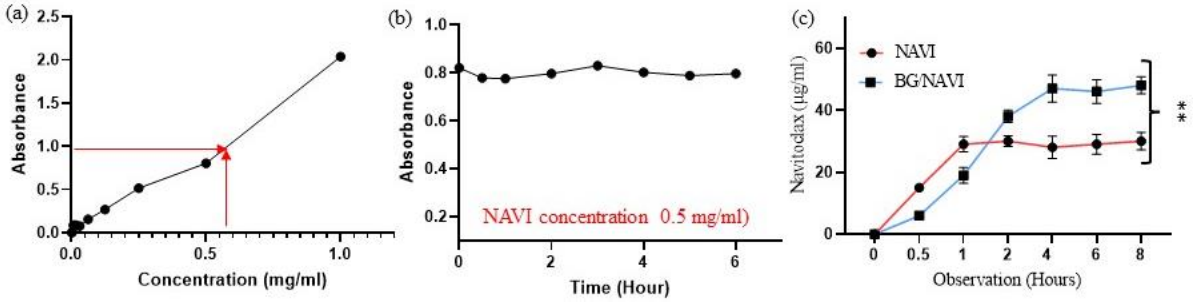

Figure 15: Drug solubility and pharmacokinetic study.

(a) Solubility of NAVI in BG oral formulation. Absorbance value y-axis indicated NAVI is soluble at around 560 µg/ml of BG. (b) Absorbance was measured at 0, 0.5, 1, 2, 3, 4, 5, and 6 h of BG/NABI (500 µg/ml) using a 96 UV plate reader. Absorbance value is consistence and indicates BG/NAVI formulation is stable at RT over 6 h time-point. 6 SD rats were randomly distributed into 2 groups, NAVI (Po) & BG/NAVI (PO). NAVI & BG/NAVI oral gavage single dose of 500 µg/dose/animal. Blood samples were collected via tail puncture at 0, 0.5, 1, 2, 4, 6 & 8 h time of oral gavage. A total of 50 µl of blood samples was collected and quantified in a UV plate reader at 345 nm. Background noise is subtracted from the absorbance value and quantified using the NAVI standard curve. NAVI (PO) C_{max} and T_{max} were two h and 38 µg, respectively. And for BG/NAVI (PO) C_{max} and T_{max} were 4 h and 47 µg. BG has slower transportation initially but can transport a higher percentage of NAVI than NAVI (PO) administration. Data represent mean ± SD, where n=3. * Indicates statistical significance with $p < 0.05$; *** indicates statistical significance with $p < 0.001$.

both NAVI and BG/NAVI were given oral gavage to each animal. 6 SD rats were taken from our animal stock aged between 3-4 months old. Right after oral dosing, the blood sample was collected at 0, 0.5, 1, 2, 4, 6, and 8 h. During collecting tail vein punctures, the animals were taken care of and given much comfort according to the animal protocol approved by the IACUC of the University of Texas at El Paso. A total of 50 µl of blood samples were collected each time, and NAVI concentration was quantified using a UV plate reader at 345 nm. In figure 15 (c), the NAVI bio-distribution of both oral gavage of NAVI and BG/NAVI was graphed. Data signified NAVI transport through GI track and reached C_{max} (maximum concentration) with 1 h of post-gavage. And BG/NAVI took longer to transport and reach its C_{max} 4 h of oral gavage. But BG/NAVI can transport 1.3 fold higher NAVI via GI tract than free NAVI transport. For 8 h observation, the

concentration of NAVI was consistent in both doses, and no body clearance was observed until 8 h time. Our bio-distribution aligns with clinical findings showing the peak concentration in humans at 9 h and a half-life of 17h with a simple first-order release profile [86]. This study confirms that BG can transport a higher NAVI percentage than free NAVI. The initial NAVI stability experiment in BG confirmed BG is suitable for transporting drugs, proteins, and antibodies via the GI tract.

4.3.3 PTXR MDA MB 231 TUMOR XENOGRAFT AND TUMOR VOLUME DURING TREATMENT:

The rodent tumor animal model is a strong tool to study drug dosing, therapeutic efficiency, and molecular pathways to target a disease. Both MDA MB 231 and MDA MB 231 PTXR cells created the tumor model in this study. Both cells were cultured and prepared a dose of 10×10^{6} cells/dose/animal for subcutaneous injection. 3 weeks after SC injection, the treatments were administered in 4 doses 5 days apart when the tumor is visible. Treatments groups were untreated, PTX, NAVI, and BG/NAVI. PTX was administered as IV, and BG/NAVI and NAVI were given oral gavage. During treatment for 20 days, the tumor volume was measured using slide calipers. The tumor volume was measured every other day of the treatment period and graphed to represent treatment efficiency. After injection, the animals were allowed to stay 3 more weeks to allow the tumor to grow. When the tumors were visible with naked eyes, the treatments were given to each group. 14 mice were chosen and initially distributed into 2 groups based on their tumor type, PTXR and 231. Then PTXR group was again divided into 4 treatment groups, untreated (UT), PTX, NAVI, and BG/NAVI. 231 groups were divided into 3 treatment groups (UT), PTX, and BG/NAVI.

Figure 16 (a) shows that the tumor volume changed during the treatment of the PTXR tumor. In 20 days, the untreated tumor volume increased to 95% of its initial volume. In the case of PTX treatment, the tumor volume decreased by 4-5% only. But the tumor volume was inhibited by 55%

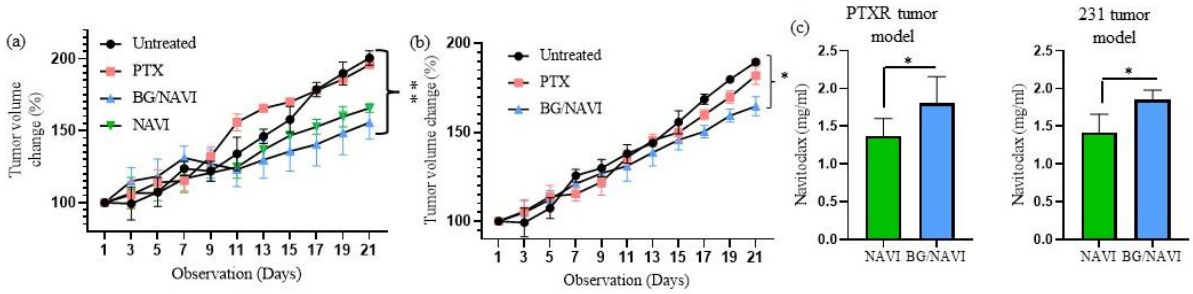

Figure 16: The treatments were paclitaxel (IV), NAVI (PO), and BG/NAVI (PO).

A total of 4 treatments were given 5 days apart. The tumor volume was measured using slide calipers from the beginning of treatment. In figure (a) left graph represent the tumor volume change in the PTXR tumor, and the right represents MDA MB 231 tumor volume change. (b) In PTXR tumors, due to BG/NAVI and NAVI treatments, the tumor volume reduced by 60% and 45% compared to the untreated group at day 20. In MDA MB 231 tumor, BG/NAVI treatment reduced the tumor volume by 35% compared to the untreated group at day 20. (c) Navitoclax concentration was quantified from serum collected after an animal experiment. Both PTXR and MB 231 tumor model BG/NAVI transport higher NAVI concentrations than NAVI (PO). This quantification proves that BG is a better vesicle for oral transportation of drugs, proteins, and antibodies. Both animal models have both BG/NAVI transport of 1.81 and 1.85 mg/ml of Navitoclax via the GI tract. Data represent mean ± SD, where n=3. * Indicates statistical significance with $p < 0.05$; *** indicates statistical significance with $p < 0.001$.

in BG/NAVI treatment and 45% in only NAVI treatment compared to untreated tumor volume. In MDA MB 231 tumor (figure 16 (b)), the untreated tumor reached an 85% increase than its initial volume within 20 days of treatment. And PTX treatment can inhibit only 5% of the tumor volume; the dose seems not enough to kill the tumor cells. Interestingly, BG/NAVI still showed 35% inhibition of tumor volume. Therefore, BG/NAVI can inhibit tumor growth in both tumors compared to only NAVI, and PTX treatment. Next, the NAVI transportation was quantified via the GI tract in the blood serum. After 4 doses of administration, the animals were sacrificed, and blood was collected via heart puncture. During the blood collection process, 0.3 ml was collected

in a low molecular weight heparin-containing tube for counting blood cell content. The biochemistry panel analysis used the remaining 0.2-0.3 ml blood serum. The serum was separated via centrifugation at 3000 rpm for 15 minutes. The serum was then quantified using UV absorbance at 345 nm. The background absorbance was subtracted, and NAVI absorbance was measured. Then NAVI concentration was quantified with a pre-measured NAVI standard curve. In figure 16(c), the NAVI concentration was graphed. The NAVI transportation was higher in BG/NAVI treatment than in both tumors compared to only NAVI oral gavage. The NAVI concentration in MDA MB 231 tumor was 1.85 mg/ml (62 mg/kg) for BG/NAVI dosing compared to 1.45 mg/ml (48 mg/kg) for NAVI dosing. And in PTXR tumors, 1.81 mg/ml (60 mg/kg) for BG/NAVI dosing compared to 1.48 mg/ml (49 mg/kg) for NAVI dosing. In both cases, the BG/NAVI concentration is statistically significant compared to the NAVI concentration. The concentration of NAVI (figure 16(c)) is also following the tumor inhibition in animal tumor volume (figure 16(a, b)). BG/NAVI dosing has the potential for tumor inhibition and higher navigation of navitoclax via the GI tract. Further, serum and blood toxicity was measured with serum biochemistry and complete blood count analysis.

4.3.4 SYSTEMIC TOXICITY EVALUATION OF PTXR MDA MB 231 TUMOR MOUSE MODEL:

Both NAVI and PTX have been reported for toxicity issues. Therefore, one of the concerns of this study was drug-induced toxicity in the animal model. The severity of Navitoclax published in phase I clinical study on multiple disease model diffuse large B-cell lymphoma (DLBCL), small lymphocytic lymphoma (SLL), chronic lymphoid leukemia (CLL), follicular lymphoma (FL), mantle-cell lymphoma (MCL), and classic Hodgkin's lymphoma, NK/T-cell lymphoma, and marginal zone lymphoma [55,103,105,142]. Compared to continuous dosing, thrombocytopenia

in patients is much higher with intermittent dosing. The authors also discuss thrombocytopenia caused by BCL-xL inhibitor; Navitoclax was developed based on preclinical investigations with lymphocytic malignancies. Authors believe that 250 mg/day of navitoclax in continuous dosing will be effective in phase II clinical study [55,143]. Therefore, oral administration of NAVI is one of the alternative routes for avoiding severe toxicity.

On the other hand, paclitaxel binds to the B subunit of tubulin selectively and reversibly, facilitating tubulin polymerization and the creation of stable microtubules even in the absence of guanosine triphosphate as an energy source ref. This action causes the tubulin dimer-polymer balance, favoring polymer assembly [144,145]. At the molecular level, PTX-associated toxicity is responsible for hyperphosphorylation of BcL-2, apoptosis mediated by caspase 3 and caspase 8, and increased BAX[146,147].

To evaluate how toxic the treatments were, the serum was analyzed. The serum panel identified six functions: total protein, glucose level, ALT, ALP, creatinine, and BUN. Figure 17 (a) shows the serum functions for MDA MB 231 and MDA MB 231 PTXR. Compared to the untreated group, NAVI showed higher kidney function. Also, PTX showed similar values in the serum analysis compared to the untreated group. Then the complete blood analysis also resembles that both NAVI and PTX showed toxicity. The platelet (PLT) number was lowered for both treatments. The reduction of platelet is lower for PTX treatment compared to NAVI treatment (figure 17(b)). The serum and complete blood count analysis signified the slight toxicity of PTX (IV) and NAVI (PO) treatment. Also, the WBC content went down in PTX treatment for both tumor types. The reduction of WBC is clinical toxicity reported against PTX [148]. Surprisingly, the tumor volume was inhibited due to NAVI and BG/NAVI treatment. Therefore, NAVI targeting mitochondria and activating apoptosis can reverse drug resistance and inhibit tumor volume. Thus, the tumor

microenvironment was further evaluated on how NAVI can inhibit tumor progression.

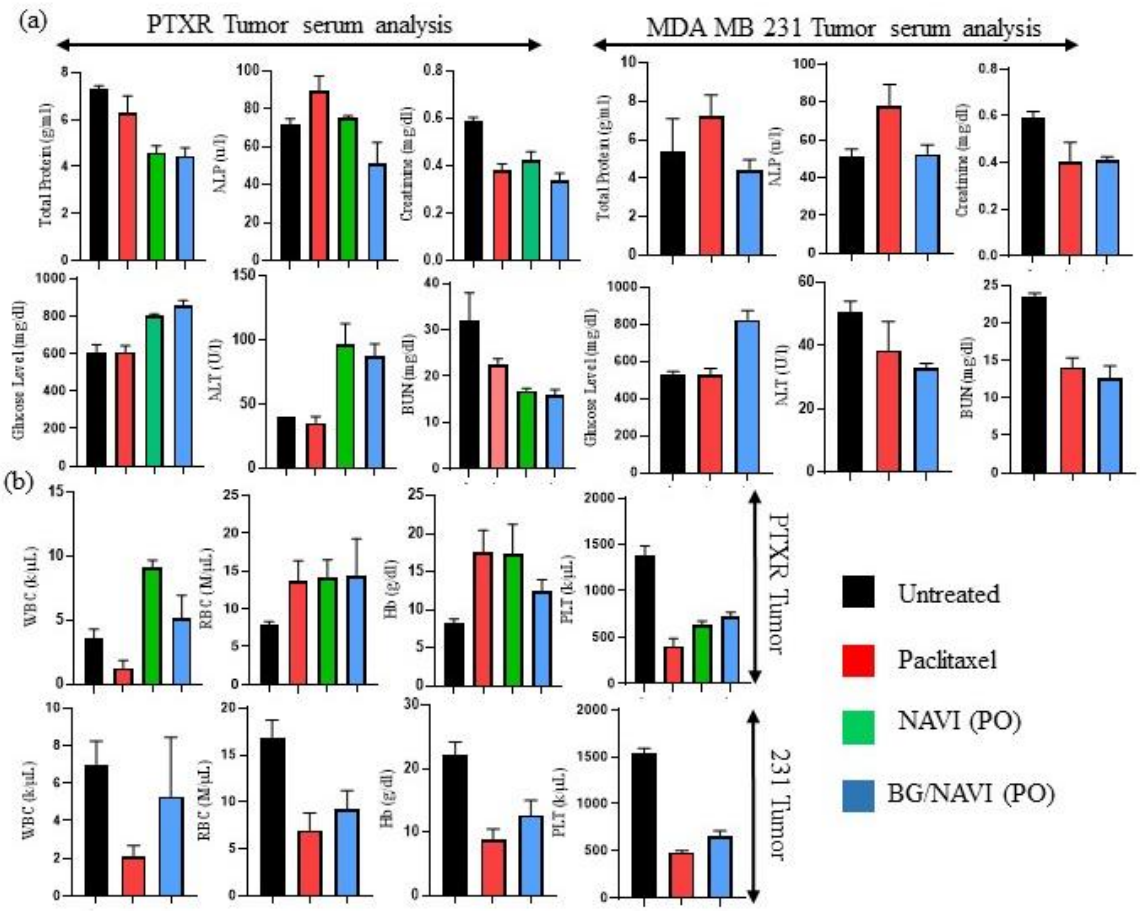

Figure 17: Serum and complete blood analysis were conducted to evaluate serum toxicity.

(a) Serum was separated via centrifugation at 3000 rpm for 15 minutes in serum analysis. The serum samples were analyzed using the Heska panel. The serum functions like total protein, blood glucose, ALT, ALP, BUN, and creatinine were analyzed and graphed according to tumor types and functions. The glucose and ALT values were higher than the untreated group in the PTXR tumor type. All other serum functions were within the normal range of healthy mice. (b) Blood count, RBC, WBC, hemoglobin, and platelet functions were analyzed and graphed to evaluate blood toxicity. The platelet (PLT) numbers were low in PTX, NAVI, and NAVI/BG treatment groups. This PTL number signifies the cytotoxicity of both PTX and NAVI in cancer treatment.

4.4. CONCLUSION AND FUTURE DIRECTION:

Despite the intimidating array of drug resistance mechanisms and the complexities caused by

tumor heterogeneity and microenvironment interactions, chemotherapeutics, and molecularly targeted therapies are effective in many disease settings, significantly prolonging patients' lives or, in some cases, producing cures. The current issue is to apply what we've learned from traditional cytotoxic medications and the first wave of molecularly targeted treatments to make the most of the growing arsenal of anti-cancer therapy. *In vitro* and *in vivo* synergy between drugs is frequently postulated in rational therapeutic combinations; nevertheless, targeting the same pathway numerous times may give a very straightforward ‘escape route' for the tumor in some circumstances. In this pilot study, we were able to show that tumor resistance can be reversed. The PTX was used as a positive control for creating drug resistance, and BG/NAVI oral delivery showed better output against drug resistance. This study provides a link to evaluate further how multiple drug combinations or drugs alone can determine the mechanism of action of drug resistance. Improved in vitro and in vivo models, such as patient-derived xenografts, that more closely model tumor-stroma interactions are needed to assess drug resistance, evaluate potential drug combinations, and determine the therapeutic value of predictive biomarkers. However, cell lines are often a good starting point. We need further study humanized tumor models and combination therapy to evaluate drug resistance reversal mechanisms. Further, the immune-cell populations and other drug resistance markers like growth factors can be evaluated in concurrent studies. This pilot study also opens the window for combination therapy applied to the animal model to elucidate the heterogeneity of drug resistance mechanisms. Following that, such preclinical research must be tested in the clinic, necessitating the development of "smart" trials that incorporate cutting-edge molecular pathology tools. Also piloted by the oncomine comprehensive panel (OCP), representing a streamlined and broadly applicable targeted NGS system to advance precision oncology, next-generation sequencing (NGS) enables genome-wide

personalized oncology efforts with the specialty and infrastructure necessary for identification and prioritization of tumor genome variants.

4.5. MATERIALS & METHODS:

4.5.1 MATERIALS AND CHEMICALS:

Navitoclax was obtained from TargetMol. Paclitaxel received from Sigma. Low molecular weight β-Glucan was obtained from Sigma Aldrich. Dulbecco's Modified Eagle Medium (DMEM), Dulbecco's phosphate buffer saline (DPBS), fetal bovine serum (FBS), trypsin/ EDTA, and penicillin/streptomycin were obtained from Gibco BRL (Carlsbad, CA, USA). Invitrogen™ eBioscience™ Annexin V-FITC Apoptosis Detection Kit (15581947) and Click-iT™ TUNEL Alexa Fluor™ 488 Imaging Assay for microscopy & HCS (C10245) were purchased from Thermo Fisher. Anti-Col1, anti-BCL-2, anti-αSMA, anti-β-actin, goat anti-rabbit Alexa 488 secondary, and goat anti-rabbit IgG H&L (HRP) were purchased from Abclonal. Mili-Q water was obtained using in-lab Milli-Q® IQ 7000 Ultrapure Water System (EMD Millipore, Bedford, MA, USA) and used for all experiments. Mitochondrial targeting peptide was ordered from GenScript and stored at -20 ˚c in powder form for stability and extended storage.

4.5.2 CELL CULTURE AND PACLITAXEL RESISTANCE CELL:

MDA MB 231 Luc cell was used for in vitro and in vivo assays purchased from ATCC. The cell was separately cultured in the DMEM medium, having 10% of FBS and 1% ABT, following the manufacturer guidelines. The cell was made paclitaxel resistance with consistent exposure for four months at a 10 nM /ml concentration. When the cell death was observed to be higher during the drug resistance process, the dose was replaced with a fresh regular cell culture medium. After regaining the desired cell number, the paclitaxel was again introduced. And this process was

maintained for four months to make the cell paclitaxel-resistant. Both MDA MB 231 and its PTXR cells were used for the study, and passages 5-8 were used in vitro and in vivo.

4.5.3: FORMULATION OF BG/NAVI:

β-Glucan (BG) was dissolved in 2 mg/ml of DI H_2O. With continuous rotation and 40 °c temperature, the BG made hydrogel and stored at RT for making BG/NAVI formulation. Then Navitoclax was dissolved in DMSO at a concentration of 1 mg/ml. Then NAVI was measured for a dose of 150 mg/kg /animal, and the rest of the 100 µl dose was BG hydrogel. In our stability test, the NAVI was stable up to 48 h of the time frame. BG was utilized as the carrier and didn't affect the biological function of NAVI. The doses were prepared fresh every time while dosing the animals.

4.5.4 CONJUGATION OF NAVI/MTP AND PTX/MTP:

Mitochondrial targeting peptide was dissolved at a 1 mg/ml concentration in DI H_2O to prepare the stock sol^n. The conjugation of NAVI & MtP was run in an overnight reaction with 1-Ethyl-3-(3-dimethyl aminopropyl) carbodiimide (EDC) and N-Hydroxysuccinimide (NHS) in Dichloromethane (DCM) solvent. The next day, the solvent was removed using Rotavapor. And conjugated NAVI/MtP was collected by dissolving in DI H_2O and dialysis using 1K MWCO membrane to remove excess EDC, NHS, and DCM. After overnight dialysis, the sample was collected the next day and lyophilized to powder from NAVI/MtP. The NAVI/MtP was stored in -20 ˚c and dissolved to make doses *in vitro* and *in vivo*.

4.5.5: *IN VITRO* APOPTOSIS-NECROSIS STUDY:

The measurement of phosphatidylserine externalization could be used as an indicator for apoptosis [120]. The Annexin V-FITC kit (Beckman Coulter, Miami, FL, USA) was used for this purpose. MDA MB 231 and PTXR MDA MB 231 cells were used for this study. The cells were grown on

24-well plate dishes at a density of $1x10^5$ cells using 1 ml media per well overnight in an incubator. The next day we washed each well with 3 X PBS and treated with treatments, saline/untreated, DMSO, H_2O_2, NAVI (50 µM), NAVI/MtP, PTX (50 nM), and PTX/MtP. Cells were treated with 0.1% DMSO (v/v) for the vehicle control study. For positive control, cells were treated with H_2O_2 (1.6 mM), and for negative control, cells were left untreated or treated with 1 X PBS. After treating the cells, they were kept in the incubator for 24 h. The cells were collected in pre-cooled 5 ml tubes for centrifugation after the incubation time. After centrifugation, the cells were suspended in a 100 µl solution (1x binding buffer containing 1 µL of Annexin V-FITC reagent and 2.5 µL of Propodeum Iodide) prepared based on previous reports [121]. The cells were then kept in the dark and incubated in 300 µl of 1x binding buffer. After incubation, each tube was examined through flow cytometry (Gallios, Beckman Coulter). FL1 and FL2 detectors captured fluorescence signals emitted by FITC and PI, respectively. Cells that showed PI positivity were identified as necrotic cells, those that were FITC positive were identified as early apoptotic cells, and both positive are late apoptosis. Cells emitting both FITC and PI signals were defined as the late apoptosis subpopulation [122]. The total percentage of apoptotic cells subpopulation was defined as the sum of both early and late phases of apoptosis (Annexin V-FITC positive), top and bottom right quadrants in the flow cytometry dot plots, respectively [64].

4.5.6: SOLUBILITY, STABILITY & NAVITOCLAX BIO-DISTRIBUTION STUDY:

BG/NAVI oral dosage prepared at 1mg/ml concentration. Then the original oral dosage was serially diluted 8 times using DI H_2O. Absorbance was measured at 345 nm using a Synergy H1 UV plate reader. For stability absorbance was measured at 0, 0.5, 1, 2, 3, 4, 5, & 6 h. Flat bottom 96 well plate was used for reading and 200 µl of samples were taken for each reading. Data was replicated thrice for statistical significance. 6 SD rats were taken from a colony of 3 months old.

The NAVI and BG/NAVI were prepared earlier on the experiment day. We collected blood at 0, 0.5, 1,2,4,6, and 8 h via tail vein puncture. The blood was collected in the heparin-coated tube and stored at 4 °c for further analysis. AT first, rats were orally gavaged with NAVI and BG/NAVI at 500 µg / 100 µl /animal. While collecting blood, the animals were taken care of and maintained in humid conditions. And right after each blood collection time, medication was administered to each animal.

4.5.7: TUMOR XENOGRAFT MOUSE MODEL AND TUMOR VOLUME MEASUREMENT:

All experiments pertaining to animals' use will perform according to the protocols approved by the Institutional Animal Care and Use Committee of the University of Texas at El Paso. Six to seven-week-old C57BL/6 (21-30 g) were purchased from Charles River Laboratories International, Inc. and maintained under specific pathogen-free conditions. Cultured MDA MB-231 and PTXR cells were trypsinized, washed twice with serum-free DMEM, and suspended at 10 X 10^6 cells/mL PBS. 100 µL of the suspended cells were subcutaneously (SC) injected into the right flank of the mice. On day 14, after tumor cell injection, the tumors were visible. Each group was again subdivided into 4 treatment groups, untreated, PTX, NAVI, and BG/NAVI. The treatment was terminated on day 34 of the injection. Mouse weight and tumor volume were measured during the treatment period and plotted tumor volume and changes in body weight against time (Day). Tumor growth was determined by measuring the longest and shortest length. Tumor volume was calculated by utilizing the following formula:

$$Tumor\ volumne\ = 0.5\{lenght\ (mm) * Width\ (mm) * Widtth\ (mm)\}$$

4.5.8: CLINICAL BIOCHEMISTRY PANEL ANALYSIS AD COMPLETE BLOOD COUNT:

In the case of animal studies, animals were divided into 2 different groups based on their tumor type. The study was continued for 4 dosages and was administered in these 20 days at 5-day intervals. These mice were sacrificed on day 20 of treatment, and 0.5-0.6 ml of whole blood was collected from the heart of each mouse. During the blood collection process, 0.3 ml was collected in a low molecular weight heparin-containing tube for counting blood cell content. The biochemistry panel analysis used the remaining 0.2-0.3 ml blood serum. To prevent the blood from coagulating EDTA containing K3EDTA bottles, a CUETTER, Greiner, Austria bottles. 0.5 ml of the whole blood sample was taken in Z Serum Sep Clot Activator bottle (VACUETTER, Greiner, Austria) and centrifuged at 3000 rpm for 15 minutes. The serum (supernatant) was collected for the biochemistry analysis. Serological parameters of the kidney and liver were determined. Furthermore, we analyzed various enzymes like aspartate aminotransferase (AST), blood urea nitrogen (BUN), alkaline phosphatase (ALP), alanine aminotransferase (ALT/GPT), creatinine (Cr), and total protein (TP). We also ran a total blood count to analyze blood functions like red blood cells (RBC), white blood cells (WBC), platelet (PLT), and hemoglobin (Hb). GraphPad Prism was used to analyze results from the biochemical assay. The total blood count was done using an Element-DC by HESKA chemical analyzer and Hemavet from Drew scientific. (Drew Scientific, Miami Lakes, FL).

4.5.9 IMMUNOHISTOCHEMISTRY OF TUMOR SAMPLES:

After freezing, the fixed tissues were cut into 20 µm size pieces using cryo-tome. The cut tissues were kept in antifreeze solution till immunohistochemistry experiments. Immunohistochemistry was performed based on a protocol that was modified from fisher scientific and Abcam. The modified protocol was optimized based on our laboratory's specifications. Initially, the tissues were washed with PBS and washing buffer (400 µl). After that, the tissues were incubated in a 400

µl blocking buffer for 45 minutes to minimize non-specific blocking. The composition of the washing buffer was 0.1% BSA in 1-X PBS. At the same time, the blocking buffer was prepared by taking 10% donkey/goat serum and 0.3% Triton® X-100 in 1X PBS [149]. According to the manufacturer's specification, the unconjugated primary antibodies were initially mixed with dilution buffer to perform the immunostaining. The tissues were incubated overnight at 4ºC with the diluted primary antibodies. The next day excess primary antibodies were washed away using washing buffer. Each tissue was washed four times for five minutes. Then the tissues were incubated for an hour at room temperature in a light protected environment with secondary antibodies. The unbounded secondary antibodies were removed using the washing buffer two times for five minutes. After that, the tissues were dried in air and mounted using the mounting media [150]. The mounting was done on a transparent coverslip, and confocal images at 20x magnification were taken using LSM 700 instrument. Finally, all the images were analyzed using ImageJ software.

4.5.10 STATISTICAL ANALYSIS:

All experiments were repeated three times to ensure reproducibility. The results were reported for the mean ± SD of these three experiments. GraphPad Prism (GraphPad Software Inc.) was utilized for performing the Student T-test, one-way analysis of variance (ANOVA), and two-way ANOVA. For all statistical analyses, when the P-value was < 0.05, it was considered significant.

4.6 ACKNOWLEDGMENT:

We acknowledge Cancer Prevention Research Institute of Texas (CPRIT) funding through Texas Regional Excellence in Cancer Award (TREC) under Award No. PR210153. Research reported in this publication was supported by the Research Centers at Minority Institutions grant funded by the National Institute on Minority Health and Health Disparities of the National Institutes of Health

under Award No. U54MD007592. This Core Facility is supported by grant 8G12MD007592 to the Border Biomedical Research Center (BBRC) from the National Institutes on Minority Health and Health Disparities (NIMHD), a component of the National Institutes of Health (NIH). Its contents are solely the authors' responsibility and do not necessarily represent the official views of NCRR or NIH.

CHAPTER 5: CONCLUSION

Non-invasive drug delivery has a higher opportunity to clinically translate than other drug delivery systems such as IV, IP, and intranasal. In this dissertation, the author focuses on topical and oral delivery of BCL-2 inhibitors. Ionic liquid (COA) was utilized delivery vesicle in chapters 2 & 3 and β-Glucan (BG) in chapter 4. COA holds intrinsic properties of increasing skin pore size and contains the drug in the deep skin layer for a longer time. BG was utilized as the delivery platform in the drug resistance pilot study. In our other projects, we have identified that BG has mucoadhesive properties attached to the mucus layer of the GI tract. Therefore, BG/NAVI oral delivery holds drugs in the GI tract for more extended and allows the transportation of drugs for a longer time.

The findings in chapter 2 suggest that COA, a new ionic liquid, might be used as a platform for topical delivery of a BCL-2 inhibitor, which could help treat cutaneous melanoma in its early stages. COA is an excellent vehicle for topical medication delivery because it improves drug solubility and allows for non-invasive transportation via the skin. NAVI is a highly effective anti-cancer medication; however, it is hydrophobic and has a high risk of hepatotoxicity. Our COA/NAVI formulation is physiologically active and has anti-cancer efficacy, according to the in vitro investigation. With enhanced topically administrable formulations like COA, this discovery has the potential to improve cutaneous melanoma treatment. In the future, we hope to conduct additional research to understand better what happens to melanoma as it metastasizes from the skin and to develop more effective therapeutic approaches to treat melanoma in its later stages.

Chapter 3 focused on skin fibrosis topical therapeutic delivery. Tissue fibrosis affects nearly every organ in our bodies and is a global health issue. There are currently few therapeutic options for reducing skin fibrosis and preventing organ failure. Certain disease situations like aging, skin

cancer and certain illnesses impair the normal skin response to fibrosis. Laser surgery, topical cream administration, and medications or therapies such as D-penicillamine, bovine collagen, methotrexate, mycophenolate mofetil, and allogeneic bone marrow transplantation are currently used as treatments. Most medications improve fibrosis symptoms; thus, we need a new therapeutic method to stop the fibrosis signaling cascade. To investigate possible systemic anti-fibrotic effects, fibrosis was generated in the skin of 4-6 week-old mice by subcutaneous BLM injection followed by wound-healing products. BLM-induced skin fibrosis would result in dysregulation of repair mechanisms, resulting in fibrosis in skin tissue and impaired wound healing, given the fibrogenic pathways and aberrant healing similarities to systemic sclerosis patients. The topical application of COA in the treatment of skin fibrosis is one of the innovative ways of this therapeutic approach. COA can increase sweat gland activity, allowing medicines to pass through the epidermal layer and reach the fibrosis site. The results also showed that fibrosis signals were reduced, which improved the tissue fibrosis situation. As a result, COA/NAVI offers a unique platform for treating skin fibrosis in mice. Fibrosis is caused by a complicated chain of events, including inflammatory effector cells and pathway dysfunction. As a result, we're looking at using COA to administer a combination medicine that targets various signaling pathways. In addition, we need to look at the COA/NAVI therapeutic efficacy across multiple fibrosis models.

Chemotherapeutic drug resistance development is a common scenario in cancer treatment. In chapter 4, we conduct the pilot study evaluating alternate therapeutic efficiency in the paclitaxel drug resistance tumor model. The present challenge is to use what we've learned from standard cytotoxic drugs and the first generation of molecularly targeted treatments to maximize the anti-cancer arsenal. In vitro and in vivo medication synergy is frequently proposed treatment combinations; yet, in some cases, repeatedly targeting the same pathway may provide a

straightforward 'escape route' for the tumor. We were able to show that tumor resistance can be reversed in our pilot trial. The drug resistance was created using the PTX as a positive control, and the BG/NAVI oral delivery exhibited improved results against drug resistance. This study serves as a baseline for additional research into how various drug combinations or single pharmaceuticals can influence the mechanism of drug resistance. To assess treatment resistance, evaluate prospective drug combinations, and determine the therapeutic utility of predictive biomarkers, improved in vitro and in vivo models, such as patient-derived xenografts, that more accurately simulate tumor-stroma interactions are needed. This pilot study also paves the way for applying combination therapy to the animal model to understand the variety of drug resistance mechanisms better. Following that, preclinical studies must be put to the test in the clinic, necessitating the creation of "smart" trials that use cutting-edge molecular pathology tools. Next-generation sequencing (NGS) enables genome-wide personalized oncology efforts with the specialty and infrastructure necessary to identify and prioritize tumor genome variants, as demonstrated by the oncomine comprehensive panel (OCP), representing a streamlined and broadly applicable targeted NGS system to advance precision oncology.

In summary, in this dissertation, the authors identify a novel topical delivery approach for skin melanoma and skin fibrosis mice model in chapters 2nd and 3rd. Both melanoma and fibrosis need alternative non-invasive treatment due to the limitations of current therapies. Our findings conclude the translational scope of topical delivery of COA/NAVI in treating local diseases. We also need further evaluation of COA/NAVI topical delivery in advanced disease stages or more aggressive forms of the disease. Also, before moving to clinical trials, we need further evaluation with non-human primate models. Our 4th chapter focuses on another significant limitation of the chemotherapeutic face during therapy. Tumors achieve drug resistance, and we identify an

alternative way to reverse this resistance mechanism. Drug resistance develops in tumors by various means such as drug efflux, vasculature, angiogenesis, and inhibition of apoptosis. This study used paclitaxel as a model drug to create drug resistance. In our findings, oral delivery of BG/NAVI can improve the drug resistance mechanism and reduce tumor volume. NAVI can inhibit the vasculature and induce apoptosis in the tumor region. Still, we need further evaluation of these proposed methods in general tumor models and combination therapy to evaluate drug resistance mechanisms.

REFERENCES

[1] A.Z. Alkilani, M.T.C. McCrudden, R.F. Donnelly, Transdermal Drug Delivery: Innovative Pharmaceutical Developments Based on Disruption of the Barrier Properties of the stratum corneum, Pharmaceutics. 7 (2015) 438–470. https://doi.org/10.3390/pharmaceutics7040438.

[2] G. Tiwari, R. Tiwari, B. Sriwastawa, L. Bhati, S. Pandey, P. Pandey, S.K. Bannerjee, Drug delivery systems: An updated review, Int. J. Pharm. Investig. 2 (2012) 2–11. https://doi.org/10.4103/2230-973X.96920.

[3] N.N. Mohamad Anuar, N.S. Nor Hisam, S.L. Liew, A. Ugusman, Clinical Review: Navitoclax as a Pro-Apoptotic and Anti-Fibrotic Agent , Front. Pharmacol. . 11 (2020) 1817. https://www.frontiersin.org/article/10.3389/fphar.2020.564108.

[4] D. Mérino, S.L. Khaw, S.P. Glaser, D.J. Anderson, L.D. Belmont, C. Wong, P. Yue, M. Robati, B. Phipson, W.D. Fairlie, E.F. Lee, K.J. Campbell, C.J. Vandenberg, S. Cory, A.W. Roberts, M.J.C. Ludlam, D.C.S. Huang, P. Bouillet, Bcl-2, Bcl-x(L), and Bcl-w are not equivalent targets of ABT-737 and navitoclax (ABT-263) in lymphoid and leukemic cells., Blood. 119 (2012) 5807–5816. https://doi.org/10.1182/blood-2011-12-400929.

[5] L.D. Osellame, T.S. Blacker, M.R. Duchen, Cellular and molecular mechanisms of mitochondrial function, Best Pract. Res. Clin. Endocrinol. Metab. 26 (2012) 711–723. https://doi.org/10.1016/j.beem.2012.05.003.

[6] V. Vigneswara, Z. Ahmed, The Role of Caspase-2 in Regulating Cell Fate., Cells. 9 (2020). https://doi.org/10.3390/cells9051259.

[7] J.C. Reed, Mechanisms of Apoptosis, Am. J. Pathol. 157 (2000) 1415–1430. https://doi.org/https://doi.org/10.1016/S0002-9440(10)64779-7.

[8] J.M. Hardwick, L. Soane, Multiple functions of BCL-2 family proteins, Cold Spring Harb. Perspect. Biol. 5 (2013) a008722. https://doi.org/10.1101/cshperspect.a008722.

[9] M. Giam, D.C.S. Huang, P. Bouillet, BH3-only proteins and their roles in programmed cell death, Oncogene. 27 (2008) S128–S136. https://doi.org/10.1038/onc.2009.50.

[10] B. Santiago, M. Galindo, M. Rivero, J.L. Pablos, Decreased susceptibility to Fas-induced apoptosis of systemic sclerosis dermal fibroblasts, Arthritis Rheum. 44 (2001) 1667–1676. https://doi.org/https://doi.org/10.1002/1529-0131(200107)44:7<1667::AID-ART291>3.0.CO;2-Y.

[11] T. Yamamoto, K. Nishioka, Possible Role of Apoptosis in the Pathogenesis of Bleomycin-Induced Scleroderma, J. Invest. Dermatol. 122 (2004) 44–50. https://doi.org/https://doi.org/10.1046/j.0022-202X.2003.22121.x.

[12] J.F. Thompson, R.A. Scolyer, R.F. Kefford, Cutaneous melanoma., Lancet (London, England). 365 (2005) 687–701. https://doi.org/10.1016/S0140-6736(05)17951-3.

[13] M.D. Jacobson, J.F. Burne, M.P. King, T. Miyashrta, J.C. Reed, M.C. Raff, Bcl-2 blocks apoptosis in cells lacking mitochondrial DNA, Nature. 361 (1993) 365–369. https://doi.org/10.1038/361365a0.

[14] P. Li, D. Nijhawan, I. Budihardjo, S.M. Srinivasula, M. Ahmad, E.S. Alnemri, X. Wang, Cytochrome c and dATP-dependent formation of Apaf-1/caspase-9 complex initiates an apoptotic protease cascade., Cell. 91 (1997) 479–489. https://doi.org/10.1016/s0092-8674(00)80434-1.

[15] C. Karimkhani, R.P. Dellavalle, L.E. Coffeng, C. Flohr, R.J. Hay, S.M. Langan, E.O. Nsoesie, A.J. Ferrari, H.E. Erskine, J.I. Silverberg, T. Vos, M. Naghavi, Global Skin Disease Morbidity and Mortality: An Update From the Global Burden of Disease Study 2013, JAMA Dermatology. 153 (2017) 406–412. https://doi.org/10.1001/jamadermatol.2016.5538.

[16] A.A. of Dermatology, BURDEN OF SKIN DISEASE, 2021. https://www.aad.org/member/clinical-quality/clinical-care/bsd.

[17] American Cancer Society, Key Statistics for Melanoma Skin Cancer, (2021). https://www.cancer.org/cancer/melanoma-skin-cancer/about/key-statistics.html.

[18] S.A. Eming, P. Martin, M. Tomic-Canic, Wound repair and regeneration: mechanisms, signaling, and translation., Sci. Transl. Med. 6 (2014) 265sr6. https://doi.org/10.1126/scitranslmed.3009337.

[19] E. Tsitoura, E. Vasarmidi, E. Bibaki, A. Trachalaki, C. Koutoulaki, G. Papastratigakis, S. Papadogiorgaki, G. Chalepakis, N. Tzanakis, K.M. Antoniou, Accumulation of damaged mitochondria in alveolar macrophages with reduced OXPHOS related gene expression in IPF, Respir. Res. 20 (2019) 264. https://doi.org/10.1186/s12931-019-1196-6.

[20] M. Schiller, D. Javelaud, A. Mauviel, TGF-beta-induced SMAD signaling and gene regulation: consequences for extracellular matrix remodeling and wound healing., J. Dermatol. Sci. 35 (2004) 83–92. https://doi.org/10.1016/j.jdermsci.2003.12.006.

[21] A.M. Curreri, S. Mitragotri, E.E.L. Tanner, Recent Advances in Ionic Liquids in Biomedicine, Adv. Sci. (Weinheim, Baden-Wurttemberg, Ger. 8 (2021) e2004819–e2004819. https://doi.org/10.1002/advs.202004819.

[22] A.C. Anselmo, Y. Gokarn, S. Mitragotri, Non-invasive delivery strategies for biologics, Nat. Rev. Drug Discov. 18 (2019) 19–40. https://doi.org/10.1038/nrd.2018.183.

[23] B. Du, M. Meenu, H. Liu, B. Xu, A Concise Review on the Molecular Structure and Function Relationship of β-Glucan, Int. J. Mol. Sci. 20 (2019) 4032. https://doi.org/10.3390/ijms20164032.

[24] American Cancer Society, How common is melanoma, (2021). https://www.cancer.org/cancer/melanoma-skin-cancer/about/key-statistics.html.

[25] M.B. Lens, M. Dawes, Global perspectives of contemporary epidemiological trends of cutaneous malignant melanoma., Br. J. Dermatol. 150 (2004) 179–185. https://doi.org/10.1111/j.1365-2133.2004.05708.x.

[26] E. Cho, B.A. Rosner, G.A. Colditz, Risk Factors for Melanoma by Body Site, Cancer Epidemiol. Biomarkers &Amp; Prev. 14 (2005) 1241 LP – 1244. https://doi.org/10.1158/1055-9965.EPI-04-0632.

[27] Y. Liu, M.S. Sheikh, Melanoma: Molecular Pathogenesis and Therapeutic Management, Mol. Cell. Pharmacol. 6 (2014) 228. https://pubmed.ncbi.nlm.nih.gov/25745537.

[28] L. Kwong, L. Chin, S.N. Wagner, Growth factors and oncogenes as targets in melanoma: lost in translation?, Adv. Dermatol. 23 (2007) 99–129. https://doi.org/10.1016/j.yadr.2007.07.015.

[29] S.R. Christensen, Recent advances in field cancerization and management of multiple cutaneous squamous cell carcinomas., F1000Research. 7 (2018). https://doi.org/10.12688/f1000research.12837.1.

[30] V. Krishnan, S. Mitragotri, Nanoparticles for topical drug delivery: Potential for skin cancer treatment., Adv. Drug Deliv. Rev. 153 (2020) 87–108. https://doi.org/10.1016/j.addr.2020.05.011.

[31] F. John P. Cunha, DO, WHAT ARE SIDE EFFECTS ASSOCIATED WITH USING HYDROQUINONE?, RxList. (2021). https://www.rxlist.com/consumer_hydroquinone_melquin_3/drugs-condition.htm.

[32] M.R. Johnson, A. Hageboutros, K. Wang, L. High, J.B. Smith, R.B. Diasio, Life-

threatening toxicity in a dihydropyrimidine dehydrogenase-deficient patient after treatment with topical 5-fluorouracil., Clin. Cancer Res. an Off. J. Am. Assoc. Cancer Res. 5 (1999) 2006–2011.

[33] J. Loyal, M. Romano, J.C. Pierson, Exuberant inflammatory reaction to occlusion of topical 5-fluorouracil (FU) under a continuous positive airway pressure (CPAP) mask: A warning to dermatologists and patients., JAAD Case Reports. 2 (2016) 278–280. https://doi.org/10.1016/j.jdcr.2016.05.011.

[34] I.G. Deaguero, M.N. Huda, V. Rodriguez, J. Zicari, T.A. Al-Hilal, A.Z.M. Badruddoza, M. Nurunnabi, Nano-Vesicle Based Anti-Fungal Formulation Shows Higher Stability, Skin Diffusion, Biosafety and Anti-Fungal Efficacy In Vitro., Pharmaceutics. 12 (2020). https://doi.org/10.3390/pharmaceutics12060516.

[35] J. Larkin, V. Chiarion-Sileni, R. Gonzalez, J.-J. Grob, P. Rutkowski, C.D. Lao, C.L. Cowey, D. Schadendorf, J. Wagstaff, R. Dummer, P.F. Ferrucci, M. Smylie, D. Hogg, A. Hill, I. Márquez-Rodas, J. Haanen, M. Guidoboni, M. Maio, P. Schöffski, M.S. Carlino, C. Lebbé, G. McArthur, P.A. Ascierto, G.A. Daniels, G. V Long, L. Bastholt, J.I. Rizzo, A. Balogh, A. Moshyk, F.S. Hodi, J.D. Wolchok, Five-Year Survival with Combined Nivolumab and Ipilimumab in Advanced Melanoma., N. Engl. J. Med. 381 (2019) 1535–1546. https://doi.org/10.1056/NEJMoa1910836.

[36] J.D. Wolchok, V. Chiarion-Sileni, R. Gonzalez, P. Rutkowski, J.-J. Grob, C.L. Cowey, C.D. Lao, J. Wagstaff, D. Schadendorf, P.F. Ferrucci, M. Smylie, R. Dummer, A. Hill, D. Hogg, J. Haanen, M.S. Carlino, O. Bechter, M. Maio, I. Marquez-Rodas, M. Guidoboni, G. McArthur, C. Lebbé, P.A. Ascierto, G. V Long, J. Cebon, J. Sosman, M.A. Postow, M.K. Callahan, D. Walker, L. Rollin, R. Bhore, F.S. Hodi, J. Larkin, Overall Survival with Combined Nivolumab and Ipilimumab in Advanced Melanoma., N. Engl. J. Med. 377 (2017) 1345–1356. https://doi.org/10.1056/NEJMoa1709684.

[37] F.S. Hodi, V. Chiarion-Sileni, R. Gonzalez, J.-J. Grob, P. Rutkowski, C.L. Cowey, C.D. Lao, D. Schadendorf, J. Wagstaff, R. Dummer, P.F. Ferrucci, M. Smylie, A. Hill, D. Hogg, I. Marquez-Rodas, J. Jiang, J. Rizzo, J. Larkin, J.D. Wolchok, Nivolumab plus ipilimumab or nivolumab alone versus ipilimumab alone in advanced melanoma (CheckMate 067): 4-year outcomes of a multicentre, randomised, phase 3 trial., Lancet. Oncol. 19 (2018) 1480–1492. https://doi.org/10.1016/S1470-2045(18)30700-9.

[38] Z. Zhao, E.E.L. Tanner, J. Kim, K. Ibsen, Y. Gao, S. Mitragotri, Ionic Liquid-Enabled Topical Delivery of Immunomodulators, ACS Biomater. Sci. Eng. 7 (2021) 2783–2790. https://doi.org/10.1021/acsbiomaterials.1c00322.

[39] D. Monti, E. Egiziano, S. Burgalassi, P. Chetoni, C. Chiappe, A. Sanzone, S. Tampucci, Ionic liquids as potential enhancers for transdermal drug delivery, Int. J. Pharm. 516 (2016). https://doi.org/10.1016/j.ijpharm.2016.11.020.

[40] M. Certo, V. Del Gaizo Moore, M. Nishino, G. Wei, S. Korsmeyer, S.A. Armstrong, A. Letai, Mitochondria primed by death signals determine cellular addiction to antiapoptotic BCL-2 family members., Cancer Cell. 9 (2006) 351–365. https://doi.org/10.1016/j.ccr.2006.03.027.

[41] A.J. García-Sáez, The secrets of the Bcl-2 family., Cell Death Differ. 19 (2012) 1733–1740. https://doi.org/10.1038/cdd.2012.105.

[42] J. Montero, A. Letai, Why do BCL-2 inhibitors work and where should we use them in the clinic?, Cell Death Differ. 25 (2018) 56–64. https://doi.org/10.1038/cdd.2017.183.

[43] J. Flieger, M. Flieger, Ionic Liquids Toxicity-Benefits and Threats, Int. J. Mol. Sci. 21 (2020) 6267. https://doi.org/10.3390/ijms21176267.

[44] K.B. Smith, R.H. Bridson, G.A. Leeke, Solubilities of Pharmaceutical Compounds in Ionic Liquids, J. Chem. Eng. Data. 56 (2011) 2039–2043. https://doi.org/10.1021/je101040p.

[45] E. Tanner, K. Piston, H. Ma, K. Ibsen, S. Nangia, S. Mitragotri, The Influence of Water on Choline-Based Ionic Liquids, ACS Biomater. Sci. Eng. 5 (2019). https://doi.org/10.1021/acsbiomaterials.9b00243.

[46] S. de Marcos, J. Galbán, C. Alonsa, J.R. Castillo, Intrinsic molecular fluorescence of lactate dehydrogenase: an analytical alternative for enzymic determination of pyruvate., Analyst. 122 (1997) 355–359. https://doi.org/10.1039/a606508b.

[47] J.C. Reed, Mechanisms of Apoptosis, Am. J. Pathol. 157 (2000) 1415–1430. https://doi.org/https://doi.org/10.1016/S0002-9440(10)64779-7.

[48] H. Thomadaki, M. Talieri, A. Scorilas, Prognostic value of the apoptosis related genes BCL2 and BCL2L12 in breast cancer, Cancer Lett. 247 (2007) 48–55. https://doi.org/https://doi.org/10.1016/j.canlet.2006.03.016.

[49] A. Strasser, S. Cory, J.M. Adams, Deciphering the rules of programmed cell death to

improve therapy of cancer and other diseases., EMBO J. 30 (2011) 3667–3683. https://doi.org/10.1038/emboj.2011.307.

[50] H.A.O. XIONG, R.S. PRADHAN, A. NADA, A.P. KRIVOSHIK, K.D. HOLEN, J.W. RHODES, G.B. GORDON, R.O.D. HUMERICKHOUSE, W.M. AWNI, Studying Navitoclax, a Targeted Anticancer Drug, in Healthy Volunteers – Ethical Considerations and Risk/Benefit Assessments and Management, Anticancer Res. 34 (2014) 3739 LP – 3746.

[51] R. Khullar, S. Saini, N. Seth, A.C. Rana, Emulgel: A surrogate approach for topical used hydrophobic drugs, IJPBS. 1 (2011) 117–128.

[52] M. Nurunnabi, K.J. Cho, J.S. Choi, K.M. Huh, Y. kyu Lee, Targeted near-IR QDs-loaded micelles for cancer therapy and imaging, Biomaterials. 31 (2010) 5436–5444. https://doi.org/10.1016/j.biomaterials.2010.03.057.

[53] A.K. Sharma, R.L. Roberts, R.D.J. Benson, J.L. Pierce, K. Yu, M.W. Hamrick, M.E. McGee-Lawrence, The Senolytic Drug Navitoclax (ABT-263) Causes Trabecular Bone Loss and Impaired Osteoprogenitor Function in Aged Mice., Front. Cell Dev. Biol. 8 (2020) 354. https://doi.org/10.3389/fcell.2020.00354.

[54] K. Dilley, J. Harb, M. Jalaluddin, J.E. Hutti, J. Potluri, A Phase 3, Open-Label, Randomized Study Evaluating the Efficacy and Safety of Navitoclax Plus Ruxolitinib Versus Best Available Therapy in Patients with Relapsed/Refractory Myelofibrosis (TRANSFORM-2), Blood. 136 (2020) 8. https://doi.org/10.1182/blood-2020-139247.

[55] L. Gandhi, D.R. Camidge, M. Ribeiro de Oliveira, P. Bonomi, D. Gandara, D. Khaira, C.L. Hann, E.M. McKeegan, E. Litvinovich, P.M. Hemken, C. Dive, S.H. Enschede, C. Nolan, Y.-L. Chiu, T. Busman, H. Xiong, A.P. Krivoshik, R. Humerickhouse, G.I. Shapiro, C.M. Rudin, Phase I study of Navitoclax (ABT-263), a novel Bcl-2 family inhibitor, in patients with small-cell lung cancer and other solid tumors., J. Clin. Oncol. Off. J. Am. Soc. Clin. Oncol. 29 (2011) 909–916. https://doi.org/10.1200/JCO.2010.31.6208.

[56] J.D. Leverson, D.C. Phillips, M.J. Mitten, E.R. Boghaert, D. Diaz, S.K. Tahir, L.D. Belmont, P. Nimmer, Y. Xiao, X.M. Ma, K.N. Lowes, P. Kovar, J. Chen, S. Jin, M. Smith, J. Xue, H. Zhang, A. Oleksijew, T.J. Magoc, K.S. Vaidya, D.H. Albert, J.M. Tarrant, N. La, L. Wang, Z.-F. Tao, M.D. Wendt, D. Sampath, S.H. Rosenberg, C. Tse,

D.C.S. Huang, W.J. Fairbrother, S.W. Elmore, A.J. Souers, Exploiting selective BCL-2 family inhibitors to dissect cell survival dependencies and define improved strategies for cancer therapy., Sci. Transl. Med. 7 (2015) 279ra40. https://doi.org/10.1126/scitranslmed.aaa4642.

[57] A. Ashkenazi, W.J. Fairbrother, J.D. Leverson, A.J. Souers, From basic apoptosis discoveries to advanced selective BCL-2 family inhibitors., Nat. Rev. Drug Discov. 16 (2017) 273–284. https://doi.org/10.1038/nrd.2016.253.

[58] M.A. Debrincat, I. Pleines, M. Lebois, R.M. Lane, M.L. Holmes, J. Corbin, C.J. Vandenberg, W.S. Alexander, A.P. Ng, A. Strasser, P. Bouillet, M. Sola-Visner, B.T. Kile, E.C. Josefsson, BCL-2 is dispensable for thrombopoiesis and platelet survival, Cell Death Dis. 6 (2015) e1721–e1721. https://doi.org/10.1038/cddis.2015.97.

[59] P.K. Smith, R.I. Krohn, G.T. Hermanson, A.K. Mallia, F.H. Gartner, M.D. Provenzano, E.K. Fujimoto, N.M. Goeke, B.J. Olson, D.C. Klenk, Measurement of protein using bicinchoninic acid, Anal. Biochem. 150 (1985) 76–85. https://doi.org/https://doi.org/10.1016/0003-2697(85)90442-7.

[60] T. Mosmann, Rapid colorimetric assay for cellular growth and survival: application to proliferation and cytotoxicity assays., J. Immunol. Methods. 65 (1983) 55–63. https://doi.org/10.1016/0022-1759(83)90303-4.

[61] D.M. Smith, J.K. Simon, J.R. Baker Jr, Applications of nanotechnology for immunology, Nat. Rev. Immunol. 13 (2013) 592–605. https://doi.org/10.1038/nri3488.

[62] G. Koopman, C.P. Reutelingsperger, G.A. Kuijten, R.M. Keehnen, S.T. Pals, M.H. van Oers, Annexin V for flow cytometric detection of phosphatidylserine expression on B cells undergoing apoptosis., Blood. 84 (1994) 1415–1420.

[63] L. Contreras, R.I. Calderon, A. Varela-Ramirez, H.-Y. Zhang, Y. Quan, U. Das, J.R. Dimmock, R. Skouta, R.J. Aguilera, Induction of apoptosis via proteasome inhibition in leukemia/lymphoma cells by two potent piperidones., Cell. Oncol. (Dordr). 41 (2018) 623–636. https://doi.org/10.1007/s13402-018-0397-1.

[64] E. Robles-Escajeda, D. Lerma, A.M. Nyakeriga, J.A. Ross, R.A. Kirken, R.J. Aguilera, A. Varela-Ramirez, Searching in mother nature for anti-cancer activity: anti-proliferative and pro-apoptotic effect elicited by green barley on leukemia/lymphoma cells., PLoS One. 8 (2013) e73508. https://doi.org/10.1371/journal.pone.0073508.

[65] R. Schuh, E. Kremmer, E. Ego, M. Wasiliu, S. Thierfelder, Determination of monoclonal antibody specificity by immunoadsorption and Western blotting, J. Immunol. Methods. 152 (1992) 59–67. https://doi.org/https://doi.org/10.1016/0022-1759(92)90089-C.

[66] E. Aksamitiene, J.B. Hoek, B. Kholodenko, A. Kiyatkin, Multistrip Western blotting to increase quantitative data output, Electrophoresis. 28 (2007) 3163–3173. https://doi.org/https://doi.org/10.1002/elps.200700002.

[67] M. Nurunnabi, K.N. Ibsen, E.E.L. Tanner, S. Mitragotri, Oral ionic liquid for the treatment of diet-induced obesity, Proc. Natl. Acad. Sci. U. S. A. (2019). https://doi.org/10.1073/pnas.1914426116.

[68] M. Nurunnabi, Z. Khatun, K.M. Huh, S.Y. Park, D.Y. Lee, K.J. Cho, Y. Lee, In Vivo Biodistribution and Toxicology of Carboxylated Graphene Quantum Dots, ACS Nano. 7 (2013) 6858–6867. https://doi.org/10.1021/nn402043c.

[69] T. Fisher, Immunohistochemistry: five steps to publication-quality images, (2021) 1–6. http://assets.thermofisher.com/TFS-Assets/BID/brochures/immunohistochemistry-steps-publication-images-brochure.pdf.

[70] Abcam, Immunohistochemistry (IHC): the complete guide, 2021. https://www.abcam.com/content/immunohistochemistry-the-complete-guide.

[71] N. Imahej, ImageJ image analysis software tutorial, 2021. https://imagej.nih.gov/ij/docs/.

[72] GraphPad, Statistical analyses with Prism, GraphPad. (2021). https://www.graphpad.com/guides/prism/latest/statistics/stat_statistical_analyses_with_pris.htm.

[73] American College of Rheumatology, Scleroderma, 2022.

[74] N. Durmus, S.-H. Park, J. Reibman, G. Grunig, Aberrant immune response with consequent vascular and connective tissue remodeling - causal to scleroderma and associated syndromes such as Raynaud phenomenon and other fibrosing syndromes?, Curr. Opin. Rheumatol. 28 (2016) 571–576. https://doi.org/10.1097/BOR.0000000000000333.

[75] N.N. Do, S.A. Eming, Skin fibrosis: Models and mechanisms, Curr. Res. Transl. Med. 64 (2016) 185–193. https://doi.org/https://doi.org/10.1016/j.retram.2016.06.003.

[76] John Hopkins Medicine, Scleroderma Treatment, 2022. https://www.hopkinsmedicine.org/health/conditions-and-

diseases/scleroderma/scleroderma-treatment.

[77] Michigan Health Lab, Systemic Scleroderma Treatments: Where Are We Now?, 2022. https://labblog.uofmhealth.org/industry-dx/systemic-scleroderma-treatments-where-are-we-now.

[78] D. Lagares, A. Santos, P.E. Grasberger, F. Liu, C.K. Probst, R.A. Rahimi, N. Sakai, T. Kuehl, J. Ryan, P. Bhola, J. Montero, M. Kapoor, M. Baron, X. Varelas, D.J. Tschumperlin, A. Letai, A.M. Tager, Targeted apoptosis of myofibroblasts with the BH3 mimetic ABT-263 reverses established fibrosis., Sci. Transl. Med. 9 (2017). https://doi.org/10.1126/scitranslmed.aal3765.

[79] J.H.W. Distler, A.-H. Györfi, M. Ramanujam, M.L. Whitfield, M. Königshoff, R. Lafyatis, Shared and distinct mechanisms of fibrosis, Nat. Rev. Rheumatol. 15 (2019) 705–730. https://doi.org/10.1038/s41584-019-0322-7.

[80] L.E. Tracy, R.A. Minasian, E.J. Caterson, Extracellular Matrix and Dermal Fibroblast Function in the Healing Wound, Adv. Wound Care. 5 (2016) 119–136. https://doi.org/10.1089/wound.2014.0561.

[81] A. Johnson, L.A. DiPietro, Apoptosis and angiogenesis: an evolving mechanism for fibrosis, FASEB J. 27 (2013) 3893–3901. https://doi.org/10.1096/fj.12-214189.

[82] S. Elmore, Apoptosis: a review of programmed cell death, Toxicol. Pathol. 35 (2007) 495–516. https://doi.org/10.1080/01926230701320337.

[83] L.L. Zhou, L.Y. Zhou, K.Q. Luo, D.C. Chang, Smac/DIABLO and cytochrome c are released from mitochondria through a similar mechanism during UV-induced apoptosis., Apoptosis. 10 (2005) 289–299. https://doi.org/10.1007/s10495-005-0803-9.

[84] A.N. Hata, J.A. Engelman, A.C. Faber, The BCL2 Family: Key Mediators of the Apoptotic Response to Targeted Anticancer Therapeutics, Cancer Discov. 5 (2015) 475–487. https://doi.org/10.1158/2159-8290.CD-15-0011.

[85] E. Er, L. Oliver, P.-F. Cartron, P. Juin, S. Manon, F.M. Vallette, Mitochondria as the target of the pro-apoptotic protein Bax., Biochim. Biophys. Acta. 1757 (2006) 1301–1311. https://doi.org/10.1016/j.bbabio.2006.05.032.

[86] W.H. Wilson, O.A. O'Connor, M.S. Czuczman, A.S. LaCasce, J.F. Gerecitano, J.P. Leonard, A. Tulpule, K. Dunleavy, H. Xiong, Y.-L. Chiu, Y. Cui, T. Busman, S.W. Elmore, S.H. Rosenberg, A.P. Krivoshik, S.H. Enschede, R.A. Humerickhouse,

Navitoclax, a targeted high-affinity inhibitor of BCL-2, in lymphoid malignancies: a phase 1 dose-escalation study of safety, pharmacokinetics, pharmacodynamics, and antitumour activity., Lancet. Oncol. 11 (2010) 1149–1159. https://doi.org/10.1016/S1470-2045(10)70261-8.

[87] C. Agatemor, K. Ibsen, E. Tanner, S. Mitragotri, Ionic Liquids for Addressing Unmet Needs in Healthcare, Bioeng. Transl. Med. 3 (2017). https://doi.org/10.1002/btm2.10083.

[88] M. Zakrewsky, K.S. Lovejoy, T.L. Kern, T.E. Miller, V. Le, A. Nagy, A.M. Goumas, R.S. Iyer, R.E. Del Sesto, A.T. Koppisch, D.T. Fox, S. Mitragotri, Ionic liquids as a class of materials for transdermal delivery and pathogen neutralization, Proc. Natl. Acad. Sci. U. S. A. 111 (2014) 13313–13318. https://doi.org/10.1073/pnas.1403995111.

[89] A. Gomes, L. Aguiar, R. Ferraz, C. Teixeira, P. Gomes, The Emerging Role of Ionic Liquid-Based Approaches for Enhanced Skin Permeation of Bioactive Molecules: A Snapshot of the Past Couple of Years, Int. J. Mol. Sci. . 22 (2021). https://doi.org/10.3390/ijms222111991.

[90] A. Shroff, A. Mamalis, J. Jagdeo, Oxidative Stress and Skin Fibrosis, Curr. Pathobiol. Rep. 2 (2014) 257–267. https://doi.org/10.1007/s40139-014-0062-y.

[91] A. Biernacka, M. Dobaczewski, N.G. Frangogiannis, TGF-β signaling in fibrosis, Growth Factors. 29 (2011) 196–202. https://doi.org/10.3109/08977194.2011.595714.

[92] E. Thunnissen, A.C. Borczuk, D.B. Flieder, B. Witte, M.B. Beasley, J.-H. Chung, S. Dacic, S. Lantuejoul, P.A. Russell, M. den Bakker, J. Botling, E. Brambilla, E. de Cuba, K.R. Geisinger, K. Hiroshima, A.M. Marchevsky, Y. Minami, A. Moreira, A.G. Nicholson, A. Yoshida, M.-S. Tsao, A. Warth, E. Duhig, G. Chen, Y. Matsuno, W.D. Travis, K. Butnor, W. Cooper, M. Mino-Kenudson, N. Motoi, C. Poleri, G. Pelosi, K. Kerr, S.C. Aisner, Y. Ishikawa, R.H. Buettner, N. Keino, Y. Yatabe, M. Noguchi, The Use of Immunohistochemistry Improves the Diagnosis of Small Cell Lung Cancer and Its Differential Diagnosis. An International Reproducibility Study in a Demanding Set of Cases, J. Thorac. Oncol. 12 (2017) 334–346. https://doi.org/https://doi.org/10.1016/j.jtho.2016.12.004.

[93] A.J. Affandi, T.R.D.J. Radstake, W. Marut, Update on biomarkers in systemic sclerosis: tools for diagnosis and treatment, Semin. Immunopathol. 37 (2015) 475–487. https://doi.org/10.1007/s00281-015-0506-4.

[94] B. Emde, A. Heinen, A. Gödecke, K. Bottermann, Wheat germ agglutinin staining as a suitable method for detection and quantification of fibrosis in cardiac tissue after myocardial infarction, Eur. J. Histochem. 58 (2014) 2448. https://doi.org/10.4081/ejh.2014.2448.

[95] R.A. Kumar, N. Papaïconomou, J.-M. Lee, J. Salminen, D.S. Clark, J.M. Prausnitz, In vitro cytotoxicities of ionic liquids: effect of cation rings, functional groups, and anions., Environ. Toxicol. 24 (2009) 388–395. https://doi.org/10.1002/tox.20443.

[96] D. Guinee Jr, E. Brambilla, M. Fleming, T. Hayashi, M. Rahn, M. Koss, V. Ferrans, W. Travis, The potential role of BAX and BCL-2 expression in diffuse alveolar damage, Am. J. Pathol. 151 (1997) 999–1007. https://pubmed.ncbi.nlm.nih.gov/9327733.

[97] A. Perelman, C. Wachtel, M. Cohen, S. Haupt, H. Shapiro, A. Tzur, JC-1: alternative excitation wavelengths facilitate mitochondrial membrane potential cytometry., Cell Death Dis. 3 (2012) e430. https://doi.org/10.1038/cddis.2012.171.

[98] E. Robles-Escajeda, U. Das, N.M. Ortega, K. Parra, G. Francia, J.R. Dimmock, A. Varela-Ramirez, R.J. Aguilera, A novel curcumin-like dienone induces apoptosis in triple-negative breast cancer cells., Cell. Oncol. (Dordr). 39 (2016) 265–277. https://doi.org/10.1007/s13402-016-0272-x.

[99] S. JO, T.A.E.K. HA, S.-H. HAN, M.I.E.U.N. KIM, I. JUNG, H.-W. LEE, S.K. BAE, J.U.N.S.I.K. LEE, Myricetin Induces Apoptosis of Human Anaplastic Thyroid Cancer Cells via Mitochondria Dysfunction, Anticancer Res. 37 (2017) 1705 LP – 1710. http://ar.iiarjournals.org/content/37/4/1705.abstract.

[100] J. Chen, M.K. Ghorai, G. Kenney, J. Stubbe, Mechanistic studies on bleomycin-mediated DNA damage: multiple binding modes can result in double-stranded DNA cleavage, Nucleic Acids Res. 36 (2008) 3781–3790. https://doi.org/10.1093/nar/gkn302.

[101] A. Vlahovic, A. Gazikalovic, O. Adjic, Bleomycin sclerotherapy for lymphatic malformation after unsuccessful surgical excision: case report, Acta Otorhinolaryngol. Ital. 35 (2015) 365–367. https://doi.org/10.14639/0392-100X-105513.

[102] D. Yang, M.-B. Chen, L.-Q. Wang, L. Yang, C.-Y. Liu, P.-H. Lu, Bcl-2 expression predicts sensitivity to chemotherapy in breast cancer: a systematic review and meta-analysis, J. Exp. Clin. Cancer Res. 32 (2013) 105. https://doi.org/10.1186/1756-9966-32-105.

[103] T.J. Kipps, H. Eradat, S. Grosicki, J. Catalano, W. Cosolo, I.S. Dyagil, S. Yalamanchili, A. Chai, S. Sahasranaman, E. Punnoose, D. Hurst, H. Pylypenko, A phase 2 study of the BH3 mimetic BCL2 inhibitor navitoclax (ABT-263) with or without rituximab, in previously untreated B-cell chronic lymphocytic leukemia., Leuk. Lymphoma. 56 (2015) 2826–2833. https://doi.org/10.3109/10428194.2015.1030638.

[104] N.S. Nor Hisam, A. Ugusman, N.F. Rajab, M.F. Ahmad, M. Fenech, S.L. Liew, N.N. Mohamad Anuar, Combination Therapy of Navitoclax with Chemotherapeutic Agents in Solid Tumors and Blood Cancer: A Review of Current Evidence, Pharm. . 13 (2021). https://doi.org/10.3390/pharmaceutics13091353.

[105] J.M. Cleary, C.M.S.R. Lima, H.I. Hurwitz, A.J. Montero, C. Franklin, J. Yang, A. Graham, T. Busman, M. Mabry, K. Holen, G.I. Shapiro, H. Uronis, A phase I clinical trial of navitoclax, a targeted high-affinity Bcl-2 family inhibitor, in combination with gemcitabine in patients with solid tumors, Invest. New Drugs. 32 (2014) 937–945. https://doi.org/10.1007/s10637-014-0110-9.

[106] B.D. Uhal, Apoptosis in Lung Fibrosis and Repair*, Chest. 122 (2002) 293S-298S. https://doi.org/https://doi.org/10.1378/chest.122.6_suppl.293S.

[107] D.R. Green, F. Llambi, Cell Death Signaling, Cold Spring Harb. Perspect. Biol. 7 (2015) a006080. https://doi.org/10.1101/cshperspect.a006080.

[108] C.-M. Park, T. Oie, A.M. Petros, H. Zhang, P.M. Nimmer, R.F. Henry, S.W. Elmore, Design, Synthesis, and Computational Studies of Inhibitors of Bcl-XL, J. Am. Chem. Soc. 128 (2006) 16206–16212. https://doi.org/10.1021/ja0650347.

[109] E.S. A., M. Paul, T.-C. Marjana, Wound repair and regeneration: Mechanisms, signaling, and translation, Sci. Transl. Med. 6 (2014) 265sr6-265sr6. https://doi.org/10.1126/scitranslmed.3009337.

[110] J. Uitto, D. Kouba, Cytokine modulation of extracellular matrix gene expression: relevance to fibrotic skin diseases., J. Dermatol. Sci. 24 Suppl 1 (2000) S60-9. https://doi.org/10.1016/s0923-1811(00)00143-2.

[111] M. Trojanowska, E.C. LeRoy, B. Eckes, T. Krieg, Pathogenesis of fibrosis: type 1 collagen and the skin., J. Mol. Med. (Berl). 76 (1998) 266–274. https://doi.org/10.1007/s001090050216.

[112] S.A. Jimenez, S. Gaidarova, B. Saitta, N. Sandorfi, D.J. Herrich, J.C. Rosenbloom, U.

Kucich, W.R. Abrams, J. Rosenbloom, Role of protein kinase C-delta in the regulation of collagen gene expression in scleroderma fibroblasts, J. Clin. Invest. 108 (2001) 1395–1403. https://doi.org/10.1172/JCI12347.

[113] A. Kaefer, J. Yang, P. Noertersheuser, S. Mensing, R. Humerickhouse, W. Awni, H. Xiong, Mechanism-based pharmacokinetic/pharmacodynamic meta-analysis of navitoclax (ABT-263) induced thrombocytopenia., Cancer Chemother. Pharmacol. 74 (2014) 593–602. https://doi.org/10.1007/s00280-014-2530-9.

[114] L.R. Jorge, L.K. Harada, E.C. Silva, W.F. Campos, F.C. Moreli, G. Shimamoto, J.F.B. Pereira, J.M. Oliveira, M. Tubino, M.M.D.C. Vila, V.M. Balcão, Non-invasive Transdermal Delivery of Human Insulin Using Ionic Liquids: In vitro Studies , Front. Pharmacol. . 11 (2020) 243. https://www.frontiersin.org/article/10.3389/fphar.2020.00243.

[115] J. Stetefeld, S.A. McKenna, T.R. Patel, Dynamic light scattering: a practical guide and applications in biomedical sciences, Biophys. Rev. 8 (2016) 409–427. https://doi.org/10.1007/s12551-016-0218-6.

[116] D.C. Murador, L.M. De Souza Mesquita, B. V Neves, A.R.C. Braga, P.L.G. Martins, L.Q. Zepka, V. V De Rosso, Bioaccessibility and cellular uptake by Caco-2 cells of carotenoids and chlorophylls from orange peels: A comparison between conventional and ionic liquid mediated extractions, Food Chem. 339 (2021) 127818. https://doi.org/https://doi.org/10.1016/j.foodchem.2020.127818.

[117] S. Matsuzaki, C. Darcha, Involvement of the Wnt/β-Catenin Signaling Pathway in the Cellular and Molecular Mechanisms of Fibrosis in Endometriosis, PLoS One. 8 (2013) e76808. https://doi.org/10.1371/journal.pone.0076808.

[118] D.A. Gutierrez, R.E. DeJesus, L. Contreras, I.A. Rodriguez-Palomares, P.J. Villanueva, K.S. Balderrama, L. Monterroza, M. Larragoity, A. Varela-Ramirez, R.J. Aguilera, A new pyridazinone exhibits potent cytotoxicity on human cancer cells via apoptosis and poly-ubiquitinated protein accumulation., Cell Biol. Toxicol. 35 (2019) 503–519. https://doi.org/10.1007/s10565-019-09466-8.

[119] R. de O. Pereira, T.C.C. Pelisson E Silva, A. de Oliveira Ferreira, M.A.F. Brandao, N.R.B. Raposo, H.C. Polonini, Ex vivo Skin Permeation Evaluation of An Innovative Transdermal Vehicle Using Nimesulide and Piroxicam as Model Drugs., Curr. Drug

Deliv. 14 (2017) 516–520. https://doi.org/10.2174/1567201813666160824142013.

[120] S.-H. Lee, X.W. Meng, K.S. Flatten, D.A. Loegering, S.H. Kaufmann, Phosphatidylserine exposure during apoptosis reflects bidirectional trafficking between plasma membrane and cytoplasm, Cell Death Differ. 20 (2013) 64–76. https://doi.org/10.1038/cdd.2012.93.

[121] M.J. Lenardo, C.K. McPhee, L. Yu, Autophagic cell death, Methods Enzymol. 453 (2009) 17–31. https://doi.org/10.1016/S0076-6879(08)04002-0.

[122] A. Varela-Ramirez, M. Costanzo, Y.P. Carrasco, K.H. Pannell, R.J. Aguilera, Cytotoxic effects of two organotin compounds and their mode of inflicting cell death on four mammalian cancer cells, Cell Biol. Toxicol. 27 (2011) 159–168. https://doi.org/10.1007/s10565-010-9178-y.

[123] M. Mishra, S. Tiwari, A. V Gomes, Protein purification and analysis: next generation Western blotting techniques, Expert Rev. Proteomics. 14 (2017) 1037–1053. https://doi.org/10.1080/14789450.2017.1388167.

[124] G.R. Turbett, L.N. Sellner, The use of optimal cutting temperature compound can inhibit amplification by polymerase chain reaction., Diagn. Mol. Pathol. 6 (1997) 298–303. https://doi.org/10.1097/00019606-199710000-00009.

[125] A.-A. Grosset, K. Loayza-Vega, É. Adam-Granger, M. Birlea, B. Gilks, B. Nguyen, G. Soucy, D. Tran-Thanh, R. Albadine, D. Trudel, Hematoxylin and Eosin Counterstaining Protocol for Immunohistochemistry Interpretation and Diagnosis., Appl. Immunohistochem. Mol. Morphol. AIMM. 27 (2019) 558–563. https://doi.org/10.1097/PAI.0000000000000626.

[126] N. Singh, P.J. Yeh, Suppressive drug combinations and their potential to combat antibiotic resistance, J. Antibiot. (Tokyo). 70 (2017) 1033–1042. https://doi.org/10.1038/ja.2017.102.

[127] Z. Khatun, M. Nurunnabi, M. Nafiujjaman, G.R. Reeck, H.A. Khan, K.J. Cho, Y. Lee, A hyaluronic acid nanogel for photo-chemo theranostics of lung cancer with simultaneous light-responsive controlled release of doxorubicin., Nanoscale. 7 (2015) 10680–10689. https://doi.org/10.1039/c5nr01075f.

[128] G. Housman, S. Byler, S. Heerboth, K. Lapinska, M. Longacre, N. Snyder, S. Sarkar, Drug resistance in cancer: an overview, Cancers (Basel). 6 (2014) 1769–1792. https://doi.org/10.3390/cancers6031769.

[129] Y. Sun, J. Campisi, C. Higano, T.M. Beer, P. Porter, I. Coleman, L. True, P.S. Nelson, Treatment-induced damage to the tumor microenvironment promotes prostate cancer therapy resistance through WNT16B., Nat. Med. 18 (2012) 1359–1368. https://doi.org/10.1038/nm.2890.

[130] Y. Sun, Tumor microenvironment and cancer therapy resistance., Cancer Lett. 380 (2016) 205–215. https://doi.org/10.1016/j.canlet.2015.07.044.

[131] J. Zugazagoitia, C. Guedes, S. Ponce, I. Ferrer, S. Molina-Pinelo, L. Paz-Ares, Current Challenges in Cancer Treatment., Clin. Ther. 38 (2016) 1551–1566. https://doi.org/10.1016/j.clinthera.2016.03.026.

[132] J.J. Cohen, Apoptosis: Mechanisms of life and death in the immune system, J. Allergy Clin. Immunol. 103 (1999) 548–554. https://doi.org/https://doi.org/10.1016/S0091-6749(99)70222-8.

[133] R.S.Y. Wong, Apoptosis in cancer: from pathogenesis to treatment, J. Exp. Clin. Cancer Res. 30 (2011) 87. https://doi.org/10.1186/1756-9966-30-87.

[134] T.M. Abu Samaan, M. Samec, A. Liskova, P. Kubatka, D. Büsselberg, Paclitaxel's Mechanistic and Clinical Effects on Breast Cancer, Biomolecules. 9 (2019) 789. https://doi.org/10.3390/biom9120789.

[135] NCI, Drugs Approved for Kaposi Sarcoma, 2021. (n.d.). https://www.cancer.gov/about-cancer/treatment/drugs/kaposi-sarcoma.

[136] Y. Jin, P. Li, F. Wang, β-glucans as potential immunoadjuvants: A review on the adjuvanticity, structure-activity relationship and receptor recognition properties., Vaccine. 36 (2018) 5235–5244. https://doi.org/10.1016/j.vaccine.2018.07.038.

[137] S.H. Albeituni, J. Yan, The effects of β-glucans on dendritic cells and implications for cancer therapy., Anticancer. Agents Med. Chem. 13 (2013) 689–698. https://doi.org/10.2174/1871520611313050003.

[138] C. Holohan, S. Van Schaeybroeck, D.B. Longley, P.G. Johnston, Cancer drug resistance: an evolving paradigm., Nat. Rev. Cancer. 13 (2013) 714–726. https://doi.org/10.1038/nrc3599.

[139] A. Singh, J. Settleman, EMT, cancer stem cells and drug resistance: an emerging axis of evil in the war on cancer., Oncogene. 29 (2010) 4741–4751. https://doi.org/10.1038/onc.2010.215.

[140] H.A.O. XIONG, R.S. PRADHAN, A. NADA, A.P. KRIVOSHIK, K.D. HOLEN, J.W. RHODES, G.B. GORDON, R.O.D. HUMERICKHOUSE, W.M. AWNI, Studying Navitoclax, a Targeted Anticancer Drug, in Healthy Volunteers – Ethical Considerations and Risk/Benefit Assessments and Management, Anticancer Res. 34 (2014) 3739 LP – 3746. http://ar.iiarjournals.org/content/34/7/3739.abstract.

[141] M. Puglisi, L.R. Molife, M.J. de Jonge, K.H. Khan, L. van Doorn, M.D. Forster, M. Blanco, M. Gutierrez, C. Franklin, T. Busman, J. Yang, F.A. Eskens, A Phase I study of the safety, pharmacokinetics and efficacy of navitoclax plus docetaxel in patients with advanced solid tumors., Future Oncol. 17 (2021) 2747–2758. https://doi.org/10.2217/fon-2021-0140.

[142] D. Yang, M.-B. Chen, L.-Q. Wang, L. Yang, C.-Y. Liu, P.-H. Lu, Bcl-2 expression predicts sensitivity to chemotherapy in breast cancer: a systematic review and meta-analysis, J. Exp. Clin. Cancer Res. 32 (2013) 105. https://doi.org/10.1186/1756-9966-32-105.

[143] A.W. Roberts, J.F. Seymour, J.R. Brown, W.G. Wierda, T.J. Kipps, S.L. Khaw, D.A. Carney, S.Z. He, D.C.S. Huang, H. Xiong, Y. Cui, T.A. Busman, E.M. McKeegan, A.P. Krivoshik, S.H. Enschede, R. Humerickhouse, Substantial Susceptibility of Chronic Lymphocytic Leukemia to BCL2 Inhibition: Results of a Phase I Study of Navitoclax in Patients With Relapsed or Refractory Disease, J. Clin. Oncol. 30 (2011) 488–496. https://doi.org/10.1200/JCO.2011.34.7898.

[144] A. Jordan, J.A. Hadfield, N.J. Lawrence, A.T. McGown, Tubulin as a target for anticancer drugs: agents which interact with the mitotic spindle., Med. Res. Rev. 18 (1998) 259–296. https://doi.org/10.1002/(sici)1098-1128(199807)18:4<259::aid-med3>3.0.co;2-u.

[145] K.H. Downing, Structural basis for the interaction of tubulin with proteins and drugs that affect microtubule dynamics., Annu. Rev. Cell Dev. Biol. 16 (2000) 89–111. https://doi.org/10.1146/annurev.cellbio.16.1.89.

[146] V. Ganansia-Leymarie, P. Bischoff, J.-P. Bergerat, V. Holl, Signal transduction pathways of taxanes-induced apoptosis., Curr. Med. Chem. Anticancer. Agents. 3 (2003) 291–306. https://doi.org/10.2174/1568011033482422.

[147] L.G. Wang, X.M. Liu, W. Kreis, D.R. Budman, The effect of antimicrotubule agents on signal transduction pathways of apoptosis: a review., Cancer Chemother. Pharmacol. 44

(1999) 355–361. https://doi.org/10.1007/s002800050989.

[148] H. Lin, E. de Stanchina, X.K. Zhou, F. Hong, A. Seidman, M. Fornier, W.-L. Xiao, E.J. Kennelly, K. Wesa, B.R. Cassileth, S. Cunningham-Rundles, Maitake beta-glucan promotes recovery of leukocytes and myeloid cell function in peripheral blood from paclitaxel hematotoxicity, Cancer Immunol. Immunother. 59 (2010) 885–897. https://doi.org/10.1007/s00262-009-0815-3.

[149] M. Pieroni, M. Santis, G. Zizzo, S. Bosello, C. Smaldone, M. Campioni, G. De Luca, A. Laria, A. Meduri, F. Bellocci, L. Bonomo, F. Crea, G. Ferraccioli, Recognizing and treating myocarditis in recent-onset systemic sclerosis heart disease: Potential utility of immunosuppressive therapy in cardiac damage progression, Semin. Arthritis Rheum. 43 (2013). https://doi.org/10.1016/j.semarthrit.2013.07.006.

[150] M. Pieroni, M. Santis, G. Zizzo, S. Bosello, C. Smaldone, M. Campioni, G. De Luca, A. Laria, A. Meduri, F. Bellocci, L. Bonomo, F. Crea, G. Ferraccioli, Recognizing and treating myocarditis in recent-onset systemic sclerosis heart disease: Potential utility of immunosuppressive therapy in cardiac damage progression, Semin. Arthritis Rheum. 43 (2013). https://doi.org/10.1016/j.semarthrit.2013.07.006.

VITA:

I am Md. Nurul Huda is a Ph.D. candidate in the Environmental science and engineering department of the University of Texas at El Paso. I have been awarded the Doctor of Philosophy in ESE from UTEP on April 22, 2022. I am originally from Bangladesh. My research focuses on targeted drug delivery in cancer and fibrosis disease models. I graduated from Dr. Nurunnabi's laboratory in the School of Pharmacy at UTEP. During my Ph.D. I have published two first-author review articles, 2 peed reviewed journals, 1 book chapter, 2 conference papers, and 2 submitted patents. I have 6 more peer-reviewed papers are under construction. During my Ph.D. I have been awarded 2 times Dodson research grant and a 1-time travel grant. I have gained research and teaching experience while working as a teaching and research assistant at UTEP. After I graduate, I am pursuing my career biotech company focused on developing regenerative medicine for age-related diseases. I am so fortunate to pursue my Ph.D. at UTEP and got the opportunity to become a better scientist.

Contact Information: mdnurunlhuda.phd@gmail.com